Silicone MEMS for Fluidics

Thesis by

Charles Grosjean

In Partial Fulfillment of the Requirements
For the Degree of
Doctor of Philosophy

California Institute of Technology
Pasadena, CA 91125

2001

(Submitted May 24, 2001)

© 2001
Charles Grosjean
All Rights Reserved

To my parents

Acknowledgements

For showing a naive undergrad that not all graduate students are "turkeys," Kwabena Boahen, Jeffrey Dickson, Chris Diorio, and Bhusan Gupta. For countless hours pleasantly lost in Steele and Moore, Art Zirger and Glen George.

To my advisor, Yu-Chong Tai, my deepest gratitude for your advice and guidance over the years. You provided me with the flexibility I desired, but always knew, even when I may not have, when I needed more structure to accomplish my goals.

To the first generation of students who showed me the ropes, Chang Liu, Jianqiang Liu, and Svetlana Tatic-Lucic, and the second generation which honed my technique, Fukang Jiang, Raanan Miller, Thomas Tsao, John Wright, and Xing Yang, I am very grateful for all the hours spent in and out of the cleanroom. Special thanks to Shuyun Wu, who while entering the Ph.D. program at the same time as myself, I always considered my elder in the best sense. Several years spent sharing an office with him was only enough time to uncover the facets of his knowledge and wonder how he could raise a family and still work so hard.

As post-docs, Weilong Tang, Tseng Yang Hsu, and Sangwook Lee proved that it is possible to work normal hours and accomplish just as much if not more than a graduate student who leaves everything to the last minute although this may also have been due to their knowledge and experience.

Tze-Jung Yao reminded me of the thirst for knowledge I once had, Yong Xu embodied patience and perseverance, and Xuan-Qi Wang admonished me to work hard.

Dr. Chih-Ming Ho and his students Gwo-Bin Lee and Po-Hao Huang helped me immensely with the delta wing project, and put up with my sporadic fabrication of actuators. Yih-Far Chen worked tirelessly preparing a number of DARPA presentations and posters related to microfluidics work and never complained when I wouldn't have results until the last minute, further increasing his workload.

Michael Gerfen, John Van Deusen, and Rodney Rojas took time out of their busy schedules to teach me enough about machining so that I could make the various structures in this thesis. Their patience is greatly appreciated.

Thanks to Linda Dozsa for making the academic paperwork disappear, Janice Tucker and later Tanya Hefner for making research related matters painless, and Lyn Hein for all the ordering, and more importantly for being there with an open door.

I could not have completed my work without the help of our technician, Trevor Roper. I probably could have done without all the cricket blather, but much of his advice was invaluable although I still don't know the lyrics to all the songs he would sing in the cleanroom.

Ken Walsh introduced me to the "if it has four legs" and potatoes diet, constantly proved that I'm getting senile, taught Sierra to use me for wiping her paws, and managed to proofread portions of this thesis without laughing or asking for a case of red pens.

Finally, Xing Yang took on the task of being a mentor, a best friend, and a voice of reason when I needed it the most. From the anonymous senior student tucked away in the corner of the Steele basement to a research partner and office mate, I owe him a debt of gratitude that is difficult to repay, but I will spend a long time trying. More so than anyone except Professor Tai, he shaped my approach to research, from the most trivial process details to solving the most complex problems.

Of course, this would not be complete without mentioning the two people who made this all possible, my parents. They made countless sacrifices over the years so that I could be where I am today. It is impossible to repay them and I can only hope that I've made them proud. My greatest regret is that I didn't finish in time for my mother to see what I've accomplished.

Abstract

Silicone MEMS for Fluidics

Thesis by
Charles Grosjean

Doctor of Philosophy in Electrical Engineering
California Institute of Technology
Professor Yu-Chong Tai, Advisor

In this thesis, silicone rubber was integrated with standard silicon based micromachining processes to allow fabrication of large deflection actuators. Taking advantage of the low Young's modulus and resulting flexibility of silicone rubber, several different devices for fluidic control were demonstrated.

A novel self-releasing process for defining large actuators on silicon substrates irrespective of backside opening size was developed and used to generate micro balloon actuators used for delta wing control. When deployed near the separation line on the rounded leading edge of a delta wing, significant aerodynamic moments were generated allowing flight control at high angle of attack. To allow more flexibility in spatial actuation, a flexible metal substrate actuator "skin" was also developed and tested on flight models. With vertical actuations of 2 mm, rolling moment coefficients up to 0.012 were obtained at high angle of attack, comparable to conventional flaps.

The low durometer and flexibility of silicone rubber membranes were exploited to fabricate a peristaltic pump. Taking advantage of the low dead volume and good sealing afforded by membranes combined with form-fitting chambers, a self-priming pump capable of pumping gas and liquid with high particle immunity was demonstrated. Due to the planar nature of the device, it is straightforward to construct integrated systems of reservoirs, channels, valves, and pumps. Standalone operation without an external pneumatic source was achieved using thermopneumatic actuation with air as the working fluid. To achieve low power consumption and reasonable operational frequency, a suspended silicon island heater process was also developed. Flow rates up to 6.3 μl/min at 291 mW power consumption were achieved with thermopneumatic actuation and flow rates above 100 μl/min can be easily obtained with external pneumatic operation.

Using technology developed for the peristaltic pump, a diaphragm pump topology suitable for complex fluidic systems was developed. By using a plurality of active valves and a single pumping chamber, fluids can be pumped from any input to any output. This can significantly reduce the number of pumps necessary for anything other than the simplest flow system. Using an improved thermopneumatic actuator, integrated flow systems can be constructed.

Table of Contents

1. Introduction **1**
1.1 Silicon Microfabrication 1
1.2 Research Objectives 1
1.2.1 MEMS for Flight Control 2
1.2.2 MEMS Micropumps 2
1.3 Thesis Outline 4
References 6

2. Silicone Rubber as a MEMS Material **8**
2.1 Introduction 8
2.2 Silicone Fundamentals 8
2.2.1 Structure 8
2.2.2 From PDMS to Silicone Rubber 9
2.2.3 Silicone Rubber Properties 10
2.3 Vinyl Addition (Platinum Cure) Silicones 11
2.3.1 Formulation 12
2.3.2 Surface Adhesion 14
2.4 Silicone for MEMS 15
2.4.1 Material Selection 15
2.4.2 Application 18
2.5 Process Development 19
2.5.1 Bulk Micromachining with Silicone 19
2.5.2 Surface Micromachining with Silicone 23
2.5.3 Simple Molding 25
2.5.4 Replica Casting 26
2.5.5 Lithography with UV Cure Silicones 29
2.6 Load-Deflection Testing 29

2.6.1 Experimental Apparatus and Samples 30
2.6.2 Results and Analysis 31
2.7 Conclusion 34
References 35

3. Actuation Methods 38
3.1 Introduction 38
3.2 Actuation Mechanisms 38
3.2.1 Electrostatic 38
3.2.2 Magnetostatic 39
3.2.3 Electromagnetic 40
3.3 Thermopneumatic Actuation 40
3.3.1 Thermal Expansion of a Gas 40
3.3.2 Thermal Expansion of a Liquid 42
3.3.3 Static Performance 42
3.4 Conclusion 44
References 45

4. Micro Balloons for Aerodynamic Control 46
4.1 Introduction 46
4.2 Previous Work 47
4.3 Silicon Substrate Actuators 48
4.3.1 Design 49
4.3.2 Fabrication 51
4.3.3 Testing Apparatus 52
4.3.4 Static Testing 53
4.3.5 Cyclic Testing 54
4.3.6 Flight Robustness 55
4.4 Wind Tunnel Testing 56
4.4.1 Facility and Delta Wing Configuration 56
4.4.2 Pitching, Yawing, and Rolling Moment Control 57
4.4.3 Balloon Actuators vs. Conventional Flaps 60
4.4.4 Spatial Distribution of Actuators 60

4.5 Metal Substrate Actuators 61
4.5.1 Design 62
4.5.2 Brass Substrates 62
4.5.3 Copper Substrates 64
4.7 Conclusion 67
References 69

5. Peristaltic Micropump 70
5.1 Introduction 70
5.2 Theory of Operation 71
5.3 Design and Fabrication 74
5.3.1 Membrane 76
5.3.2 Chamber 77
5.3.3 Heater 80
5.4 Pneumatic Operation 84
5.4.1 Testing Setup 84
5.4.2 Testing Results 86
5.4.3 Three Phase Analysis 88
5.4.4 Six Phase Analysis 90
5.5 Thermopneumatic Operation 91
5.5.1 Pump Assembly 92
5.5.2 Testing 93
5.5.3 Operation as a Valve 96
5.6 Enhancements 96
5.6.1 Asymmetric Sealing 96
5.6.2 Integrated Heater/Membrane 98
5.7 Conclusion 100
References 102

6. Planar Fluidic System 104
6.1 Introduction 104
6.2 Diaphragm Pump Operation 105
6.3 Integrated Heater and Membrane 106

6.3.1 Design and Fabrication 107
6.3.2 Discussion 109
6.4 Improved Nitride Membrane Heater 112
6.4.1 Design and Fabrication 112
6.4.2 Process Specifics 114
6.4.3 Heater Testing 116
6.5 Diaphragm Pump 119
6.5.1 Membrane 120
6.5.2 Fluidic Substrate 120
6.5.3 Thermopneumatic Actuator 121
6.5.4 Thermopneumatic Pumping 124
6.6 Conclusion 128
References 129

7. Conclusion 130
7.1 Summary of Research 130
7.2 Directions for Future Work 132

Figures

2-1: Basic structural units of polyorganosiloxanes. 9

2-2: Platinum catalyzed addition reaction between vinyl and hydride. 10

2-3: Adding functionality to substrate through deposition of silanes. 15

2-4: Using KOH etching and RIE to create free standing rectangular silicone rubber membranes. 21

2-5: (a) Circular MRTV1 silicone rubber membranes with rigid boss in center. (b) Backside of dies showing thin silicon membrane formed by KOH and RIE definition of membrane boundary and boss structures. 22

2-6: Circular (clear) silicone rubber membrane formed over DRIE defined silicon meandering beam (100 μm wide) using photoresist sacrificial layer. 24

2-7: Process flow for a membrane with integrated pillars to control membrane crush when clamping to a fluidic structure. 26

2-8: Silicone rubber (RTV615) replica made by casting. This is a second generation part, made by casting on a first generation silicone rubber mold made from the original silicon master. The large square and oval reservoirs were defined by DRIE along with the channels, while the smaller groups of three hexagonal pits were defined by KOH followed by HNA. 28

2-9: Small channel and chamber formed by spinning silicone rubber over a photoresist pattern and later removing the photoresist with acetone. The small square holes are 100 x 100 μm openings from the backside formed by KOH etching to a nitride membrane etch stop which is later removed with SF_6 plasma. 28

2-10: Circular membranes for testing the properties of Shin Etsu X32-1502. A small eyelet is used for connecting pneumatic tubing to the samples. 29

2-11: The microscope (Bausch & Lomb MicroZoom™) and stage used to measure vertical deflection of the membrane vs. pressure. A high power objective is used to minimize depth of field to obtain accurate focus on membrane surface. 30

2-12: Pressure vs. deflection for sample #4, a 178 μm thick, 2.13mm diameter circular membrane. A theoretical fit is also shown that was used to determine the Young's modulus and residual stress. 31

2-13: Measured profile of an inflated membrane with a theoretical fit assuming a sinusoidal profile as in Equation 2.2. 33

3-1: Deflection for a 1.4 mm diameter membrane as a function of air temperature inside the cavity (assuming it was filled at 298°K) 43

3-2: Deflection vs. temperature for a water filled cavity. 44

4-1: Visualization of counter-rotating vortices over a delta-wing. 46

4-2: A simple mechanical actuator consisting of a metal strip rolled into a tube on the leading edge. By rotating the strip, a certain protrusion from the surface can be obtained. 47

4-3: Conceptual assembly of actuator strip to backing plate. 48

4-4: First generation actuator design (2 mm) and extreme deformation during inflation (also referred to as the "dogbone" shape). 49

4-5: Second (3 mm) generation design. Note the rounded edges of the release layer and two instead of three backholes. 50

4-6: Process flow for silicone balloon actuators and a completed wafer prior to dicing. Dicing tape was used to mask the silicone rubber so that reference marks on the wafer could be used for alignment during dicing. 51

4-7: Testing apparatus for pressurizing silicone balloon actuators. 52

4-8: Pressure vs. deflection for a 3 mm actuator after various experiments to determine the change in properties with use. 53

4-9: Side view of a 3 mm actuator inflated with various pressures. 54

4-10: Typical pressure vs. deflection data for a 3 mm actuator after cycling at 5.1 psi showing minimal change in shape. 55

4-11: Large UCLA wind tunnel schematic. 56

4-12: Schematic of delta wing model and detail of leading edge rod. 57

4-13: Rolling moment (normalized to a single vortex) at an AOA of 25°. 57

4-14: With selective spatial actuation, rolling, pitching, and yawing moments can be achieved. All of these are normalized to a single vortex 58

4-15: Moment coefficients vs. Reynolds number at an AOA of 25° 59

4-16: Flow visualization of vortex movement vs. actuator position. 60

4-17: Conventional vs. MEMS control for double sided actuation assuming positive and negative components on opposite sides being added together. 61

4-18: Simple process for metal substrate balloon actuators. 62

4-19: Brass substrate actuators and asymmetric actuation when inflated due to the metal island left on the membrane. 63

4-20: Etching apparatus with bubbler (left) and substrate holder (right) with photoresist patterned copper substrate clipped on for $FeCl_3$ etching. 65

4-21: A closeup detail of the pneumatic inlets for each row of balloon actuators (left) and an early prototype X32-1502 on brass substrate actuator skin bonded to a tube. The grooves in the tube distribute pressure to each row. The final actuators were made using copper instead of brass. 67

5-1: Operational sequence of a conventional peristaltic pump. 71

5-2: Peristaltic operation with discrete linear actuators. 72

5-3: Different actuation patterns for a three stage peristaltic pump. Intermediate patterns are shown in gray for A & B and show the transitory behavior assuming that the actuators have equal rise and fall times. 73

5-4: A conceptual three chamber peristaltic pump structure. 75

5-5: Poor matching causing leakage between easily fabricated chamber shapes and deflected membranes along with two possible solutions. 75

5-6: Top and bottom views of the composite silicone rubber/Parylene C membrane die. Each membranes measures 2.0 x 2.8 mm. The pressure vs. deflection curve illustrates how flexible the membranes are. 76

5-7: The vertical machining center (VMC) used for fabricating chamber prototypes along with the fixture used to hold the acrylic during machining. 78

5-8: Acrylic pump plate with three sequential chambers, connections for tubing on the sides, and four holes for clamping to a base plate. A Wyko scan of an inlet/outlet chamber is on the right with details of the channel and chamber. 79

5-9: Island suspension from the top (a) vs. below (b). 80

5-10: Process flow for suspended island heater using TMAH release. 82

5-11: (a) A view of the heater die. (b) A single heater showing the meandering gold resistor on a silicon island suspended by a silicon nitride membrane. (c) A closeup of one corner (white dotted outline) with detail of the corner compensation, silicon nitride bridge for the resistor, and through holes. 82

5-12: A view of the top nitride/gold bridge viewed from the back through the suspension nitride. Note the crack in the beam on the left initiated by the incompletely etched silicon outcropping vs. the good beam on the right. 83

5-13: Pneumatic testing setup. A silicone membrane die is glued to an aluminum block which serves serves as a manifold for connection to the three solenoid valves. Acrylic pump plates are clamped onto the membrane. A calibrated capillary is attached to the outlet for flow rate measurement. 84

5-14: Flow vs. frequency for three phase pneumatic operation (Pattern B). Operation is shown for air and water pumping with two membrane actuation pressures. The inset graph shows volume pumped per cycle.

Lower actuation pressures result in less membrane deflection which results in less swept volume. 85

5-15: Offset membrane location (to the left) to improve sealing. The blue dye illustrates the resulting dead volume. 86

5-16: Flow rate vs. frequency for 6 phase pneumatic operation as compared to 3 phase for water at an actuation pressure of 8 psi 87

5-17: Backpressure vs. normalized flow rate (the equivalent flow rate if operated at 1 Hz) for pneumatic operation (six phase) at two pressures. 88

5-18: Vacuum (measured at the inlet) vs. flow rate using Pattern C at 8 Hz. 88

5-19: Thermopneumatic pump assembly. Heater/membrane package is sandwiched between an aluminum plate and the acrylic chamber plate. The inlet and outlet are stainless steel hypodermic tubing while electrical connections are made to the green 4-pin header on the bottom. 93

5-20: Thermal image of a heater showing strong heat localization on the silicon island. Input power is 190 mW and the substrate is on a 60°C hot chuck. 94

5-21: Power vs. deflection for air and PF5080 filled actuators and flow rate vs. backpressure for an air filled pump operating at 2 Hz. 94

5-22: Step response of air filled actuator in response to 161 mW input 95

5-23: Flow rate of air vs power for a single chamber and thermopneumatic actuator used as a valve. Data for two different inlet pressures is shown. 96

5-24: Optimization of pumping speed and power by using an asymmetric chamber to seal the inlet side of the chamber before the full stroke is complete. 97

5-25: Process flow for a DRIE heater with integrated membrane. 99

5-26: Top and bottom views of a meandering silicon beam formed by DRIE. A gold resistor is deposited on the beam to serve as a heater. The cross section below shows the vertical sidewalls and high aspect ratio of the beam. 100

6-1: Conceptual diaphragm pump with passive check (one-way) valves 104

6-2: A conceptual fluidic system. The rectangles represent active valves with the large circle a pumping chamber. The actuator die on the left has four inputs that can be arbitrarily pumped to the sensor chip in the top center. 107

6-3: Process flow for integrated heater and membrane. 109

6-4: Top (left) and bottom (right) view of the integrated heater/membrane. The silicone layer is transparent. Gold is used for the heater metallization. 110

6-5: Front and back views of actuators assembled to the acrylic fluidic plate along with backside electrical connections. 111

6-6: Process flow for the nitride membrane heater made with DRIE........................ 113

6-7: Heater TCR measurements... 117

6-8: Thermal image of small heater on the left and large heater on the right. The gray regions are areas where no data was acquired due to the low emissivity of gold. 118

6-9: Thermal image of a small heater with 233 mW applied power. The membrane suspending the heater is composed of silicon nitride and silicon resulting in very high thermal conduction to the substrate. 119

6-10: Power vs. deflection for valve actuator.. 121

6-11: Transient response of small valve actuator in response to 2.0V input............... 122

6-12: Basic 6 phase sequence for diaphragm pump. Note that a valve is always closed to prevent free flow through the structure... 124

6-13: Modified sequence used for thermopneumatic operation. The slow filling of the pump chamber and fast rise vs. fall times of the valves allows the transition from phase 2 to phase 3.. 126

Tables

1-1: Various Diaphragm Pumps 3

1-2: Several Peristaltic Pump Designs 4

2-1: Selected thermal and electrical properties of two silicone rubbers. 11

2-2: Various silicone properties. 18

2-3: Sample dimensions and calculated values for E and σ. 32

3-1: Theoretical displacement vs. pressure for silicone rubber membrane. 38

3-2: Required voltage for a given membrane deflection. 39

6-1: Time constants for thermopneumatic actuators. 122

6-2: Measurements to determine effects of air on time constants 123

6-3: Channel dimensions for two different acrylic fluidic substrates and the corresponding pressure drops assuming a flow rate of 0.1 μl/s. 126

Chapter 1

Introduction

1.1 Silicon Microfabrication

Since the 1950's, integrated circuit (IC) technology has also been used to make mechanical structures in silicon. While the term MEMS (Micro Electro Mechanical Systems) dates from the late 1980's, people have been fabricating devices from silicon and associated materials for quite some time. For the most part, silicon based MEMS follows the semiconductor industry in terms of materials and processes. The price paid for the convenience of using existing technology is some limitation in the scope of materials available and thus the range of properties that can be exploited.

Traditional materials for silicon microfabrication include single crystal as used for integrated circuit fabrication; silicon dioxide, polysilicon, amorphous silicon, and silicon nitride in the form of thin films; many metals; polyimide, and photoresist. As certain limitations are encountered in the IC industry, for instance the need for low-k dielectrics for multilevel metallization, new materials are investigated and used. Two examples of new materials for IC fabrication are Parylene and silicon carbide. There are also other materials with interesting properties which while not commonly used in the IC industry, can be integrated with silicon microfabrication. One such material is silicone rubber.

1.2 Research Objectives

The goal of this work was to explore the potential of silicone rubber as a MEMS material and its usefulness in fabricating microactuators. Silicone rubber exhibits a number of

interesting properties including a very low Young's modulus—three to five orders of magnitude lower than other common materials used for silicon microfabrication. It also has very high elongation which allows the construction of very large displacement actuators. Finally, silicone rubber can be formulated with very low durometer which allows it to seal well on rough or uneven surfaces. As it can be easily fabricated into membranes, a variety of actuators can be made. Two applications were investigated.

1.2.1 MEMS for Flight Control

A number of methods have been used for vortex control on delta wing aircraft. These include moveable strakes or nose tips [1, 2], forebody blowing [3, 4], and mechanical flaps [5, 6]. The mechanical flaps implemented as magnetically actuated MEMS flaps offer distributed control and rapid actuation. However, for flight applications, they tend to be fragile and not robust enough for the rough handling encountered in practice. Also, their highly angular nature during actuation potentially makes the development of low radar return wing structures difficult. Pneumatically actuated silicone membranes overcome many of these problems. They can be made small enough so that multiple rows can be situated on the leading edge of a wing. They are conformal in nature until deployed and very robust, even at high velocities. Thus, they are well suited for distributed control applications.

1.2.2 MEMS Micropumps

There has been a great deal of interest in microfluidics as enabled by MEMS technology. Applications encompass genetic analysis [7, 8, 9], medical diagnostics [10], drug delivery [11], and chemical analysis. [12] A necessary component of a microfluidic system is a micropump. In this case, the micro refers to fluid volumes rather than package size.

Depending on the exact nature of usage, it may or may not be necessary for the device itself to be on the same scale as the fluidic volume. However, for devices such as handheld diagnostics and implanted insulin pumps, a small device is also required.

Most work has focused on diaphragm pumps with passive check valves. A number of designs are summarized in Table 1-1. These are popular as only a single active element is required. Common to most designs are externally bonded piezoelectric actuators and membrane or flap style check valves. Thermal methods of actuation are also used and some designs replace the mechanical check valves with diffusor/nozzle structures. The primary intent has been the design of small single devices so fabrication has not been optimized for usage in a microsystem. Flow rates are also reasonably large (100 μl/min) as these devices need to be interfaced with more macroscopic fluidic systems. Self-priming and resistance to particles are common problems that have only been overcome by a few designs. In general, most check valves are not completely immune to particle induced leakage as a strong seal is dependent on the conformality of two relatively flat rigid surfaces. Diffusor structures offer no flow resistance at very low flow rates and thus such designs are subject to leakage during rest which requires an additional passive check valve or active valve.

Reference	**Type**	**Actuation**	**Self-Priming**	**Flow Rate (μl/min)**
13	Check Valve	Piezoelectric	No	8
14	Check Valve	Thermopneumatic	No	34
15	Diffusor	Piezoelectric	No	230
16	Check Valve	Piezoelectric	Not Specified	20
17	Check Valve	Electrostatic	Not Specified	850
18	Check Valve	Piezoelectric	Yes	400

Table 1-1: Various Diaphragm Pumps

It is also possible to use multiple valves or actuators to form a quasi-peristaltic pump. Three such designs are summarized in Table 1-2. While flow rate data is provided for two designs, a lack of complete information with respect to size, frequency of operation, and backpressure vs. flow rate makes it difficult to judge them quantitatively. While peristaltic designs are much less common, they are attractive due to the lack of passive check valves and bi-directional flow. This allows the fluid flow to remain planar which in turn greatly simplifies the integration of such pumps into a fluidic system. While the achieved flow rates are not as high, in the context of a self-contained microsystem, flow rate plays less of a role as there is minimal dead volume and in fact, the suction and pressure head capabilities of the pump become more important. Also, the robustness of the pump, especially with regards to mixed phase fluids is key. Potentially, taking advantage of the flexibility and sealing properties of silicone rubber, a structure well suited to fluidic integration can be made.

Reference	Actuation	Membrane	Self-Priming	Flow Rate
19	Piezoelectric	Glass	No	100
20	Thermopneumatic	Silicon Nitride	No	0
21	Electromagnetic	Silicon	Not Specified	20

Table 1-2: Several Peristaltic Pump Designs

1.3 Thesis Outline

Chapter 2 investigates the structure of silicone rubber, aspects of the formulation that affect its properties, and the performance of various commercial products. A number of processes are outlined for fabricating a variety of structures that can be integrated with conventional silicon micromachining processes.

Chapter 3 considers actuation methods for large displacement silicone membrane actuators. It is concluded that thermopneumatic operation provides a balance of large

forces through large displacements with reasonable power dissipation and speed provided that the heater design is optimized.

Chapter 4 covers the design, fabrication, and testing of micro balloon actuators for delta wing control. Silicone rubber membranes form robust actuators that can be used to interact with the boundary layer near the separation point on the rounded leading edge of a delta wing. This allows small perturbations to create large aerodynamic rolling moments. Such devices are useful for developing highly maneuverable aircraft such as Unmanned Aerial Vehicles.

Chapter 5 details the design of a peristaltic micropump using silicone rubber membrane actuators. Both externally pneumatically controlled and self-contained thermopneumatic devices are covered. Robust, self-priming operation is achieved for both modes of operation.

In Chapter 6, an integrated pumping and valving architecture for a microfluidic system is described. Making improvements to devices developed in Chapter 5, a fairly generic pumping scheme is developed that is well suited for various applications including sample preparation for diagnostic devices.

Finally the thesis is summarized in Chapter 7 and directions for future work are suggested.

References

[1] R. W. Guyton, R. F. Osborn, and S. P. LeMay, "Forebody Vortex Control Aeromechanics," AGARD CP-497, Nov. 1991.

[2] L. A. Darden, and N. M. Komerath, "Forebody Vortex Control at High Incidence Using A Moveable Nose Stagnation Point," AIAA Paper 95-1775, 1995.

[3] N. J. Wood, and L. Roberts, "The Control of Vortical Lift on Delta Wings by Tangential Leading Edge Blowing," AIAA Paper No. 87-0158.

[4] J. K. Chow, *The Transient Roll Moment Response Due to Forebody Tangential Blowing at High Angles of Attack*, Ph.D. Thesis, Stanford University, 1999.

[5] C. Liu, T. Tsao, and Y. C. Tai, "Out of Plane Permalloy Magnetic Actuators for Delta-Wing Control," MEMS 1995, Amsterdam, The Netherlands, pp. 7-12, 1995.

[6] G.-B. Lee, *Control of a Delta-Wing Aircraft by Micromachined Sensors and Actuators*, Ph.D. Thesis, University of California Los Angeles, 1998.

[7] M. A. Burns, B. N. Johnson, S. N. Brahmasandra, K. Handique, J. R. Webster, M. Krishnan, T. S. Sammarco, P. F. Man, D. K. Jones, D. Heldsinger, C. H. Mastrangelo, and D. T. Burke, "An Integrated Nanoliter DNA Analysis Device," Science, Vol. 282, pp. 484-487, October 1998.

[8] R. C. Anderson, G. J. Bogdan, and R. J. Lipshutz, "Miniaturized Genetic Analysis System," Technical Digest, Solid-State Sensor and Actuator Workshop, pp. 258-261, Hilton Head Island, South Carolina, USA, June 1996.

[9] M. Albin, R. Kowallis, E. Picozza, Y. Raysberg, C. Sloan, E. Winn-Deen, T. Woudenberg, and J. Zupfer, "Micromachining and Microgenetics: What Are They and Where Do They Work Together?" Technical Digest, Solid-State Sensor and Actuator Workshop, pp. 253-257, Hilton Head Island, South Carolina, USA, June 1996.

[10] C. Bisson, J. Campbell, R. Cheadle, M. Chomiak, J. Lee, C. Miller, C. Milley, P. Pialis, S. Shaw, W. Weiss, and C. Widrig, "A Microanalytical Device for the Assessment of Coagulation Parameters in Whole Blood," Technical Digest, Solid-State Sensor and Actuator Workshop, pp. 1-6, Hilton Head Island, South Carolina, USA, June 1998.

[11] D. Maillefer, H. van Lintel, G. Rey-Mermet, and R. Hirschi, "A High-Performance Silicon Micropump for an Implantable Drug Delivery System," Proceedings of IEEE Workshop on Micro Electro Mechanical Systems (MEMS '99), pp. 541-546, Orlando, FL, USA, January 1999.

[12] S. C. Terry, J. H. Jerman, and J. B. Angell, "A Gas Chromatographic Air Analyzer Fabricated on a Silicon Wafer," IEEE transactions on Electron Devices, Vol. ED-26, No. 12, pp.1880-1886, 1979.

[13] H. T. G. Van Lintel, F. C. M. Van De Pol, and S. Bouwstra, "A Piezoelectric Micropump Based on Micromachining of Silicon," Sensors and Actuators 15, pp. 153-167, 1988.

[14] F. C. M. Van De Pol, H. T. G. Van Lintel, M. Elwenspoek, and J. H. J. Fluitman, "A Thermopneumatic Micropump Based on Micro-Engineering Techniques," Sensors and Actuators A21-A23, pp. 198-202, 1990.

[15] A. Olsson, P. Enoksson, G. Stemme, and E. Stemme, "A Valve-Less Planar Pump Isotropically Etched in Silicon," Journal of Micromechanical Microengineering 6, pp. 87-91, 1996.

[16] M. Esashi, S. Shoji, and A. Nakano, "Normally Closed Microvalve and Micropump Fabricated on a Silicon Wafer," Sensors and Actuators 20, pp. 163-169, 1989.

[17] R. Zengerle, J. Ulrich, S. Kluge, M. Richter, A. Richter, "A Bidirectional Silicon Micropump," Sensors and Actuators A50, pp. 81-86, 1995.

[18] K.-P. Kämper, J. Döpper, W. Ehrfeld, and S. Oberbeck, "A Self-Filling Low-Cost Membrane Micropump," Proceedings of IEEE Workshop on Micro Electro Mechanical Systems (MEMS '98), pp. 432-437, Heidelberg, Germany, January, 1998.

[19] J. G. Smits, "Piezoelectric Micropump with Three Valves Working Peristaltically," Sensors and Actuators A21-A23, pp. 203-206, 1990.

[20] J. A. Folta, N. F. Raley, and E. W. Hee, "Design, Fabrication and Testing of a Miniature Peristaltic Membrane Pump," Technical Digest, IEEE Solid-State Sensor and Actuator Workshop, pp. 186-189, Hilton Head Island, South Carolina, USA, June 1992.

[21] W. Zhang and C. H. Ahn, "A Bi-Directional Magnetic Micropump on a Silicon Wafer," Technical Digest, Solid-State Sensor and Actuator Workshop, pp. 94-97, Hilton Head Island, South Carolina, USA, June 1996.

Chapter 2

Silicone Rubber as a MEMS Material

2.1 Introduction

Conventional silicon micromachining has been limited to materials typically used in VLSI processing. Given the common fabrication technology, this is a natural consequence. One direction for MEMS research is the exploration of alternative materials to broaden the scope of possible devices. However, new materials must be compatible with the available process technology and at the same time must not pose a contamination hazard for circuit processes which will also be run in the same fabrication facility. Silicone rubber is a well characterized material used in many aspects of modern manufacturing including medical and biological components. With a Young's modulus orders of magnitude smaller than most metals and silicon, it allows the fabrication of extremely flexible structures, especially membranes. The low durometer also serves very well in sealing applications. With a wide variety of products available, it is important to understand the properties of the material and how it can be best integrated into MEMS devices while retaining as much conventional process technology as possible.

2.2 Silicone Fundamentals

2.2.1 Structure

The term silicone encompasses a wide range of technical products with the following common features. They are polymeric, they are made up of silicon atoms bound to each other by oxygen, and they have hydrocarbon radicals directly bonded to the silicon

valences not taken up by oxygen. These features place silicones between organic and inorganic compounds with interesting results. The more precise name for these compounds is polyorganosiloxanes where siloxane refers to an Si–O–Si unit. Polyorganosiloxanes are made up of four structural units, M, D, T, and Q as shown in Figure 2-1 which can be combined in a multitude of ways to form complex polymers. The R groups are typically methyls (denoted as CH_3 or Me) although other groups such as phenyls, hydrides, silanols, and vinyls are used.

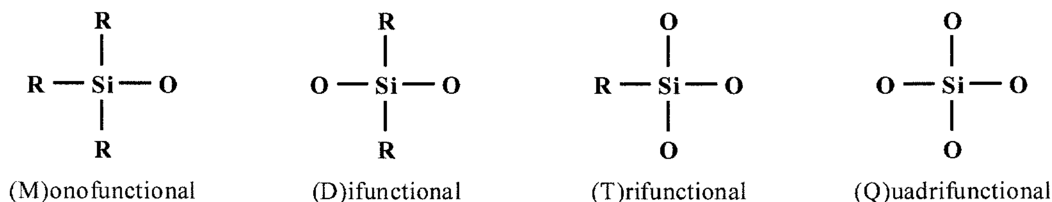

Figure 2-1: Basic structural units of polyorganosiloxanes.

The simplest silicones are polydimethylsiloxanes (PDMS). A linear polydimethylsiloxane can be expressed as MD_nM. Depending on molecular weight, PDMS is a clear fluid with viscosities ranging from 1 to over 1,000,000 cSt. These fluids have many useful applications. However, the conversion by crosslinking from a viscous to elastic state results in a versatile family of silicone rubbers or elastomers.

2.2.2 From PDMS to Silicone Rubber

Although silicone rubber is sometimes referred to as PDMS, it is a technical product made up of three components; polymers (modified PDMS fluids), fillers, and curing agents or catalysts. To facilitate crosslinking, some methyl groups can be replaced with other groups including vinyl, hydride, and silanol. There are four processes that can be used for crosslinking; peroxide, condensation, metal salt, and vinyl addition [1]. These

methods can fall into one or more categories of room (RTV), low (LTV), or high (HTV) temperature vulcanizing systems depending on the catalyst.

Perhaps the most common form of silicone rubber available is the one part condensation or moisture cure sealant. These contain silanol terminated PDMS chains mixed with a silane crosslinker. The silanol on the end is displaced by the silane resulting in end groups very susceptible to hydrolysis. On exposure to moisture, the end groups are hydrolyzed with a concomitant condensation reaction and crosslinking. Since the reaction is dependent on moisture, the cure takes longer for thick sections. Hydrolysis of the silanes along with the condensation cure results in byproducts such as acetic acid or alcohol depending on the chemistry used (Acetoxy, Enoxy, Oxime, Alkoxy, Amine). There is also a shrinkage of the material during cure. These characteristics make one part systems unattractive from the point of view of semiconductor processing. As it turns out, the only process that forms no byproducts during cure is vinyl addition. The crosslinking process is a hydrosilyation reaction between hydride and vinyl groups catalyzed by platinum as shown in Figure 2-2.

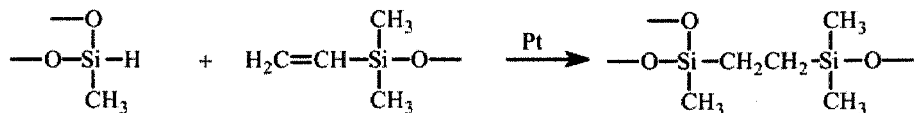

Figure 2-2: Platinum catalyzed addition reaction between vinyl and hydride.

2.2.3 Silicone Rubber Properties

While it is called a rubber, there are some significant differences. Silicone rubber has a very broad operating temperature range, typically from –60°C to 200°C with fluorosilicone based elastomers going above 250°C. Silicone is also porous due to the open structure afforded by the flexibility of the siloxane backbone and free orientation of

the methyl groups. While silicone is very hydrophobic due to the methyl groups, it is permeable to steam and attacked at high temperatures. The permeability to some common gases is 10 to 100 times higher than common rubbers [2] and cured elastomers tend to swell in many organic solvents and oils. Silicone is destroyed by strong acids and bases and hydrofluoric acid directly attacks the siloxane backbone. Very few materials adhere to cured silicone and it serves as a good release agent. In addition, vinyl addition systems exhibit poor adhesion to most materials. Silicone rubbers are naturally transparent. Unfilled vinyl addition elastomers have a refractive index of 1.4. For applications that require higher indices for matching, this can be increased above 1.5 by adding phenyl groups. Filled systems are not used for optical applications. General thermal and electrical properties for cured silicone films are summarized in Table 2-1 for an unfilled and filled system.

	Unfilled (RTV615)	Filled (RTV-1556)
Thermal Conductivity (W/m-°K)	0.19	0.23
Specific Heat (cal/gm-°C)	0.3	NA
Dielectric Strength (kV/mm)	20	18
Dielectric Constant (100 Hz)	2.7	3.0
Volume Resistivity (Ω-cm)	1.2×10^{15}	7×10^{14}

Table 2-1: Selected thermal and electrical properties of two silicone rubbers.

2.3 Vinyl Addition (Platinum Cure) Silicones

As previously shown, a vinyl addition cure system catalyzed with platinum has no byproducts. This results in a cured material with very little shrinkage and no potential for corrosive damage to the substrate or other substances that may come in contact with the elastomer. These systems can also be tailored to cure in specific temperature ranges, and the cure of RTV systems can be accelerated when necessary by low temperature bakes.

As most addition cure systems are packaged in two parts which are mixed prior to use, storage is simplified and performance is fairly consistent over the rated shelf life (and often even longer).

2.3.1 Formulation

Most addition cure systems are split into two parts, A & B. Part A normally contains the base polymer, a vinyl-terminated polydimethylsiloxane fluid, the filler and catalyst. For RTV systems, the catalyst is often a complex of chloroplatinic acid in vinyldisiloxanes. Part B contains the crosslinker a hydride functional polymer, typically a methylhydrosiloxane-dimethylsiloxane copolymer and some balance of vinyl fluid. Along with the length/molecular weight of the PDMS fluid, the crosslinking density can be used to adjust the physical parameters of the final elastomer. In general, long chain lightly crosslinked systems are softer and have higher elongation, while systems with high hydride content and short chains produce material with higher strength and higher durometer [3].

Significant changes to the properties of the elastomer can be made by the addition of fillers. Unfilled silicones have very poor mechanical properties. Fillers are used to control a variety of properties such as conductivity (carbon black), uncured processing characteristics (calcium carbonate, diatomaceous mineral fillers, etc.), and pigmentation (titanium dioxide). Most importantly, fumed and precipitated silicas are commonly used as reinforcing fillers. The reinforcing effect can be both physical and chemical depending on the type and treatment of filler. High surface area silicas work very well as reinforcing fillers due to the similarity in bond angles and interatomic spacing between the silica aggregate and the polymer [4]. Fumed silica typically has higher BET (Brunauer, Emmett

and Teller) surface area (50 to 400 m^2/gm) than precipitated silica (50 to 200 m^2/gm) [cat]. Precipitated silicas have typically been a lower performance filler with improved flowability, potentially due to their lower surface area and tendency to form less effective networks compared to fumed silica aggregates [5].

Untreated silica has silanol (Si–OH) and hydrogen bonded hydroxyl groups on the surface that make the particles hydrophilic [5]. These hydroxyl groups can hydrogen bond to each other so that when the silica is dispersed in a liquid, silica aggregates can bond with each other to form three-dimensional networks. Products with large amounts of untreated filler can exhibit crepe hardening and high viscosity although that can be temporarily reversed by shearing the liquid to break interaggregate hydrogen bonds. This tendency can be reduced by treating the fillers, either with silane agents, typically hexamethyldisilazane (HMDS) or capped PDMS chains [6]. These treatments can also improve the dispersability of the filler in the polymer. In the case of silanization of the filler, not all of the isolated silanol groups are capped; in the specific case of Wacker HDK the density is reduced from roughly 2 to 0.5 - 1 Si–OH/nm^2 [7]. Besides treatments with HMDS or similar compounds, it is also possible to treat fillers with vinyl or allylsilanes to provide reactive groups on the surface that can participate in the addition cure reactions. High tear strength systems potentially result from this technique [3]. In certain cases where high clarity is necessary, silica fillers aren't used. Instead, vinyl Q-resins are used as "molecular sand" typically with some combination of vinyl and methyl termination. These resins can also be used with silica fillers to produce very high strength systems.

The choice and loading of filler can greatly affect application of the silicone rubber. Products designed for liquid injection molding or extrusion are high viscosity, the latter sufficiently so that the extruded material is self supporting during cure, and have high filler loadings and high molecular weight base fluids. The resulting materials exhibit superb strength in comparison to moldmaking products which are typically the strongest family of vinyl addition cure RTV systems. The flowability and relatively low viscosity of mold making formulations is obtained at some expense in mechanical strength.

2.3.2 Surface Adhesion

Most addition cure systems do not bond well to nonporous substrates including glass, metal, and most plastics. A few products are specifically formulated with an adhesive component, but in general, a surface must be primed in order to form a strong bond between it and the cured elastomer film. One exception to this is pure silicon. Under certain conditions, the vinyl may crosslink with hydride groups on the silicon surface resulting in a very strong bond when it works. This effect is more likely after a high temperature bake (around 100°C).

In general, there are two strategies that can be used, chemically bonding to the filler, or bonding to the silicone itself, possibly through the crosslinker. In both cases, silane coupling agents are used. When bonding to the filler, a silane is chosen with several hydrolyzable groups and an organic radical that controls wetting. After hydrolysis, reactive silanol groups are formed which can then condense with other hydroxyl groups on the substrate. Bonds are also formed to the silanol groups on the fillers thus providing the coupling between silicone and substrate. In a similar manner, the radical group can be chosen to provide a certain functionality. In the case of addition

cure silicones, a vinyl or allyl group can be used which can crosslink with the hydride capped silicone chains in the same manner as the reactions that form the silicone rubber. These silanes can either be added to the rubber formulation during manufacture to provide adhesive functionality, or substrates can be pretreated with a primer or in solution and then a standard silicone applied and cured. The hydrolysis and condensation is shown in Figure 2-3.

2.4 Silicone for MEMS

2.4.1 Material Selection

In this work, silicone rubber was used as a mechanical material, specifically a flexible membrane. As such, the necessary properties differ from applications where silicone is used as an o-ring [9], a gasket [10], a structural material [11, 12], or soft lithography/replica molding [13, 14]. What is shared are the methods of application. For most MEMS devices, the desired film thickness ranges from tens to thousands of

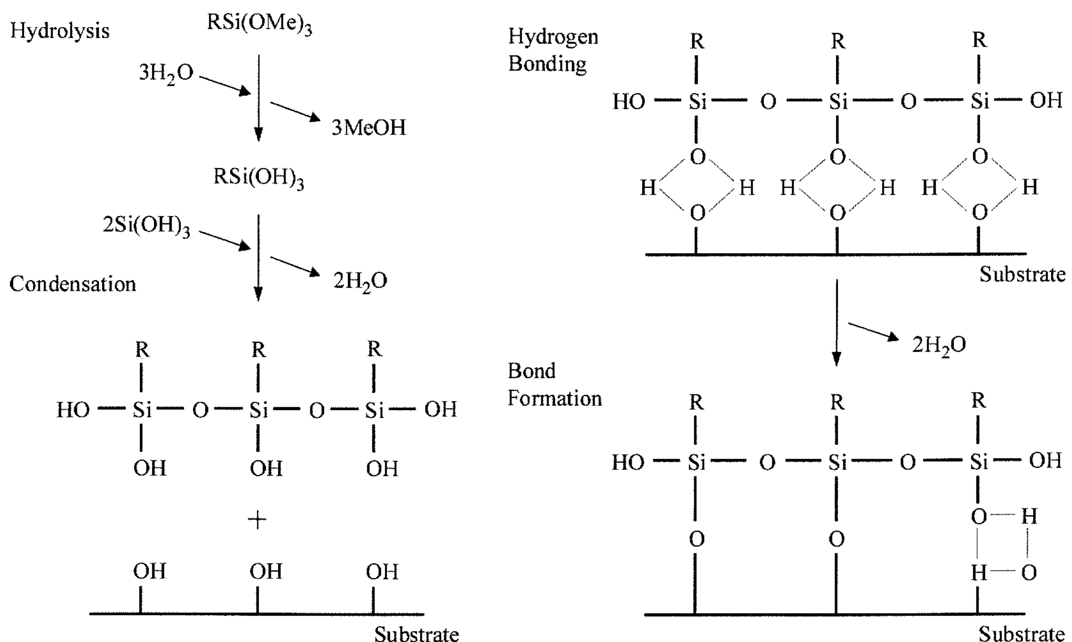

Figure 2-3: Adding functionality to substrate through deposition of silanes [8].

microns. The substrates are usually very flat (usually silicon or glass wafers) and uniform thickness is often important. Application is usually done manually, thus spin coating and casting tend to be the most commonly used methods. Both of these require lower viscosity formulations, below 100,000 cps. For replica casting, highly flowable mixtures are preferable for better image transfer. At the same time, the uncured rubber shouldn't be so thin as to flow off the substrate during cure leading to a practical lower range of viscosity in the hundreds of centipoise.

Important characteristics include tensile strength, tear strength, elongation, and clarity. Most other physical properties are very similar with some differences in thermal parameters, density, and index of refraction depending on filler. Clear silicones are particularly advantageous for many microfluidic applications with some penalty in physical parameters for highly transparent variants. Table x lists a representative sample of commercial silicones that have applications in MEMS.

Since membranes with fairly high deflection are central to this work, MRTV1 was initially chosen for its elongation. At 60,000 cps, it is very difficult to spin coat. Initially, a mixture of part A diluted by the supplier with 5% low viscosity PDMS fluid was used (MRTV1-5%). The approximate viscosity of this formulation is 45,000 cps. This was still high enough to be problematic in spinning smooth films of 200 μm or less. A second mix (MRTV1-8%) was tried with better results. Spin rates from 500 to 1000 rpm provided the best results with thicknesses in the range of 150 to 200 μm. The addition of nonreactive silicone fluid affects the physical properties of the cured film adversely. Also, a slightly lower viscosity was desired, but in greater than 10% concentration, the dilutent fluid tends to bleed out as there is no crosslinking to the polymer. A version of MRTV1 diluted

with 10% reactive fluid was obtained (MRTV1-10RE). In this case, the low viscosity fluid (200cps) is most likely vinyl terminated. The viscosity of this mixture is approximately 30,000 cps. MRTV1 and its diluted forms have the surprising property of strong adhesion to clean silicon and silicon nitride surfaces. Since it is a moldmaking product, it is designed to release well from smooth nonporous surfaces. Other addition cure systems don't exhibit this behavior. The vendor hypothesized that this might be due to residual silane leftover from the filler treatment. However, one would expect such a treatment to also be effective on glass substrates which is not the case. It is possible that there is sufficient catalyst in the mixture that bonding is occuring between vinyl groups in the polymer and hydride groups on the surface of the substrate. This would explain in part why there is no adhesion to glass (primarily hydroxyl groups) surfaces.

For certain high deflection actuators, the MRTV1-10RE formulation proved to have insufficient tear and tensile strength leading to failures after extended operation. At the same time, it was felt that a translucent product would be desirable for alignment reasons. Shin-Etsu KE1300 and Rhodia RTV1556 were both tried. The KE1300 is very strong, but the viscosity is far too high for spin coating. The RTV1556 was similar in performance with a much lower viscosity that allows easy formation of layers less than 100 μm thick. Both of these products exhibit little to no adhesion to silicon, though, as expected. Also, they are both fairly transparent, due to careful control of silica filler size during processing. RTV1556 would seem to be an ideal silicone for many MEMS applications requiring high strength. However, Shin Etsu introduced a low viscosity, high tear strength moldmaking silicone known as X-32-1502. A comparison of this product with others in Table 2-2 shows that it is stronger than every one except Dow Corning Q7-

4850 which is a Liquid Injection Molding (LIM) product unsuitable for spin coating or casting. X-32-1502 uses allylsilane treated precipitated silica filler along with vinyl methyl Q-resins to achieve this combination of properties. The only feature lacking is strong adhesion to unprimed substrates which can be achieved by priming the surface separately, or mixing with Shin Etsu KE1800 which is formulated to bond well to many substrates.

Manufacturer and Product	Tensile Strength (psi)	Tear Strength (psi)	Elongation (%)	Color	Viscosity (cps)
General Electric RTV-615	920	NA	120	Clear	4000
Dow Corning Sylgard 184	NA	NA	NA	Clear	3900
Dow Corning Silastic T-2	800	120	300	Translucent	55,000
Permagile MRTV1	500	125	1,000	White	60,000
Shin Etsu KE1300	850	125	400	Translucent	75,000
Rhodia RTV1556	750	110	450	Translucent	12,000
Shin Etsu X-32-1302	1,000	150	600	Translucent	20,000
Dow Corning Q7-4850	1,375	250	690	Translucent	NA

Table 2-2: Various silicone properties.

2.4.2 Application

Most RTV addition cure products are supplied in two parts to be mixed in a 10:1 ratio. The components should be weighed to ensure the ratio is accurate. Thorough mixing is essential, especially for systems that have a large disparity in viscosity between the two parts as in most mold making formulations. Material should be scraped off the walls of the container and mixed thoroughly to form a homogenous mixture. Most likely, the uncured mixture will be full of air bubbles. Low viscosity mixtures can be left to sit for a couple of minutes, but thick mixtures will have to be vacuum deaired. As the mixed

silicone will expand to several times its original volume under vacuum, it is important to use a large enough container. If vacuum is not available, the mixture can be left in a refrigerator for several hours to settle. When pouring the uncured silicone into a mold or onto a wafer for spin coating, it is important to avoid entrapment of air.

Best results when spin coating are had by performing a low speed (500 rpm) spin to disperse the material across the wafer followed by a second spin at higher rpm to obtain the desired film thickness. If necessary, multiple low speed spins can be performed until the substrate is uniformly covered with a bubble free layer. It is also possible to "pop" air bubbles at this stage without affecting the final film. Very low viscosity silicones such as RTV615 and Sylgard 184 can be dispersed and coated in a single spin.

2.5 Process Development

Unlike most MEMS materials, it is difficult to pattern cured silicone rubber using photolithography and etching. The surface is very inert and photoresist adhesion is very poor, unless a plasma treatment is used. Also, most chemicals that attack silicone also attack photoresist. Thus, different techniques must be used to develop structures.

2.5.1 Bulk Micromachining with Silicone

Practically speaking, a flexible membrane needs to be attached to some sort of rigid frame to define the geometry. Macroscopically, one might make a membrane by bonding or clamping a layer of silicone rubber sheet to a frame, or in a more automated process by compression or injection molding silicone rubber with a frame insert. These methods don't lend themselves to prototype fabrication, especially for microstructures. Bonding a sheet to a substrate requires premanufactured material in the correct thickness, cut to the proper shape, and then controlled adhesive application to the substrate, such as by screen

printing. Molding requires specific tooling for each substrate geometry and film thickness.

Since the primary substrates used in this work are 4" single crystal silicon wafers, spin coating seems to be a natural choice for silicone application. The process has been well developed in the past for photoresist, polyimide, and other polymers although these layers are usually less than 10 μm thick. No special equipment is needed for different size substrates besides the correct chuck and film thicknesses can be easily changed by adjusting viscosity and spin speed. Also, the application introduces very little pressure on the substrate which is important if there are fragile structures that would be crushed by compression or injection molding. The primary drawback to spin coating is the necessity of a fairly flat substrate with no holes. Given then a silicon substrate with a layer of cured silicone rubber, how do we make a freestanding membrane?

Wet etchants for silicon etching such as potassium hydroxide (KOH) and hydrofluoric acid (HF) as a component of HNA attack silicone rubber aggressively. This precludes applying the silicone first and then etching a hole through the wafer to form a membrane unless a one sided etching apparatus is used to minimize chemical exposure. Achieving sufficient clamping force to seal an o-ring without breaking the wafer is difficult and most masking materials that could be applied on top of silicone rubber cannot withstand 24 hours in 60°C KOH or 1 hour in 49% HF. Dry etching, such as RIE with SF_6 plasma is attractive as the chemical attack is primarily on the exposed surface. However, it is impractical to etch through 500 μm of silicon due to the slow etch rate and large undercut. DRIE changes this, due to the fast etch rate (3 – 10 μm/min) and high mask selectivity with either photoresist or silicon dioxide. Unfortunately, the substrate

gets quite hot and is typically cooled from the backside with a helium gas flow. Since the silicone rubber layer would be between the cooling gas and wafer, the cooling efficiency would be very poor due to the very low thermal conductivity of silicone. Conceivably, such an etch could be done in many small steps with frequent removal of the wafer for cooling, but this is impractical.

Instead, suppose that the silicone coating step is left until late in the process. Then it is possible to pre-etch cavities or holes from the backside in a substrate leaving thin rigid membranes, spin coat and cure silicone rubber on the front side and then finish the etch, using either a gentler chemistry or relying on the much lower exposure time to minimize damage to the silicone. Using KOH as an etchant, two similar approaches are described as shown in Figure 2-4. In the first case, 1.8 to 2.0 μm of thermally grown silicon dioxide are grown on both sides of the wafer. Photoresist is spun on the backside and etch windows are patterned. Buffered hydrofluoric acid (BHF) is used to etch the windows after which the wafer is etched in KOH until thin silicon membranes are left. Due to thickness variations in the wafer and etching nonuniformity in the reflux unit, the nominal membrane thickness is usually 10 to 20 μm to ensure that the wafer isn't etched all the way through. Then, in the case of MRTV1 (5%, 8%, or 10RE), the oxide layer on the front side is stripped to provide a clean silicon surface for strong adhesion. The

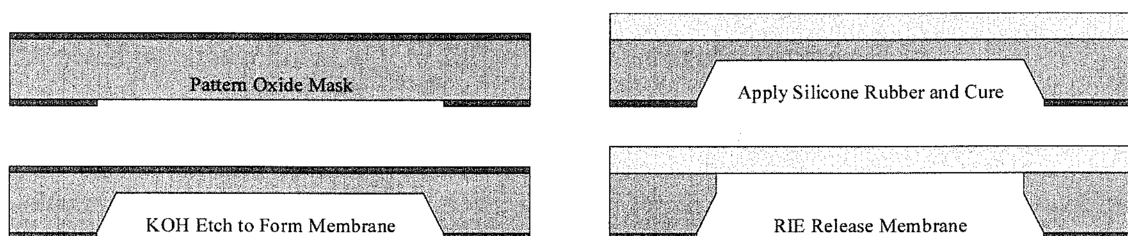

Figure 2-4: Using KOH etching and RIE to create free standing rectangular silicone rubber membranes.

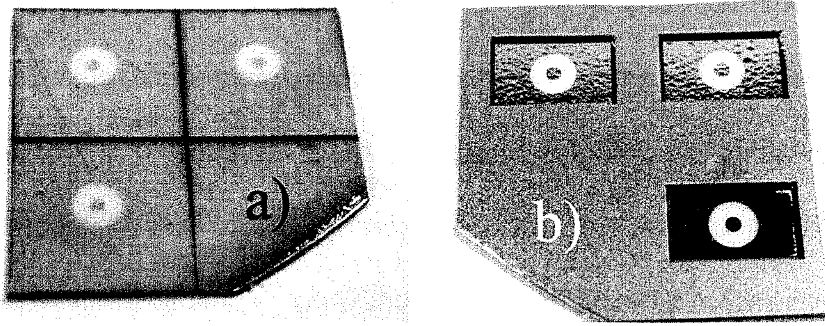

Figure 2-5: (a) Circular MRTV1 silicone rubber membranes with rigid boss in center. (b) Backside of dies showing thin silicon membrane formed by KOH and RIE definition of membrane boundary and boss structures.

silicone is spin coated on the wafer and cured. Afterwards, the remaining silicon is removed using RIE with SF_6/O_2 or potentially a short etch in TMAH. The same process can be done using LPCVD silicon nitride as the membrane material. No oxide is required in this case as the nitride serves as the mask and mechanical material. In this case, the silicon is etched until only a silicon nitride membrane is left. After spin coating and curing the silicone, the nitride is removed by plasma etching with SF_6/O_2 or CF_4/O_2. The exposed silicon sidewalls cause loading and the edges of the nitride membrane tend to etch very slowly exposing the central portion of the underside of the silicone membrane to the reactive species. This exposure and the limitations on geometry caused by anisotropic etching (mainly rectangular structures) are drawbacks to this method. The same approach can be used with combinations of wet and dry etching as shown Figure 2-5. Here, anisotropic etching with KOH is used to define a thin silicon membrane, followed by conventional RIE to define a non rectangular geometry.

In the case of substrates other than silicon, there are etchants that exhibit high selectivity with silicone, in particular ferric chloride ($FeCl_3$) which etches a variety of metals including copper based alloys very quickly. A number of materials are effective

masks including photoresist and various tapes such as vinyl electrical tape (Scotch Super 33+) and dicing tape (Nitto brand). Etch rates up to 20 μm/min can be easily obtained in copper or brass. With proper surface treatment, good adhesion can be had between most silicones and copper. Due to the isotropic nature of the etchant, arbitrary geometry structures can be made as long as the feature size is on the same order or larger than the thickness of material etched.

2.5.2 Surface Micromachining with Silicone

Using the simple method described above, the resulting membrane shape is determined by the geometry of the through hole in the substrate. There are times when it would be preferable to independently define the geometry of the membrane and the frame. This requires a sacrificial layer. Traditional MEMS sacrificial layers have primarily been some form of silicon dioxide or polysilicon. Silicon dioxide is primarily removed with Hydrofluoric acid whereas polysilicon is etched with TMAH [15], HNA, XeF_2 [16], and BrF_3 [17]. Plasma and RIE processes exhibit poor undercutting characteristics and are not commonly used. All of the etchants listed with the exception of TMAH attack silicone rubber. Also, given the porous nature of silicone rubber, it is preferable to use an etchant that doesn't attack the substrate or other materials used in a device.

Photoresist, while unsuitable for processes involving high temperature depositions such as PECVD or LPCVD nitride, is an excellent sacrificial material for structures based on polymers such as Parylene [18, 19], and silicone rubber [11]. It also serves as an excellent etch stop for RIE or DRIE processes to prevent damage to the silicone layer and contamination of the etching chamber from silicone rubber etch byproducts. Photoresist is not normally used as a membrane material and cracks, but this does not affect the final

performance of the released structure. As long as the silicone layer is defined and cured while the substrate is rigid, any changes in the sacrificial layer will only be temporarily transferred to the membrane.

With the addition of photoresist, nonuniformity in the etching of the supporting silicon nitride or silicon membrane during release is no longer a problem. Several microns of photoresist is more than sufficient for most applications. Most importantly, the final membrane geometry is completely independent of the through hole as demonstrated in Figure 2-6. This structure which is described in more detail in Section 6.3.1 has a circular membrane formed over a meandering silicon beam. Starting with an oxidized silicon wafer (<100> although orientation is unimportant since DRIE is being used), 6 μm of AZ4400 photoresist is applied and patterned on the backside. The openings are transferred into the 5000 Å oxide layer using BHF while the front side oxide is stripped at the same time. The backside is etched in DRIE until membranes 20 to 40 μm thick are left. The remaining photoresist layer is removed in ACSI photoresist stripper. A 4 μm layer of AZ4400 is patterned on the front side to form the sacrificial layer. An O_2 plasma descum is performed to clean the surface along with an HF dip to

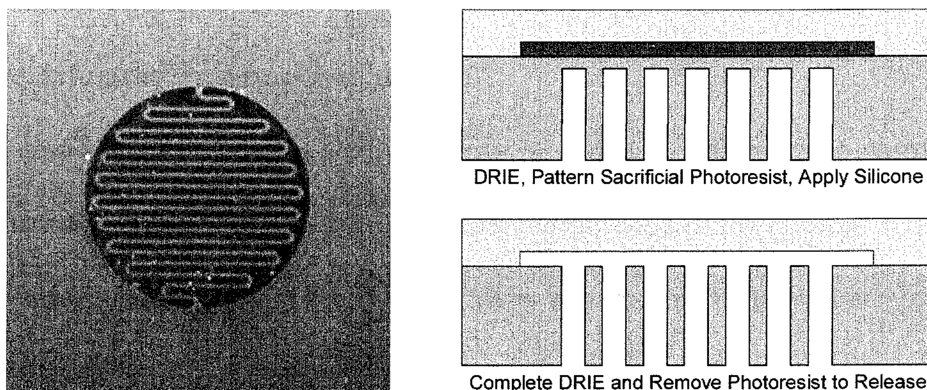

Figure 2-6: Circular (clear) silicone rubber membrane formed over DRIE defined silicon meandering beam (100 μm wide) using photoresist sacrificial layer.

remove any trace of HMDS adhesion promoter. At this point, the surface is primed if necessary and then the silicone rubber is spin coated and cured. After curing, the remaining silicon membranes are etched in the DRIE using the 5000 Å oxide layer as a mask. The resulting structure is a composite silicone rubber/photoresist membrane. The photoresist is easily removed with acetone at room temperature followed by an isopropanol and DI water rinse.

2.5.3 Simple Molding

For structures that have large amounts of topography, spin coating will not always planarize the surface. It is possible to cast silicone rubber on top and let gravity level the surface, but precise thickness control is impractical. In these situations, some form of molding is more suited to the task. One particular example is a membrane that is designed to be clamped to another structure to form a sandwich with fluidic channels in between. Most silicone rubber formulations have sufficiently low durometer that excessive clamping force will extrude the rubber into the channels. A desirable structure might be a rubber surface that is level with a surrounding frame. This way, the clamping force is transferred to the frame rather than the silicone, and minimal extrusion of the rubber occurs. Another possibility is the incorporation of rigid pillars in the membrane that serve as posts to define the compression of the film.

By using a squeegee process in a cavity, a structure with a frame surrounding a silicone membrane can be fabricated. However, the adhesion of the uncured rubber to the squeegee blade combined with the high viscosity and wetting of the rubber results in a concave membrane [20]. A flatter membrane would be better made by molding the cavity structure against a rigid plate. In this case, the excess rubber would need a path to flow

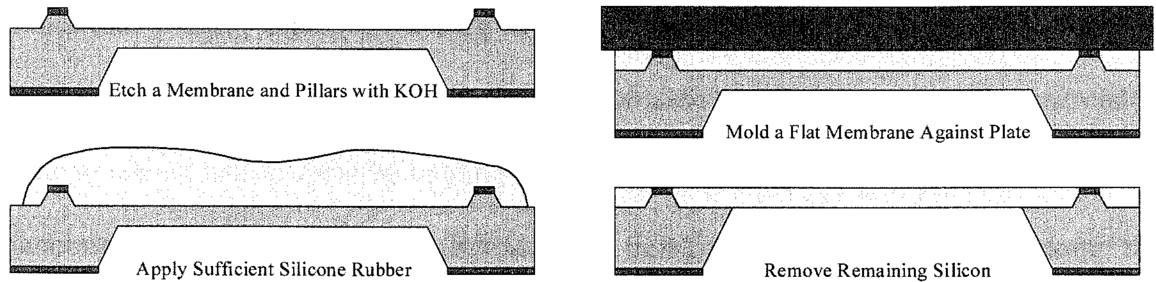

Figure 2-7: Process flow for a membrane with integrated pillars to control membrane crush when clamping to a fluidic structure.

out and this is in part why such high pressures are required for compression and injection molding along with proper filling of the mold. However, another approach can be used. A silicon substrate is covered with small pillars by patterning squares in a mask layer (either silicon dioxide or nitride) and etching the front surface in KOH or TMAH. A rectangular mask pattern results in truncated pyramids with some amount of corner rounding. Then a thick layer of silicone rubber is cast on the surface while ensuring that all the bubbles are removed. The wafer is compressed against a flat surface and allowed to cure. The pillars control the thickness of the resulting silicone layer and in compression, prevent the rubber from extruding into the fluidic part clamped to the membrane. A process flow is shown in Figure 2-7.

2.5.4 Replica Casting

Casting or "soft lithography" has become a popular method of rapidly prototyping fluidic structures [13, 14]. In general, silicone rubber is cast on a form, typically patterned photoresist on silicon. After the silicone rubber is cured, the film is removed from the pattern. A mold release is often used to prevent adhesion to the silicon and photoresist. Channels and chambers or membranes can be easily formed using this technique. As in injection molding, the mold is the inverse of the desired structure. However, there are

times that is more expedient to form the desired pattern in the silicon or glass mold. In this case a reverse pattern can be made and then used for further casting. Commercially, this process would be done by making multiple generations of nickel electroforms. In the laboratory, it can be easily done by casting a first generation silicone part, treating the surface with a mold release, and then casting another generation from that part. This process can be repeated ad infinium with the caveat that there is a very small amount of shrinkage each time, even more so if an elevated temperature cure is used against a low TCE mold like silicon.

For deep and high aspect ratio structures, it is often better to etch the actual structures in the substrate. It is often easier to remove material in a specific shape than add it. With very complex masking, it is possible to make most geometries in a layer of photoresist, but one is limited to 100 μm or so in thickness. LIGA can be used with the limitation of sharp, high aspect ratio features. A combination of etching techniques including precision machining when necessary on a silicon substrate offers the most flexibility. DRIE can be used for high aspect ratio structures such as microchannels, standard RIE can be used to pattern transfer 3-D photoresist structures imaged with grayscale masks into silicon, and wet etching with KOH or TMAH can be used for reservoirs.

A silicone replica made from a silicon master using DRIE and KOH is shown in Figure 2-8. The curved chambers were defined by an initial KOH etch followed by HNA to round the edges while the channels and large reservoirs were defined in two levels with DRIE. GE RTV615 was cast on the silicon master, cured at 80°C for two hours and then removed. The silicone copy, a male part, was then coated with a layer of plasma

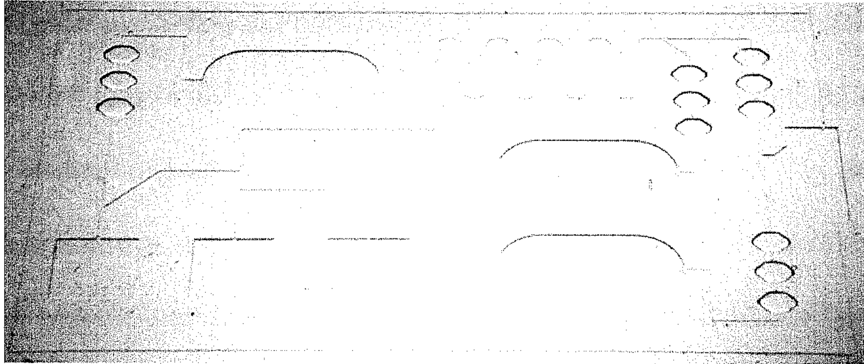

Figure 2-8: Silicone rubber (RTV615) replica made by casting. This is a second generation part, made by casting on a first generation silicone rubber mold made from the original silicon master. The large square and oval reservoirs were defined by DRIE along with the channels, while the smaller groups of three hexagonal pits were defined by KOH followed by HNA.

Teflon using CHF_3 to act as a mold release. A second layer of GE RTV615 was then cast on the silicone rubber part and cured in a similar manner forming an exact replica except for being about 0.2% smaller in each dimension (0.1% for each generation). The channels are the smallest features measuring 200 µm wide and 100 µm deep.

When photoresist is used to define the features of the mold, rather than peeling the silicone rubber off after cure, the photoresist can be dissolved out with acetone. Large structures can be easily freed due to the rapid dissolution rate [21] although stiction between the freed silicone and substrate can be a serious problem. Figure 2-9 shows a simple structure formed by spin coating RTV615 over a 20 µm thick layer of patterned

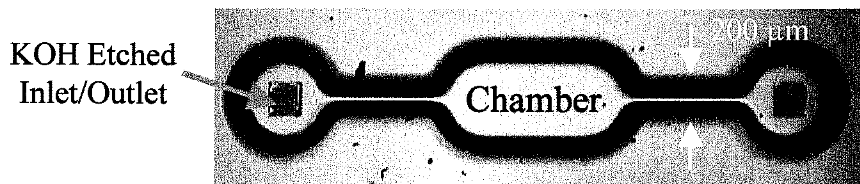

Figure 2-9: Small channel and chamber formed by spinning silicone rubber over a photoresist pattern and later removing the photoresist with acetone. The small square holes are 100 x 100 µm openings from the backside formed by KOH etching to a nitride membrane etch stop which is later removed with SF_6 plasma.

AZ4620 and then dissolving the photoresist out with acetone. Holes are etched through the silicon wafer to provide inlet and outlet ports for the channel structure and are also used for the acetone release.

2.5.5 Lithography with UV Cure Silicones

While traditional photoresist patterning and etching processes aren't practical, it is still possible to perform conventional lithography by using a UV cure silicone formulation. These are usually one part systems that are cured on exposure to UV with some products [22] also having condensation cure functionality. The cure of some formulations is inhibited by oxygen which can be solved by using a nitrogen or argon blanket or covering the uncured film with Mylar [23]. After UV exposure, the uncured material can be removed by rinsing in Xylene.

2.6 Load-Deflection Testing

Mold making silicones which have mechanical properties most suited to high strength membranes (for RTV products) are not typically characterized as mechanical materials except for tensile and tear strength. By performing load deflection testing on membranes, we can extract values for residual stress and Young's modulus.

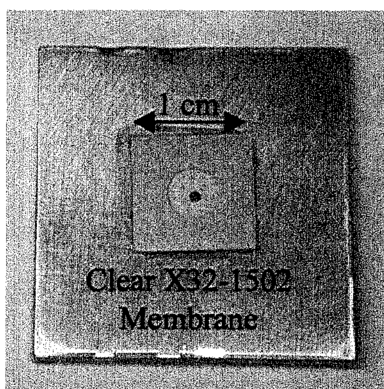

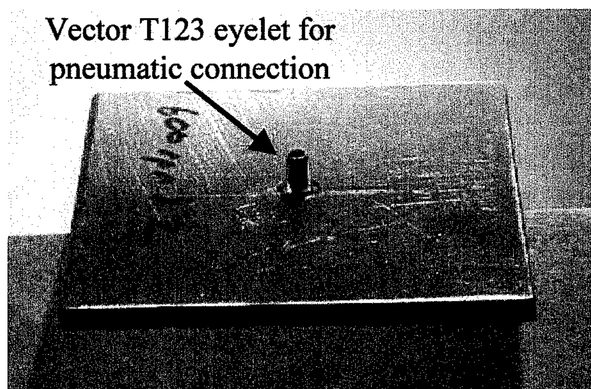

Figure 2-10: Circular membranes for testing the properties of Shin Etsu X32-1502. A small eyelet is used for connecting pneumatic tubing to the samples.

2.6.1 Experimental Apparatus and Samples

Using the process and parameters described in detail in Section 4.5.3, circular membranes were fabricated and mounted to aluminum plates (Figure 2-10) for testing the mechanical properties of X32-1502. The use of an isotropic etchant and copper substrates allowed the easy fabrication of circular membranes compared to the rectangular silicon structures normally used [24]. Two different membrane diameters and nominal thicknesses of silicone were used. A Vector T123 eyelet, 0.054" OD on the back of the plate was connected to a pressure source through Dow Corning Silastic silicone rubber tubing of 0.040" ID. The load-deflection setup is shown in Figure 2-11. The pressure applied to the sample was measured with an Omega PCL100-30 (resolution 0.01 psi). The sample was mounted on the X-Y stage of a microscope. A 25X, 0.31 NA objective was used to focus

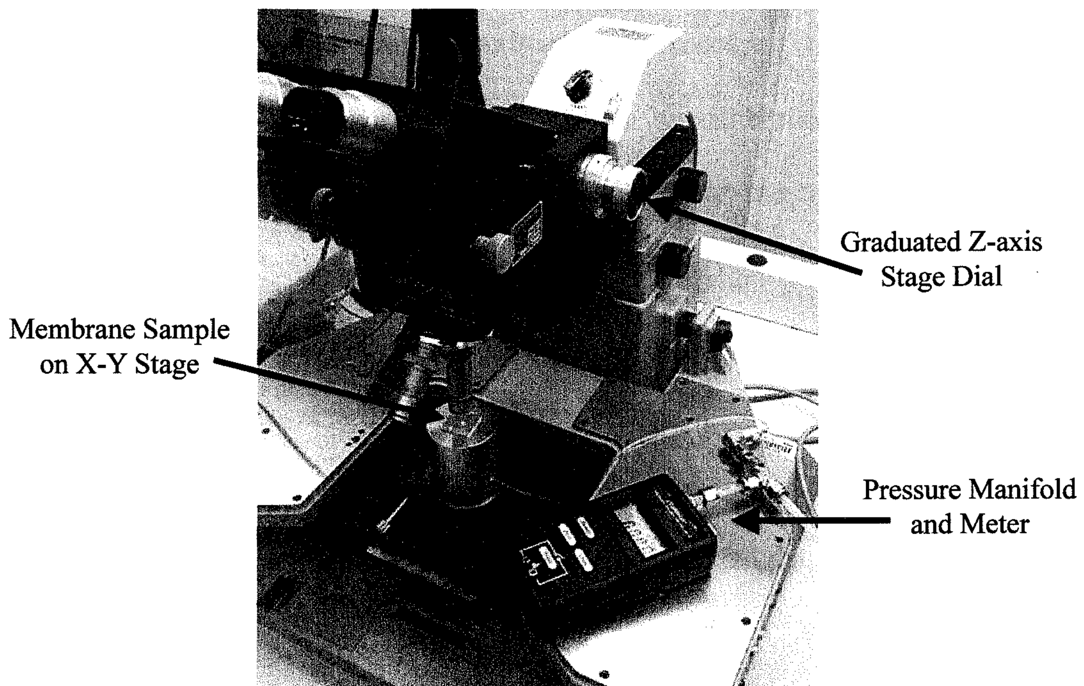

Figure 2-11: The microscope (Bausch & Lomb MicroZoom™) and stage used to measure vertical deflection of the membrane vs. pressure. A high power objective is used to minimize depth of field to obtain accurate focus on membrane surface.

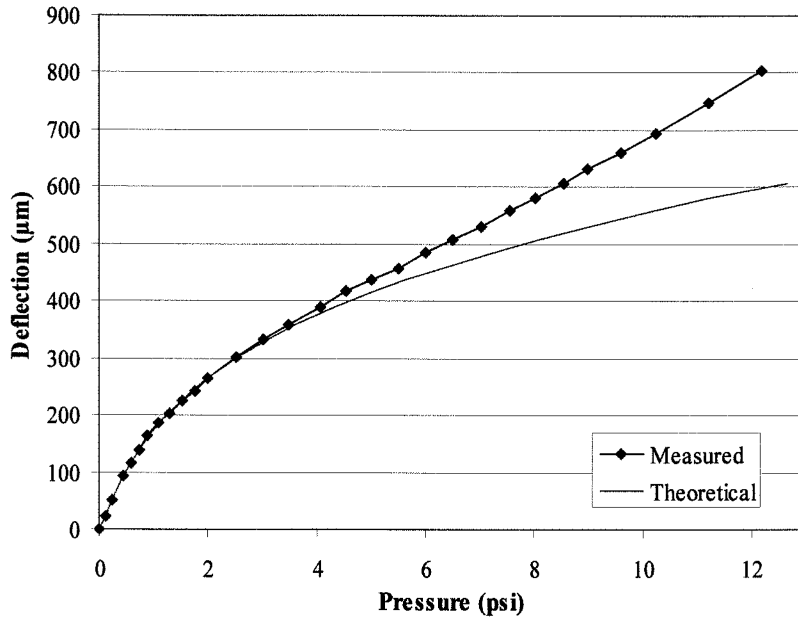

Figure 2-12: Pressure vs. deflection for sample #4, a 178 µm thick, 2.13mm diameter circular membrane. A theoretical fit is also shown that was used to determine the Young's modulus and residual stress.

on the center of membrane. Deflection was measured by refocusing on the membrane and noting the change on the graduated Z-axis of the microscope. The conversion from stage Z-axis translation to actual deflection was done by calibrating the dial with several samples of precise height (as measured with a digital indicator accurate to 1 µm). Repeatability of the deflection measurements is within 5 µm including both mechanical play in the stage and errors in focusing on the surface. Depending on the size and thickness of membrane, pressures up to 15 psi were used.

2.6.2 Results and Analysis

The following equation [25] was used to fit the experimental data

$$P = \frac{C_1 t}{r^2}\sigma d + \frac{C_2 t}{r^4}\frac{E}{1-\nu}d^3 \tag{2.1}$$

where P is the applied pressure, C_1 and C_2 are geometry dependant constants, ν is Poisson's Ratio, E is Young's modulus, σ is the residual stress, r is the radius of the membrane, and d is the deflection in the center. The values for E and σ are summarized in Table 2-3. A value of 0.48 [26] was used for Poisson's ratio.

Sample	Radius (μm)	Thickness (μm)	E (MPa)	σ (kPa)
1	2080	277	0.41	32.3
3	2070	185	0.53	28.4
4	1065	178	0.43	48.4

Table 2-3: Sample dimensions and calculated values for E and σ.

Since the Young's modulus is derived from the cubic portion of the fit, it is important to window the data correctly as the deflection deviates from at higher deflections. Figure x shows the data vs. the theoretical fit for sample #4. Agreement is very good at low deflections which is the regime that this model will be used for. As can be seen from Table 2-3, the Young's modulus of X32-1502 silicone is on the order of 0.5 MPa which is approximately 5-6 orders of magnitude smaller than that of traditional silicon processing materials. This confirms that silicone rubber is a very flexible material.

The behavior of membrane under uniform pressure load has been studied by several authors [24, 25, 27]. It is generally accepted that the deflection of a membrane has two regimes. For a membrane with clamped boundaries, when the deflection is much smaller than the thickness of the membrane, the applied pressure is proportional to the deflection. This linear relationship is called plate behavior. In the small deflection regime, the membrane tends to bend into a quasi-spherical shape in the center but reverses its curvature at a finite distance from the center. When the deflection is much larger than the thickness of the membrane, the applied pressure is a cubic function of the membrane

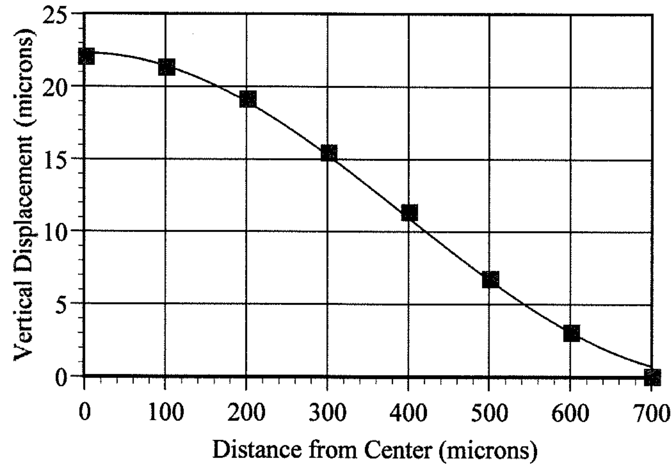

Figure 2-13: Measured profile of an inflated membrane with a theoretical fit assuming a sinusoidal profile as in Equation 2.2.

deflection. This cubic relationship is called membrane behavior. In this large deflection regime, the deflected membrane has the shape of a hemispherical cap.

The shape of the deflected silicone membrane was measured using a Wyko NT2000 and is shown in Figure 2-13. Empirically it was found that a sinusoidal fit was better as shown. The actual fit used takes the form of:

$$z(x) = \frac{d}{2}\left(1 + \cos\left(\frac{\pi x}{r}\right)\right) \tag{2.2}$$

where d is the deflection in the center of the membrane and x is the distance from the center of the membrane. The radius of the membrane and deflection at the center were left as parameters to be fit and came out to 800 μm and 22.2 μm respectively vs. the actual measured values of 700 μm and 22 μm. While this is not an exact fit, it is useful for approximating volume changes for small deflections and for designing chambers for pumping and valving structures.

2.7 Conclusion

The integration of silicone rubber into silicon based MEMS processes has been investigated. Silicone rubber is a very versatile material with a number of desirable characteristics, not the least of which is its great flexibility which makes it an ideal membrane material for many applications. Desirable characteristics for process integration have been identified along with several commercial products well suited for MEMS. Several processes that are compatible with standard MEMS materials and processes have been described along with several devices. Using these techniques, several different actuators will be described in the following chapters.

References

[1] B. Arkles, "Look What You Can Make Out of Silicones," Chemtech, Vol. 13, pp. 542-555, 1983.

[2] W. Noll, *Chemistry and Technology of Silicones*, Academic Press, New York, 1968.

[3] Gelest Inc., *Reactive Silicones: Forging New Polymer Links*, Catalog, 1999.

[4] E. G. Rochow, *Silicon and Silicones*, Springer-Verlag, Germany, 1987.

[5] D. G. Miller, W. F. Moll, V. W. Taylor, "Rheology Control of High-Solids Coatings," Modern Paint and Coatings, April 1983. http://www.cabot-corp.com

[6] B. E. Wolf, "Comparing Liquid and High Consistency Silicone Rubber Elastomers: Which Is Right for You?," Medical Plastics and Biomaterials, July 1997. http://www.devicelink.com/mpb/archive/97/07/003.html

[7] Wacker HDK® fumed silica catalog. http://www.wacker.com

[8] B. Arkles, "Tailoring Surfaces with Silane," Chemtech, Vol. 7, pp. 766-778, 1977.

[9] T.J. Yao, S.W. Lee, W. Fang, and Y.C. Tai, "A Micromachined Rubber O-ring Microfluidic Coupler," Proceedings of IEEE International Conference on Micro Electro Mechanical Systems (MEMS '00), pp. 624-627, Miyazaki, Japan, January, 2000.

[10] D. Jaeggi, B. L. Gray, N. J. Mourlas, B. P. van Drieenhuizen, K. R. Williams, N. I. Maluf, and G. T. A. Kovacs, "Novel Interconnection Technologies for Integrated Microfluidic Systems," Technical Digest, Solid-State Sensors and Actuators Workshop, pp. 112-115, Hilton Head Island, South Carolina, USA, June 1998.

[11] L. Bousse, E. Dijkstra, and O. Guenat, "High-Density Arrays of Valves and Interconnects for Liquid Switching," Technical Digest, Solid-State Sensor and Actuator Workshop, pp. 272-275, Hilton Head Island, South Carolina, USA, June 1996.

[12] C. Vieider, O. Ohman, and H. Elderstig, "A Pneumatically Actuated Microvalve with a Silicone Rubber Membrane for Integration with Fluid Handling Systems," Technical Digest, International Conference on Solid-State Sensors and Actuators (Transducers '95), Vol. 2, pp. 284-286, Stockholm, Sweden, June 1995.

[13] H. Chou, C. Spence, A. Fu, A. Scherer, and S. Quake, "Disposable Microdevices for DNA Analysis and Cell Sorting," Technical Digest, Solid-State Sensor and Actuator Workshop, pp. 11-14, Hilton Head Island, South Carolina, USA, June 1998.

[14] Y. Xia and G. M. Whitesides, "Soft Lithography," Annual Review Of Materials Science, Vol. 28, pp. 153-184, 1998.

[15] O. Tabata, H. Funabashi, K. Shimaoka, R. Asahi, and S. Sugiyama, "Surface Micromachining Using Polysilicon Sacrificial Layer," Proceedings of International Symposium on Micromachine and Human Science, pp.163-172, Nagoya, Japan, October 1991.

[16] P. B. Chu, J. T. Chen, R. Yeh, G. Lin, J. C. P. Huang, B. A. Warneke, and K. S. J. Pister, "Controlled Pulsed Etching with Xenon Difluoride," Technical Digest, International Conference on Solid-State Sensors and Actuators (Transducers'97), Vol. 1, pp. 665-668, Chicago, USA, June 1997.

[17] X. Q. Wang, X. Yang, K. Walsh, and Y.C. Tai, "Gas Phase Silicon Etching with Bromine Trifluoride," Technical Digest, International Conference on Solid-State Sensors and Actuators (Transducers'97), Vol. 2, pp. 1046-1415, Chicago, USA, June 1997.

[18] P. Man, D. Jones, and C. Mastrangelo, "Microfluidic Plastic Capillaries on Silicon Substrates: A New Inexpensive Technology for Bio Analysis Chips," Proceedings of IEEE Workshop on Micro Electro Mechanical Systems Workshop (MEMS '97), pp. 311-316, Nagoya, Japan, January 1997.

[19] X.Q. Wang, A. Desai, and Y.C. Tai, "Polymer-Based Electrospray Chips for Mass Spectroscopy," Proceedings of IEEE International Conference on Micro Electro Mechanical Systems (MEMS '99), pp. 523-528, Florida, USA, January, 1999.

[20] X. Yang, *Micromachined Silicone Rubber Membrane Valves for Fluidic Applications*, Ph.D. Thesis, California Institute of Technology, 1998.

[21] K. Walsh, J. Norville, and Y. C. Tai, "Photoresist as a Sacrificial Layer by Dissoluion in Acetone," Proceedings of IEEE International Conference on Micro Electro Mechanical Sytems (MEMS'01), pp. 114-117, Interlaken, Switzerland, January, 2001.

[22] Loctite UV silicone data sheets.

[23] J. C. Lötters, *A Highly Symmetrical Capacitive Triaxial Accelerometer*, Ph.D. Thesis, University of Twente, 1997.

[24] O. Tabata, K. Kawahata, S. Sugiyama, and I. Igarashi, "Mechanical Property Measurements of Thin Films Using Load-Deflection of Composite Rectangular Membranes," Sensors and Actuators, 20, pp. 135-141, 1989.

[25] J. Y. Pan, P. Lin, F. Maseeh, and S. D. Senturia, "Verification of FEM Analysis of Load-Deflection Methods for Meausuring Mechanical Properties of Thin Films,"

Technical Digest, Solid State Sensor and Actuator Workshop (Hilton Head '90), pp. 70-73, Hilton Head Island, South Carolina, USA, June 1990.

[26] G. P. O'Hara, "Mechanical Properties of Silicone Rubber in a Closed Volume," Large Caliber Weapon Systems Lab, Army Armament Resource Development Center, Watervliet, NY, 1983.

[27] M. Sheplak, J. Dugundji, "Large Deflections of Clamped Circular Plates Under Initial Tension and Transitions to Membrane Behavior," Journal of Applied Mechanics, 65, pp. 107-115, 1998.

Chapter 3

Actuation Methods

3.1 Introduction

Since we can use silicone rubber to generate very flexible membranes, it is necessary to find a complementary form of actuation that can generate large forces through long displacements. While pneumatic operation was used for material characterization, devices often require self-contained or miniature methods of actuation. Several different forms of actuation are evaluated.

3.2 Actuation Mechanisms

Clearly, the results of Section 2.5.x demonstrate that pneumatic operation is ideal for actuation of silicone membranes. However, the following sections consider the feasibility of several other actuation methods. For some examples, a membrane made of Shin Etsu X32-1502 1.4 mm in diameter and 150 μm thick being deflected a total of 50 μm vertically from its rest position is considered. The calculated pressure required for various deflections is shown in Table 3-1.

Displacement (μm)	0	10	20	30	40	50
Pressure (Pa)	0	447	903	1377	1877	2412

Table 3-1: Theoretical displacement vs. pressure for silicone rubber membrane.

3.2.1 Electrostatic

The force between the plates of a parallel plate capacitor can be expressed as follows

$$F_{electrostatic} = \frac{d}{dx}\left(\frac{1}{2}C(x)V^2\right) = \frac{\varepsilon_0 A V^2}{2(d-x)^2} \tag{3.1}$$

where ε_0 is the permittivity of free space, A the electrode surface area, V the applied voltage, d the nominal electrode separation, and x the displacement from rest. If we make an approximation and assume that the membrane deflects as a flat plate, we can calculate the force vs. deflection and compare to the theoretical pressure vs. deflection curve of our sample membrane. Assuming a 51 μm gap, the voltage required to obtain the necessary force at a given deflection for our silicone membrane is tabulated below.

Displacement (μm)	10	20	30	40	50
V (V)	411	442	370	226	23

Table 3-2: Required voltage for a given membrane deflection.

Clearly, except for small gaps, these voltages are very high and electrostatic actuation is not optimal for structures of this size. Also, electrostatic actuation requires an electrode opposing the membrane which is not always feasible, especially given possible failure of a metal electrode due to the change in surface area under deflection.

3.2.2 Magnetostatic

While a number of different structures could be made, one straightforward one is magnetic plates embedded in the membrane which tend to align themselves to an external field thus generating torques. Such a device has been fabricated [1] and tested. With an external magnetic field of 2.85×10^5 A/m, greater than 200 μm displacement was realized for a 40 μm thick 2 mm square membrane. This membrane is approximately 10 times softer than the hypothetical membrane proposed above and with the resultant loss in surface area, the smaller magnetic plates would generate significantly less torque. In

general, magnetostatic actuation has potential for soft membranes and large external fields.

3.2.3 Electromagnetic

Given a coil with a current flowing through it in a non-uniform magnetic field, the force on the coil can be expressed as [2]

$$F_x = m\frac{\partial B_x}{\partial x} \tag{3.2}$$

where the magnetic moment m = IA, with I the current and A the sum of the areas of the coils. If we use a value of 86.7 Tesla/m [2] for the gradient of magnetic flux density, and assume 5 turn coils that measure 1.0 mm square with a current of 1 A, the resulting force is approximately 216 μN which corresponds to a pressure of 216 Pa. This falls short of the necessary pressure required for our hypothetical membrane, but it is possible with more coils (stacked layers of metallization) and a softer structure (both larger in diameter and thinner) that this form of actuation could work.

3.3 Thermopneumatic Actuation

The volume of a gas or liquid can be changed by heating or cooling it. If a fluid is sealed in a cavity and heated, the volume and/or pressure will increase depending on the flexibility of the cavity. There are three cases to consider, thermal expansion of a gas, thermal expansion of a liquid, and mixed systems. A detailed study of the latter can be found in [3] and only the first two will be considered here.

3.3.1 Thermal Expansion of a Gas

Assuming an ideal gas, we have

$$PV = nRT \tag{3.3}$$

where R is 8314 kPa-ml/mol-°K, P is pressure, V is volume, n is moles of gas and T is temperature. We know that the volume of our cavity will change with pressure due to the flexible membrane. This change in volume can be expressed as [3]:

$$\lambda = \frac{1}{V}\frac{\partial V}{\partial P} \tag{3.4}$$

For our membranes, assuming a sinusoidal profile for small deflections, we can approximate the volume vs. deflection as follows where d is the deflection at the center of the membrane and r is the radius.

$$\Delta V(d,r) = \int_0^r d\pi x\left[1+\cos\left(\frac{\pi x}{r}\right)\right]dx \tag{3.5}$$

The deflection z is a function of pressure, and thus λ can be solved explicitly. If the cavity is filled with gas at a certain pressure and temperature, we can write

$$P = \frac{nRT}{V_i + V_i\lambda(P - P_{ambient})} \text{ where } V_i = \frac{nRT_i}{P_i} \tag{3.6}$$

where V_i, T_i, and P_i are the properties of the gas when the cavity was filled and $P_{ambient}$ is the surrounding pressure when the cavity is heated. Solving 3.6 for P, we obtain the following expression for pressure as a function of temperature taking into account the flexibility of the membrane.

$$P = \frac{\lambda P_{ambient} - 1 + \sqrt{(1-\lambda P_{ambient})^2 + \frac{4\lambda P_i T}{T_i}}}{2\lambda} \tag{3.7}$$

Of interest is the independence of pressure on the type of gas. Air is used in this work due to its convenience for filling.

3.3.2 Thermal Expansion of a Liquid

We can also seal a liquid in the cavity and heat it. The change in pressure for a fixed amount of liquid that undergoes a volume change is

$$\Delta P = E\frac{\Delta V}{V} \tag{3.8}$$

If we heat a liquid, the change in volume can be expressed in terms of β, the thermal coefficient of expansion

$$\beta = \frac{1}{V}\frac{\Delta V}{\Delta T} \tag{3.9}$$

Given a liquid in a sealed cavity that is flexible to some extent, if we heat the liquid the cavity will expand causing a corresponding volume change. The resulting pressure change can then be expressed as the difference of two volume change terms, one an increase due to temperature, and the other a decrease due to the expansion of the cavity.

$$\Delta P = E\left(\beta\Delta T - \frac{\Delta V}{V}\right) \tag{3.10}$$

If we recall the definition of λ from 3.4, we can rewrite this as

$$\frac{\Delta P}{\Delta T} = \frac{E\beta}{1+\lambda E} \tag{3.11}$$

Of interest, if λ is large, the changes in pressure tend to be small. Liquid systems excel at providing large pressures for relatively fixed volumes.

3.3.3 Static Performance

Given the dimensions of our membrane (1.4 mm in diameter, 150 μm thick silicone), we can calculate the volume change vs. deflection assuming that Equation 3.5 holds. As it turns out, the deflection of the membrane comes out of the integral for the following linear relationship

$$\Delta V = \left(\frac{\pi}{2} - \frac{2}{\pi}\right) d r^2 \tag{3.12}$$

Also, considering Equation 2.1, the first term dominates at very small deflections (in this case, when d << r), we can make the following linear simplification

$$\Delta P = \frac{C_1 t}{r^2} \sigma d \tag{3.13}$$

which gives us the following linear relationship between pressure and volume

$$\Delta V = \left(\frac{\pi}{2} - \frac{2}{\pi}\right) \frac{r^4}{C_1 t \sigma} \Delta P \quad \text{so} \quad \Delta V(\mu m) = 1.03 \times 10^4 \Delta P(Pa) \tag{3.14}$$

Consider first the case of an ideal gas (air) as a working fluid. For our structures, the typical cavity size is the diameter of the membrane and the thickness of two 4" silicon wafers, nominally a total of 1.0 mm. For our 700 μm radius membrane, we calculate λ as defined in Equation 3.4 to be 6.69×10^{-6} (1/Pa). Now we can calculate the deflection vs. temperature using Equations 3.4 and 3.7. Figure 3-1 shows that small increases in temperature can result in sizable deflection.

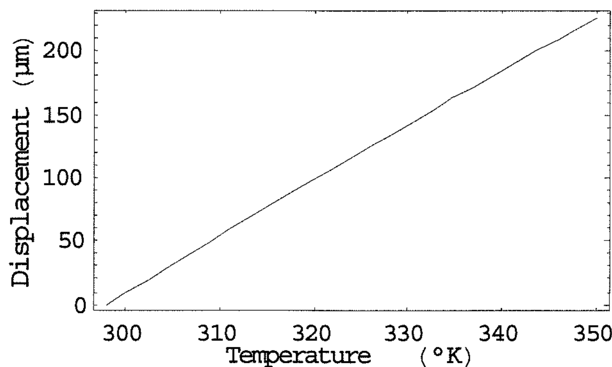

Figure 3-1: Deflection for a 1.4 mm diameter membrane as a function of air temperature inside the cavity (assuming it was filled at 298°K).

We can also consider the case of liquid as a working fluid. A very representative liquid would be water with a bulk modulus (E) of 2.28 GPa and a thermal coefficient of expansion (β) of 2.3×10^{-4}/°C. Since λE >> 1, Equation 3.11 can be simplified and

$$\Delta P = \Delta T \frac{\beta}{\lambda} \tag{3.15}$$

The resulting deflection vs. temperature is shown in Figure 3-2.

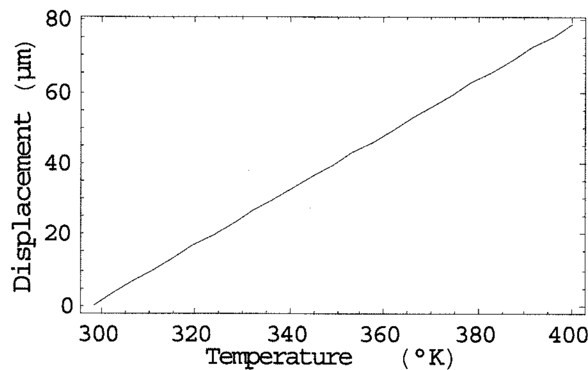

Figure 3-2: Deflection vs. temperature for a water filled cavity.

3.4 Conclusion

Several types of actuation have been analyzed. The most promising seem to be magnetic and thermopneumatic actuation. Since magnetic actuation does not generate a uniform pressure on the membrane, thermopneumatic actuation would seem to be more ideal for pumps and valves. Given the flexibility of silicone rubber membranes, operation with a gas for the working fluid offers greater deflection for a given temperature increase. Also, as air has much lower thermal conductivity than most liquids, it may offer a power advantage.

References

[1] M. Khoo, L. Lu, and C. Liu, "Development of a Magnetic Flexible Membrane Micropump," Late News Supplemental Digest, Solid State Sensor and Actuator Workshop (Hilton Head '00), pp. 3-4, Hilton Head Island, South Carolina, USA, June 2000.

[2] E. M. Purcell, *Electricity and Magnetism*, McGraw-Hill, New York, 1985.

[3] M. J. Zdeblick, *A Planar Process for an Electric-to-Fluidic Valve*, Ph.D. Thesis, Stanford University, 1988.

Chapter 4

Micro Balloons for Aerodynamic Control

4.1 Introduction

At medium angles of attack (AOA or α), the flow over a sharp edge delta wing is characterized by a pair of counter-rotating vortices which separate from the leading edge and reattach on the surface as shown in Figure 4-1. For a sharp edge, separation occurs at the leading edge. The general nature of the vortices stays similar over a wide range of Reynolds numbers, from laminar through turbulent flow [1]. The vortices contribute lift which can be predicted using a leading edge suction analogy [2]. As the size and strength of the vortices increases with angle of attack (until vortex breakdown), the lift contributed by the vortices can be as much as 40% of the total lift [2] at high AOA ($\alpha = 30°$ for a 75° delta wing). This implies that significant rolling torques can be generated by breaking the symmetry of the vortices which could be done by moving the separation points.

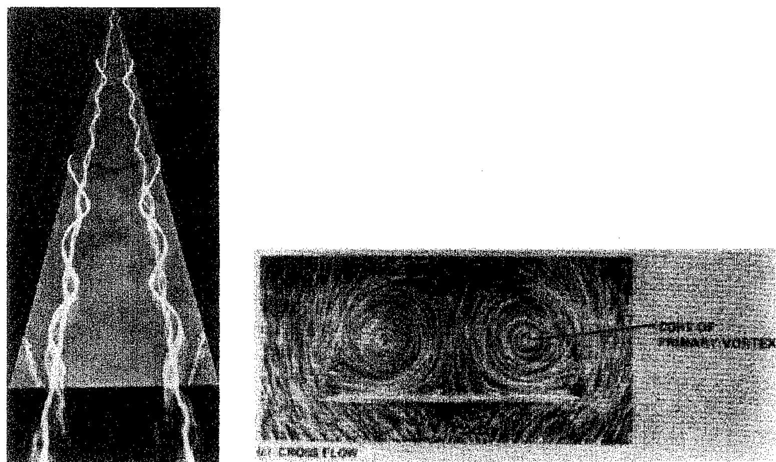

Figure 4-1: Visualization of counter-rotating vortices over a delta-wing [1].

Unfortunately, for a sharp edge, the separation point is defined by the geometry of the sharp leading edge. For a rounded leading edge, the separation point can depend on the Reynolds number, AOA, and local curvature which determines the flow field distribution. Depending on the shape of the leading edge, vortices may not develop until large AOA's and/or Reynolds number. However, this is balanced by the ability to affect the separation point by small perturbations on the leading edge. By interacting with the boundary layer using microactuators, it is possible to control large vortex structures and generate significant aerodynamic torques. This chapter explores the use of silicone rubber micro balloon actuators as vortex control elements for delta wing control.

4.2 Previous Work

To determine the length scale necessary for actuators to interact with the boundary layer before separation, a number of experiments were done with mechanical actuators, a simple metal strip that could be extended a specific distance from a circular leading edge as shown in Figure 4-2. The necessary length scales were found to be on the order of one millimeter. Magnetically actuated surface and bulk micromachined flaps were used for delta wing control surfaces [3]. Because the length scales of the actuators and boundary

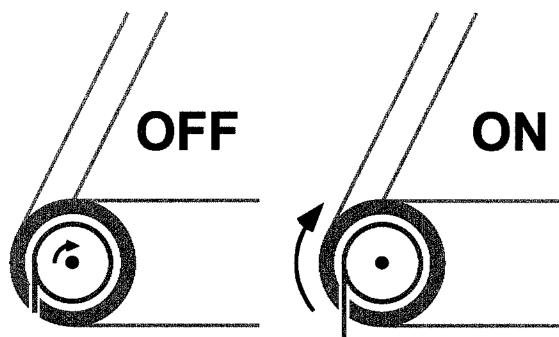

Figure 4-2: A simple mechanical actuator consisting of a metal strip rolled into a tube on the leading edge. By rotating the strip, a certain protrusion from the surface can be obtained.

layer before separation at the leading edge are similar, small surface perturbations can generate large aerodynamic control moments (pitch, yaw, and roll) through fluid amplification. However, the magnetic flap actuators were designed only for wind tunnel testing (<50 m/s) and were not robust enough for flight tests on real aircraft or high speed (>50 m/s) wind tunnel testing as the beams would break. More robust beams would require very large magnetic forces and the resulting structures would still suffer from debris damage during flight. For practical aircraft, requirements for a microactuator control surface then have to include robustness (e.g., resistance to particles), large deflection and load, low power consumption, surface conformability, and small size along the thickness of the wing. Pneumatically driven silicone membranes satisfy the first four requirements, but it can be difficult to design robust membranes that have small dead areas, as the frame can be very large.

4.3 Silicon Substrate Actuators

The desired geometry of the microactuators for wind tunnel testing and flight testing on a scale airfoil model were strips two to three mm wide, and stackable end to end for a total

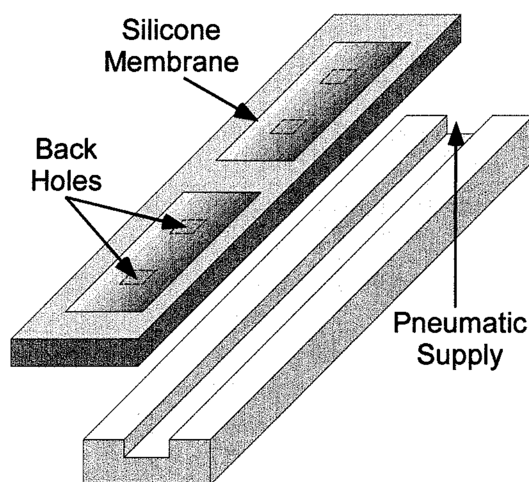

Figure 4-3: Conceptual assembly of actuator strip to backing plate.

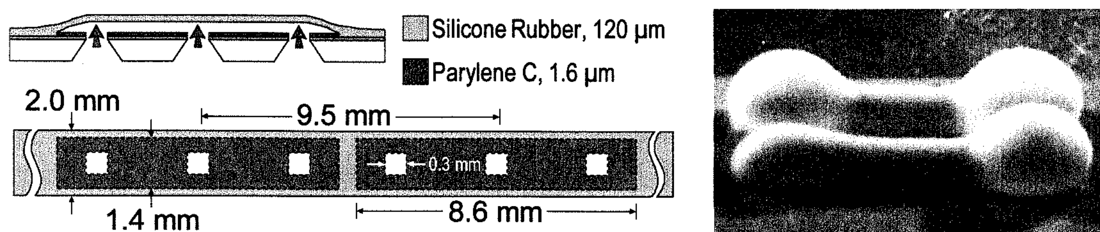

Figure 4-4: First generation actuator design (2 mm) and extreme deformation during inflation (also referred to as the "dogbone" shape).

length as necessary depending on the wing configuration. A vertical deflection on the order of one to two mm was needed for sufficient interaction with the boundary layer. Large deflection can be obtained from silicone rubber membranes operated pneumatically. Micro "balloons" could be made on substrates of silicon using silicone rubber for the balloon material. Strips of actuators would then be attached to a suitable backing strip and pneumatically actuated. It was decided to put the groove for air flow in the backing strip so as to make the silicon wafer less prone to cracking during fabrication and the final actuator strips as robust as possible (Figure 4-3).

4.3.1 Design

To achieve maximum deflection for a given width strip, the frame overhang must be as small as possible. Practically speaking, such a structure fabricated from a silicon wafer would be very fragile with the frame only being 300 µm by 500 µm in some areas. A process using a sacrificial layer to allow the retention of as much silicon as possible except for several pneumatic access holes is necessary. Photoresist was used to define a large membrane over very small through hole openings in a silicon wafer. However, the large unsupported silicone membrane would stick to the substrate after release with acetone. While working with composite Parylene/silicone rubber membranes for thermopneumatic actuators, it was discovered that silicone rubber has very poor adhesion

to Parylene, both during the cure process and afterwards. Thus, a patterned layer of Parylene can be used as a release layer to form large area silicone membranes without the complications associated with etching a sacrificial layer. Using this technology, several generations of actuators were designed.

A first generation of micro balloon actuators was fabricated with dimensions shown in Figure 4-4. These actuators could deflect about 1 mm before undergoing severe deformation at the edges as shown. They also failed fairly often by losing adhesion at the edges, especially at the sharp corners. Initial wind tunnel tests also showed that a larger deflection was desirable, this in part due to the gentle curvature of the inflated balloon vs. the sharp metal strip used prior. The design was revised in three ways (Figure 4-5) to increase reliability, both of the silicone itself and the adhesion to the silicon frame. The width of exposed silicon on either side of the Parylene release layer was increased from 0.3 mm to 0.35 mm to increase the adhesion area. The corners of the release layer were rounded to decrease stress from the boundary conditions, and one inlet hole was removed while the remaining two were moved closer together to equalize the pressure exerted on the membrane during release. A third generation was later fabricated that was 3.4 mm wide to achieve even higher deflection (2 mm).

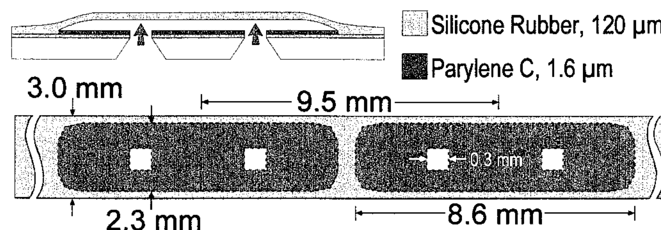

Figure 4-5: Second (3 mm) generation design. Note the rounded edges of the release layer and two instead of three backholes.

4.3.2 Fabrication

The use of the Parylene release layer greatly simplifies the process. The geometry of the silicone membrane is defined by a simple lithography and no harsh chemicals are required to release it. Because the access holes for release and pneumatic operation are independent of the membrane geometry, they can be very small so that the silicon substrate is reasonably robust.

The process along with a completed wafer prior to dicing is shown in Figure 4-6. Starting with a <100> silicon wafer, 0.5 μm of LPCVD silicon nitride is deposited on both sides. The back side is patterned using RIE, and cavities are etched anisotropically using KOH forming 300 μm square free-standing membranes. 1.6 μm of Parylene C is deposited on the front side and patterned using O_2 plasma. Without removing the photoresist on the Parylene, the front side is roughened with SF_6/O_2 plasma. The photoresist is stripped and 100 to 200 μm of MRTV1 silicone rubber is spin-coated on the front side. The first devices made used MRTV1-8% silicone rubber. Because of

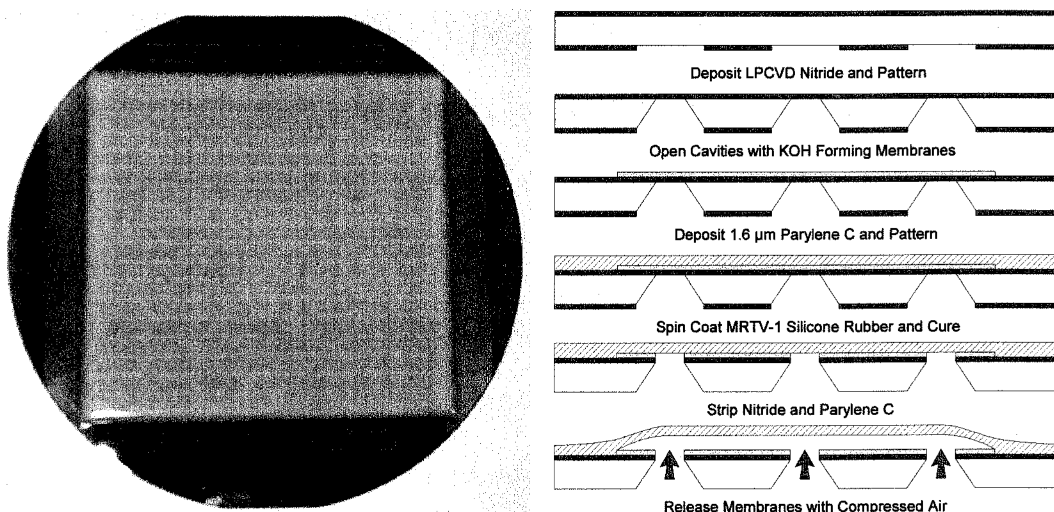

Figure 4-6: Process flow for silicone balloon actuators and a completed wafer prior to dicing. Dicing tape was used to mask the silicone rubber so that reference marks on the wafer could be used for alignment during dicing.

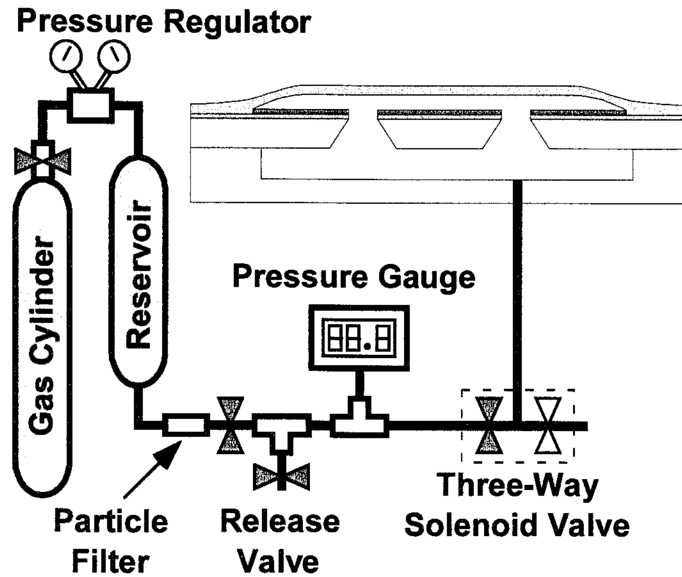

Figure 4-7: Testing apparatus for pressurizing silicone balloon actuators.

reduced strength, a switch was made to MRTV1-10RE. The wafers are cured and the composite nitride/Parylene membranes are removed from the backside with SF_6/O_2 plasma followed by O_2 plasma. Application of pressurized gas to the inlet holes frees the silicone membranes with very high yield. Since lithography has to be done on both sides of the wafers and reasonable alignment accuracy is required, extra membranes were formed during the KOH etch. These terminated on the front side of the wafer as small windows that could be used as alignment squares with the GCA stepper thus eliminating the additional process of putting alignment marks on both sides of the wafer.

4.3.3 Testing Apparatus

Completed actuators were tested after fabrication to determine the pressure vs. deflection relationship using the experimental apparatus in Figure 4-7. It was found that approximately 3 psi of pressure was necessary to free the silicone membranes from the substrate after release, prior to testing. Also, if the membranes were allowed to "stick" to the substrate, a similar pressure was necessary, i.e. there was some hydrogen bonding or

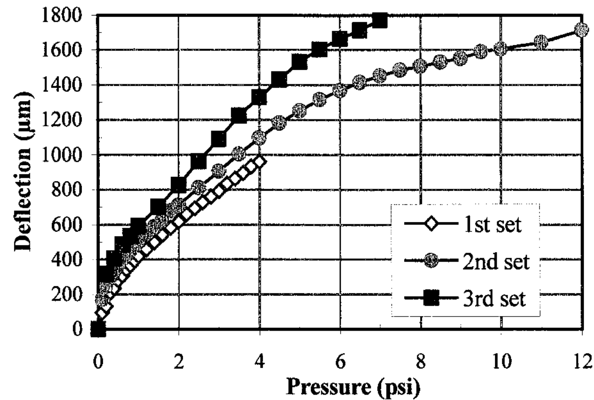

Figure 4-8: Pressure vs. deflection for a 3 mm actuator after various experiments to determine the change in properties with use.

Van der Walls interaction between the silicone and Parylene. For the proposed usage as an aircraft control surface, this is not an issue as the operational pressures are much greater than that required to free the membranes.

4.3.4 Static Testing

Due to the excessive plastic deformation of the first generation of actuators, extensive testing was limited to the second generation (3 mm). Figure 4-8 shows three sets of data for the same actuator taken at different times. The first (and lowest) trend line was taken directly after fabrication. At the low pressures used, no plastic deformation was noted visually, or as a rapid slope change in the curve. The actuator was then inflated with a wide range of pressures up to 12 psi to observe the behavior of the membrane (and generate the series in Figure 4-9). A second set of data was taken and plastic deformation was observed at 10+ psi although the "dog bone" shape exhibited by the first generation actuators wasn't noticed. The actuator was then tested past 15 psi and more permanent deformation was observed. A third set of data was then taken. At higher pressures, the

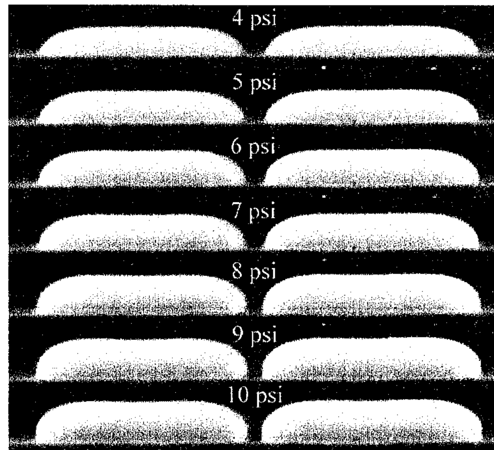

Figure 4-9: Side view of a 3 mm actuator inflated with various pressures.

deflection increased 350 μm or more over the first set of data indicating permanent stretching of the silicone membrane and the "dog bone" shape was observed.

4.3.5 Cyclic Testing

To determine the reliability of the actuators under continuous use, eight actuators were cycled using a three-way solenoid valve at frequencies from one to two Hz at a pressure of 5.1 psi which was chosen to be out of the plastic regime. Pressure vs. deflection curves were taken after 0, 2000, 5000, and 11000 cycles for each actuator. Deflection was recorded from an initial pressure of 0.2 psi to take any slack out of the membrane and provide a consistent starting point.

Actuators failed at 4500, 5000, 7100, 7900, and 10000 cycles leaving three actuators after 11000 cycles. In each case failure was preceded by a slight peeling of the silicone at the edges of the Parylene release layer (at the point of highest stress during actuation) and failure consisted of a pinhole along the center of the long edge of the actuator. As the pressure was sufficiently low, none of the failures were due to bursting membranes.

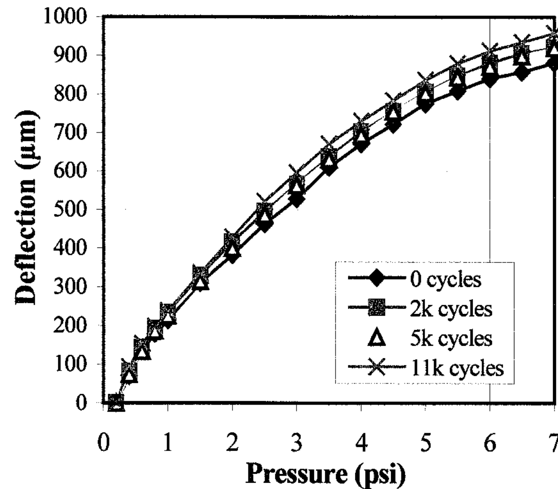

Figure 4-10: Typical pressure vs. deflection data for a 3 mm actuator after cycling at 5.1 psi showing minimal change in shape.

Figure 4-10 shows the pressure vs. deflection trend for one of three actuators that survived past 11,000 cycles (although the trend is similar for the actuators that failed). From 0 through 5,000 cycles, the curves are almost identical with a slight stretching occurring after 2,000 cycles. After 11,000 cycles, all three actuators showed signs of the silicone membrane losing adhesion at the edges and the higher deflection is partly due to this effect. The shape of the pressure vs. deflection curve doesn't change indicating that cyclic stress below the plastic region does not induce plasticity in the membrane which might lead to early membrane failure.

4.3.6 Flight Robustness

Several strips of 2 mm actuators (first generation) were attached to a small section of F-15 fighter jet wing and flight tested to assess their resistance to temperatures and pressures seen at high velocity. The aircraft achieved a maximum speed of 0.9 Ma and temperatures fluctuated from –9 °F to 110 °F. It was found that all the actuators survived the harsh flight test several times which demonstrates the robustness.

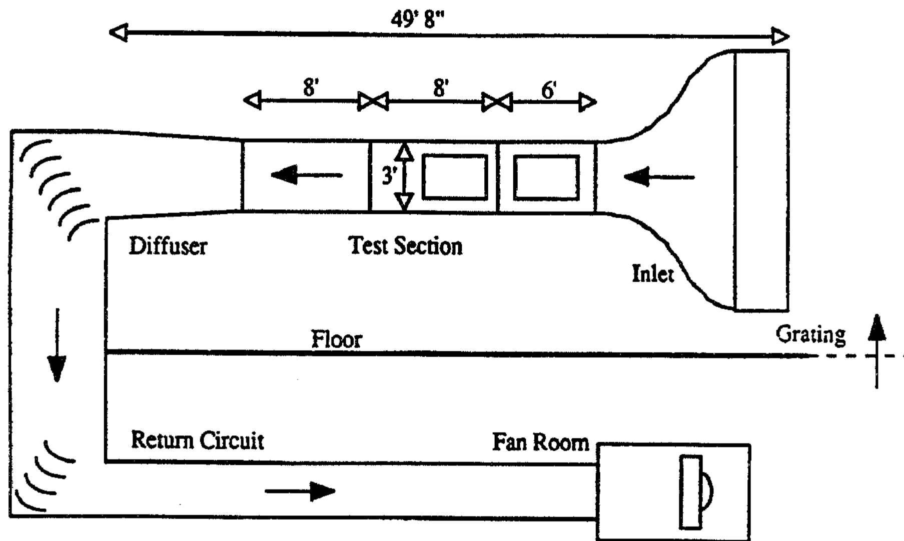

Figure 4-11: Large UCLA wind tunnel schematic.

4.4 Wind Tunnel Testing

To verify the feasibility of using micro balloon actuators for control of a macro aerodynamic device such as an Unmanned Aerial Vehicle (UAV), the actuators were tested on a delta wing model at UCLA in their wind tunnel. Theoretically, the similarity in scale of the actuators and the thin boundary layer before separation near the leading edge should allow the use of small perturbations to change the separation point. The development of leading edge vortices, which contribute a significant portion of the total lift at high angles of attack, are then modified. By manipulation of the vortex asymmetries, moments for flight control can be generated.

4.4.1 Facility and Delta Wing Configuration

An open-return wind tunnel was used for aerodynamic testing at UCLA (Figure 4-11). The test-section is 91 cm by 91 cm by 730 cm long. The maximum operating speed of the wind tunnel is 45 m/s. A delta wing model (Figure 4-12) with a swept angle of 56.5° and chord length of 30 cm was employed. The delta wing model has round leading edges

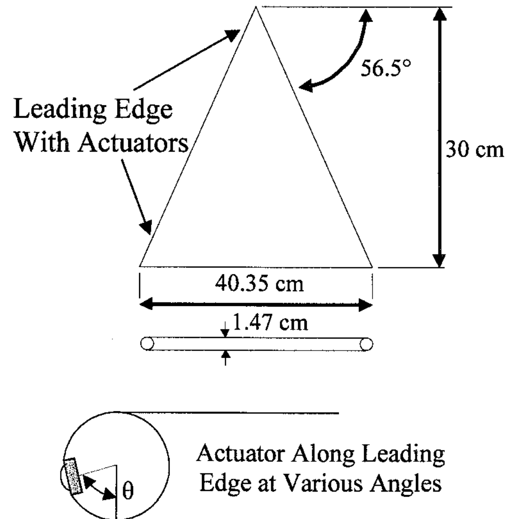

Figure 4-12: Schematic of delta wing model and detail of leading edge rod.

formed by a rod on which the micro balloon actuators are mounted. By rotating the rod, the position of the actuators can be varied over the entire leading edge. The angular position of the actuator on the leading edge is defined between 0° at the bottom of the wing and 180° at the top. A six component force/moment transducer (AMTI Inc.) was used to measure aerodynamic forces and moments. This transducer was used to record changes in the 3-axis torques caused by the micro balloons.

4.4.2 Pitching, Yawing, and Rolling Moment Control

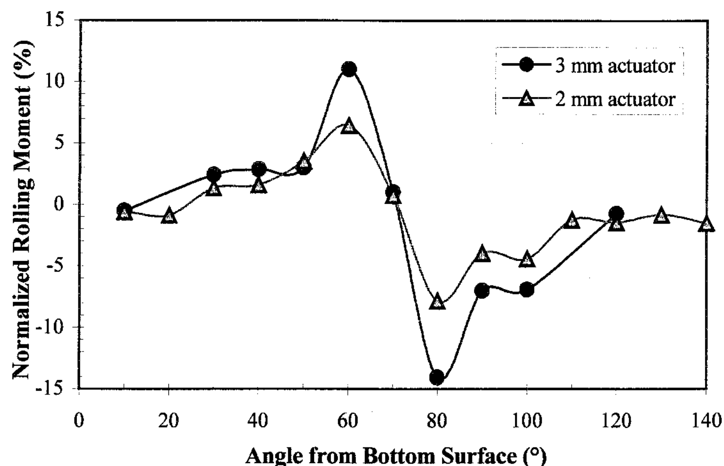

Figure 4-13: Rolling moment (normalized to a single vortex) at an AOA of 25°.

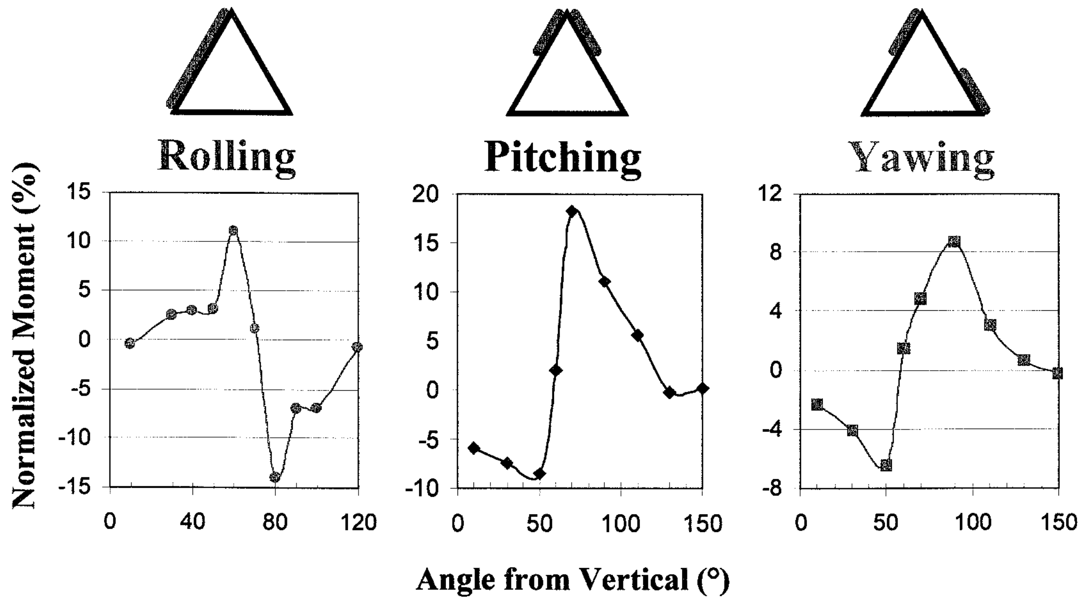

Figure 4-14: With selective spatial actuation, rolling, pitching, and yawing moments can be achieved. All of these are normalized to a single vortex.

To investigate the rolling moment generated by the two generations of actuators (2 mm and 3 mm wide strips with respective deflections of 1 mm and 1.6 mm), actuators were positioned and actuated along one leading edge from the apex to wing tip. Figure 4-13 represents the effects of the 2 mm and 3 mm actuators on rolling moment at an AOA of 25°. The data shows that 14% and 25% increments of the rolling moment can be obtained by two-sided actuation (adding the positive and negative moments together by using actuators on both leading edges at different positions) if we normalize these results to the experimentally obtained moment generated by a single leading-edge vortex (the product of the lift force of a single vortex and the distance from the center line to the centroid of the half wing).

In addition to rolling moments, we can also generate pitching and yawing with the same actuation by operating pairs of actuators strips on different portions of the leading edge as shown in Figure 4-14. In order to compare the data with that generated by

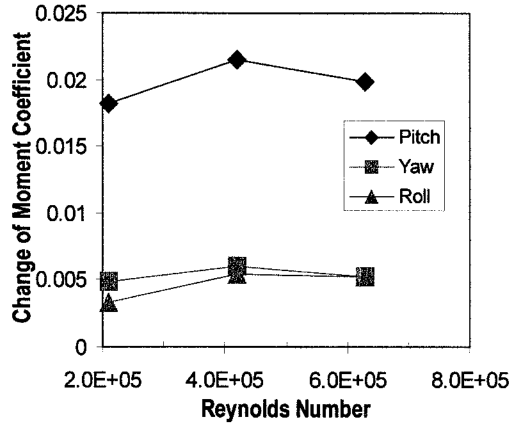

Figure 4-15: Moment coefficients vs. Reynolds number at an AOA of 25°.

conventional control surfaces, like rudders, we plot the data for the 3 mm actuators as pitching, yawing, and rolling moment coefficients in Figure 4-15. The pitching, yawing, and rolling moment coefficients, C_p, C_y, and C_r are defined in the following way

$$C_p = \frac{\Delta M_p}{QSc} \quad C_y = \frac{\Delta M_y}{QSb} \quad C_r = \frac{\Delta M_r}{QSb} \tag{4.1}$$

where Q is the dynamic pressure, S the wing area, b the trailing edge length, and c the distance from the apex to the centroid of the wing. The moment coefficients are relatively insensitive to Reynolds number as expected. Their values are on the low side for flight control which led to the fabrication of larger deflection actuators.

To better understand the interaction between the vortices and micro actuators, flow visualization [4] was done in the wind tunnel using a laser-sheet technique. These tests were performed in a low-speed suction-type wind tunnel with a maximum speed of 18 m/s. A different type of microactuator was used, but the results in Figure 4-16 are illustrative of the general vortex behavior. For an actuator at θ=50° which corresponds to a positive rolling moment, the vortical structure moves outboard as compared to no

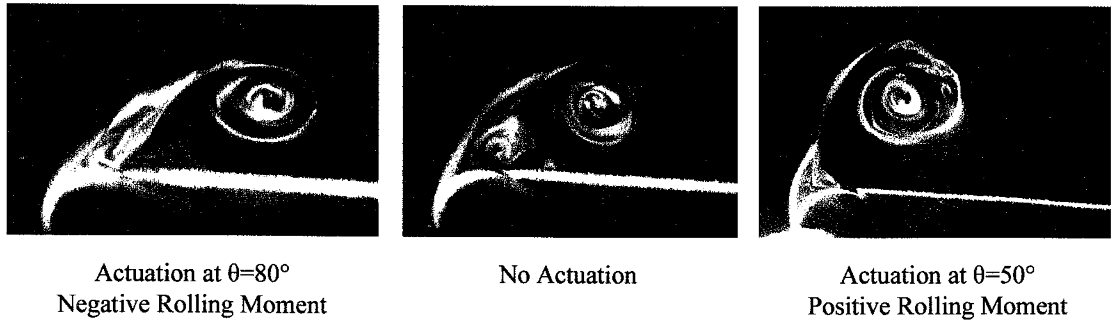

Actuation at θ=80°
Negative Rolling Moment

No Actuation

Actuation at θ=50°
Positive Rolling Moment

Figure 4-16: Flow visualization of vortex movement vs. actuator position.

actuation. For an actuator at θ=80°, the vortical structure moves inboard with a corresponding negative rolling moment.

4.4.3 Balloon Actuators vs. Conventional Flaps

To achieve increased rolling moments, a new batch of actuators was made with a 3.4 mm width strip for a deflection of 2 mm. The performance of a strip of actuators covering one leading edge of the delta wing model was compared to conventional flap style control surfaces attached to the trailing edge of the model. Figure shows the moment coefficients for balloon actuators (assuming double-sided actuation) vs. a conventional outboard aileron (also assumed to be actuated on both sides). At higher AOA, the MEMS actuators can achieve more than 50% of the rolling moment of a large conventional flap.

4.4.4 Spatial Distribution of Actuators

All of the wind tunnel data was taken with a single strip of actuators mounted on a tube that could be rotated in the leading edge. In this manner, the strip could be positioned at various angles between 0° and 180°. While this is acceptable for characterizing the moments vs θ, actual flight control on a plane requires actuators that can address arbitrary angular locations depending on AOA, orientation, and the location of the separation line. Ideally, the entire leading edge would be covered with thin strips of balloon actuators so

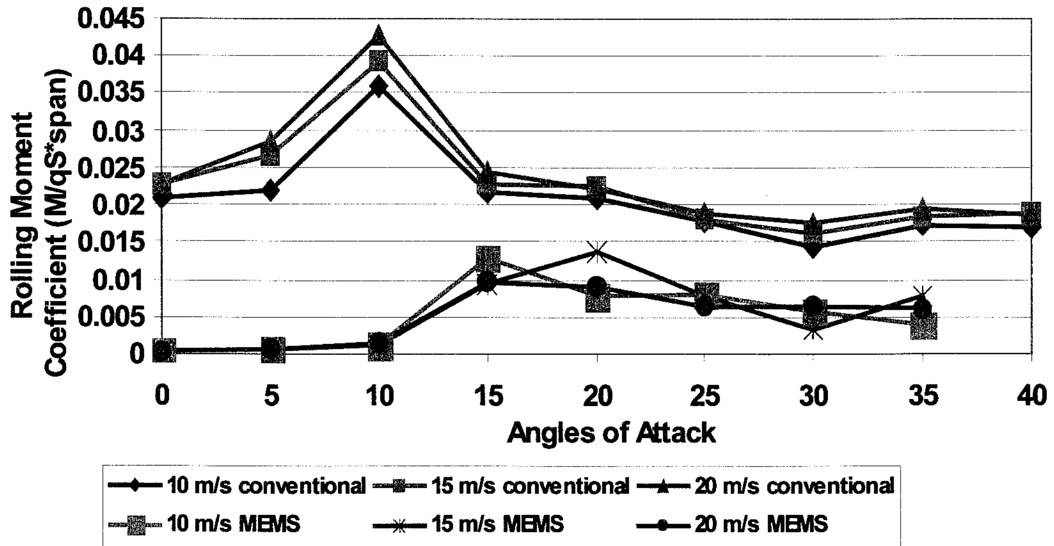

Figure 4-17: Conventional vs. MEMS control for double sided actuation assuming positive and negative components on opposite sides being added together.

that reasonably small angular segments could be addressed individually. Given the size of the leading edge (6.4 mm radius) and the width of the strips (3.4 mm), only six strips can be fit over a 180° section of leading edge which gives 30° granularity. However, this may still be sufficiently dense for flight control.

4.5 Metal Substrate Actuators

While the silicon substrate actuators are flight ready, packaging presents a problem. In flight, the leading edge can't be rotated dynamically to locate the actuator at the optimal angle so a distributed array or "skin" of bubbles is required. Bonding multiple silicon strips to a round leading edge is a poor solution as the final surface would be segmented, not to mention the labor required to align and glue each strip. Also, the long term adhesion and strength of the MRTV1 based actuators was found to be inconsistent, and the tear strength was always lower than desired.

4.5.1 Design

One solution to the packaging problem is a flexible actuator skin. In this way, all of the strips are combined on a single substrate which is then bonded to the leading edge. As the skin is flexible, the leading edge is smooth even though the actuators are still separate membranes. Initially, the possibility of using a Parylene release layer on a metal substrate was considered. While this would work very well, the metal skin is sufficiently ductile that breakage is not a concern and the actual frame area available for adhesion to the silicone layer is the same whether or not a Parylene release layer is used. Thus, the simple process outlined in Figure 4-18 was used to make actuator skins. First a metal substrate is primed with an adhesion promoter and then a layer of silicone is spin coated and cured. The other side of the substrate is patterned with photoresist and then a wet etchant is used to define the membranes.

4.5.2 Brass Substrates

Initially, it was decided to use copper or brass as both metals can be aggressively etched with Ferric Chloride ($FeCl_3$). A number of materials can be used as an etch mask including standard AZ positive photoresist, dicing tape, and electrical tape. Also, $FeCl_3$ doesn't attack cured silicone rubber. Brass shim stock 125 μm thick was originally chosen due to ready availability in very flat sheets (K&S #250 .005" x 4" x 10"). Copper

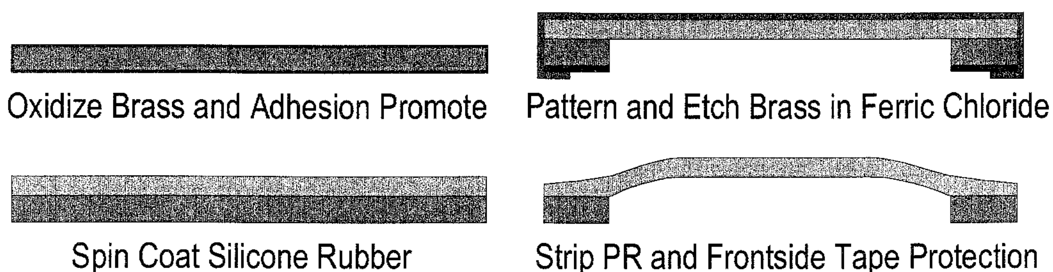

Figure 4-18: Simple process for metal substrate balloon actuators.

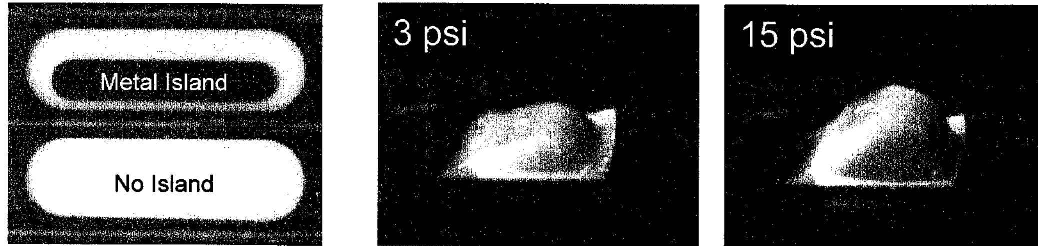

Figure 4-19: Brass substrate actuators and asymmetric actuation when inflated due to the metal island left on the membrane.

and brass tend to oxidize rapidly and some of these oxides are very weakly bound. Since the coupling agents are binding to the metal oxides, it's important that they be strongly bound. In the printed circuit board industry, copper interlayers are commonly given what is called a brown or black oxide treatment. Most of these treatments are proprietary and one was procured from RD Chemical, ChemBond™ RD-12/RD-13.

Brass sheets were cut into 4" x 4" squares. After degreasing in acetone, isopropanol, and rinsing in DI water, a layer of brown oxide was grown on the substrates using the vendors recommended procedure. Following this, the substrates were baked and then treated with General Electric SS4155 adhesion primer. A small amount of primer was applied to a Tekwipe and then wiped onto the brass substrate. The substrates were then left out for 1 hour at room temperature in a 50% RH environment. MRTV1-10RE was spin coated and cured on the brass substrates. Then 4.0 μm of AZ4400 was spun on the backside, softbaked at 100°C, and patterned using a contact mask in the UV cannon. At this point, the metal substrates were trimmed almost to final size. Since the brass was partially hardened as provided, it was difficult to bend smoothly after etching the membranes as it would tend to bend in the weakest regions. Instead, the skins would be preformed on a 1/2" diameter rod so that they were almost ready to bond after etching.

Initial etching was done at 50°C in a beaker with a spin bar and/or nitrogen bubbler. The silicone was protected from the etchant by a layer of dicing tape sealed at the edges with electrical tape. Etching was extremely nonuniform and samples had to be rotated often for any semblance of uniform etching. Commercial vendors use sophisticated spargers or spray nozzles for printed circuit board etching. 125 μm of brass would etch in anywhere from 15 to 60 minutes depending on the location of the sample in the beaker. For longer etch times, the resist would begin to erode. Clearly, very fast etch rates can be achieved, but the distribution of fresh etchant must be very uniform in the beaker. Figure 4-19 shows an example of some brass substrate actuators with and without metal islands on the membrane. The island provides asymmetric deflection.

4.5.3 Copper Substrates

With the mixed success of the brass substrate process, two changes were made at once. First, the substrate was switched to soft temper (or annealed) Alloy 110 copper. This was done to eliminate the preforming step. The silicone was also switched to Shin Etsu X32-1502 for its superior strength and ease of alignment when gluing afforded by its transparency. Initially, 6" x 12" sheets of .005" copper foil were obtained from McMaster-Carr (8944K25). The sheets were not very flat and the edges were often damaged, but the material was suitable for testing. The same recipe for adhesion as used for brass was tried, a brown oxide treatment, GE SS4155 primer, and then X32-1502 application. Adhesion of the cured silicone was very poor. What worked very well for MRTV1 didn't for X32-1502. Some attempts were made to treat the copper surface with various vinyl silanes from solution as outlined in [5] with no success. While the copper could be easily functionalized with a vinyl surface (by observing the behavior of water on

the surface before and after treatment), the silicone wouldn't form a strong adhesive bond. Silanes added directly to the prepolymer were also unsuccessful and such practice is tricky as the silanes can bond very rapidly to the fillers or other groups resulting in thixotropic mixtures that won't cure. After some testing, it was found that Dow Corning Sylgard Prime Coat worked very well. This contains allyltrimethoxysilane along with a condensation catalyst. This primer is potentially bonding to the filler and silicone chains. In the case of vinyl silane treatment, the surface only had vinyl functionality as the bake after soaking the substrate in solution would tend to condense all the silanes.

Interestingly enough, a brown oxide treatment prior to application of Sylgard Prime Coat reduced the strength of the bond. It was found that freshly cleaned copper provided the best surface. At this time, precut and flattened Alloy 110 substrates were ordered [6]. Upon receipt, it was found that there was a varnish like coating on the material. The vendor had no knowledge of this, and standard degreasing agents would not remove it. Finally, the following procedure was used to remove the coating and prepare the substrates for priming. The substrates were soaked in 12:1:1 DI:H_2SO_4:H_2O_2 until fresh

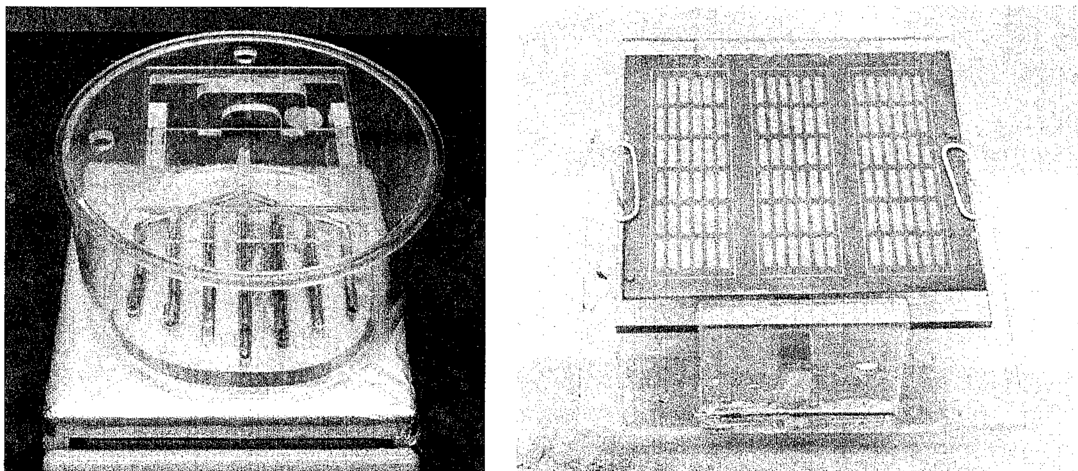

Figure 4-20: Etching apparatus with bubbler (left) and substrate holder (right) with photoresist patterned copper substrate clipped on for $FeCl_3$ etching.

copper was exposed and no coating remained. They were then quickly etched in clean 8:1:1 DI:H_2SO_4:H_2O_2, rinsed in DI water and blow dried. After a 15 minute bake at 100°C and cooling, Sylgard Prime Coat was wiped onto the substrate with a Tekwipe. The substrates were then left at RT and 50% RH for 2 to 3 hours for the primer to react. Following this, the X32-1502 was mixed and spin coated on the substrates. The tendency at this point is to bake the silicone for a quick cure. However, it was found that the quick cure in concert with the very low humidity in the convection ovens led to poor film adhesion. While the humidity in the oven could have been increased with a pan of water, the silicone was instead left to cure overnight followed by a 1-2 hour bake at 100°C to complete curing. The atmospheric moisture is necessary for the coupling agents, not the addition cure silicone reaction. Most samples were spin coated with two 40 second 600 rpm spins for a final film thickness of approximately 260 to 280 μm. A 600 rpm followed by 800 rpm spin would provide films about 200 μm thick. It is important to note that these numbers are specific to the copper substrates used. Silicone films spun on silicon wafers at the same speeds are thinner.

Because of the poor copper etching uniformity, a special apparatus was made for $FeCl_3$ etching. An acrylic plate was machined with channels and small holes to implement a nitrogen "showerhead" bubbler in the bottom of a Pyrex crystallization dish. A holder was made that suspended the copper substrates above the bubbler. In this setup (Figure 4-20), substrates were completely etched after 16 minutes in 40°C $FeCl_3$ with four rotations for an approximate etch rate of 8 μm/min. Following a through rinse in DI water and baking, individual actuator skins were cut out using a razor blade. To package the actuators on the leading edge, aluminum tubes (Figure 4-21) with grooves for

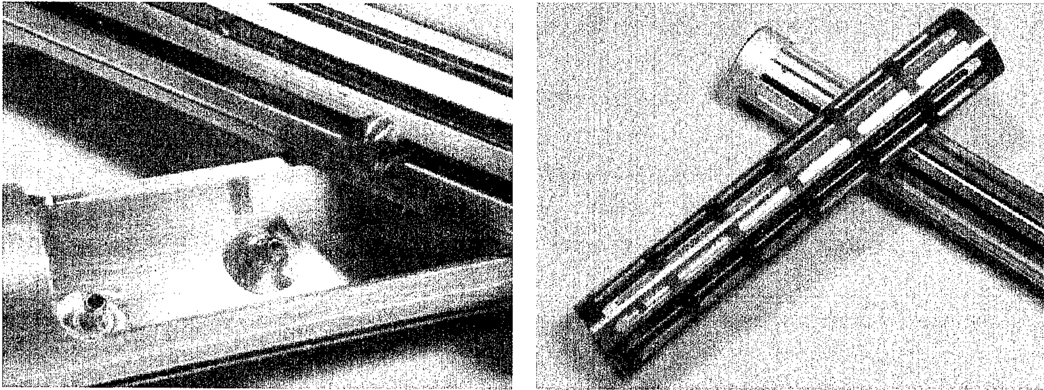

Figure 4-21: A closeup detail of the pneumatic inlets for each row of balloon actuators (left) and an early prototype X32-1502 on brass substrate actuator skin bonded to a tube. The grooves in the tube distribute pressure to each row. The final actuators were made using copper instead of brass.

pneumatic distribution along the actuator strip were made using a 4-axis setup in a CNC mill. After cutting 1/2" OD aluminum tube stock to length, they were drilled and contoured in a single fixture on the milling machine. 3M Scotch-Weld ™ DP-110 epoxy was used to glue actuator skins to the aluminum holders.

While the deflection performance of these new copper substrate actuators is very similar to the older 3.4 mm wide silicon based parts, they are considerably more robust, in part due to the use of X32-1502 silicone rubber. They are modular and can be easily configured for a variety of aircraft assuming all share the same leading edge radius.

4.7 Conclusion

A novel, high yield fabrication process has been developed for silicone rubber balloon actuators on a silicon substrate. By using a dry release method taking advantage of the poor adhesion of silicone rubber to Parylene, close to 100% yield is achieved (with failures dependent on flaws in the silicone rubber film). Actuator strips have been tested in the wind tunnel and shown to create aerodynamic moments suitable for flight control.

Since the optimal actuation point depends on the separation line which varies depending on flight conditions, it is necessary to have an array of actuators covering the leading edge. To facilitate this, a flexible metal substrate process was developed along with the corresponding packaging. These actuator skins have been tested successfully in the wind tunnel along with shear stress sensors used to detect the separation line for optimal spatial actuation and the combination is currently being flight tested on a full scale model.

References

[1] J. Rom, *High Angle of Attack Aerodynamics*, Springer-Verlag, New York, 1992.

[2] E. C. Polhamus, "Predictions of Vortex-Lift Characteristics by a Leading-Edge Suction Analogy," Journal of Aircraft, Vol. 8, No. 4, pp. 193-199, April, 1971.

[3] C. Liu, T. Tsao, and Y. C. Tai, "Out of Plane Permalloy Magnetic Actuators for Delta-Wing Control," MEMS 1995, Amsterdam, The Netherlands, pp. 7-12, 1995.

[4] G.-B. Lee, *Control of a Delta-Wing Aircraft by Micromachined Sensors and Actuators*, Ph.D. Thesis, University of California Los Angeles, 1998.

[5] United Chemical/Petrarch 2000 Catalog

[6] Integrity Metals & Slitting, 592 W. Explorer Street, Brea, CA 92821.

Chapter 5

Peristaltic Micropump

5.1 Introduction

An essential component of a general-purpose microfluidic system is a pump. While systems have been demonstrated using external pumping with integrated valves and channels, a micropump is required for most standalone systems. A number of methods can be used for pumping depending on the fluid and flow requirements. Some techniques such as electroosmotic pumping are very elegant for specific applications [1, 2]. However, for a general system, some form of mechanical pumping offers the most robust operation in the presence of mixed phase fluids, particulates, and varying chemical and electrical properties over a wide range of flow rates. A number of MEMS micropumps [3, 4] have been diaphragm pumps. Diaphragm pumps are commonly formed with a single pumping chamber and two passive check (one-way) valves. Low power consumption and reasonable flow rate have been demonstrated, but the resulting structures often have out-of-plane fluid flow due primarily to the implementation and location of the check valves. Until recently [5], most MEMS check valves have had the direction of fluid flow perpendicular to the plane of the substrate. As a result, for a diaphragm pump, the liquid must flow through the check valve, make a 90° turn to the pumping chamber, and then make another 90° turn to the outlet check valve. This non-planar flow complicates the design of integrated fluidics. More recent planar fluid flow check valve designs [6, 7] alleviate this problem to some extent.

In comparison, a peristaltic pump design uses multiple actuators that are very similar to the structure that would be used for an active normally open valve. Since a good technology for integrated fluidics must include the facility for many active valves, this pumping structure lends itself very well to integration. In addition, peristaltic pumps are self-priming by nature whereas diaphragm pumps must be designed with an eye towards adequate compression ratio as defined below. Peristaltic designs can be operated over a wide range of frequencies for a variety of fluids with varying viscosities, and can pump in either direction making them very flexible.

5.2 Theory of Operation

A peristaltic pump can be defined as a pump where fluid is transferred by mechanical contraction along a flexible tube. In typical laboratory pumps, a flexible tube is occluded between a rotor with three or more rollers and the pump housing. As the rotor rotates a pocket of fluid is moved through the pump. The section of tube behind the rotor returns to its normal shape generating a vacuum that draws more fluid from the input. The use of three or more rollers ensures that there is always a seal in the tube so there is no backflow or suction. Pulsation occurs as the occluded section of tube is released at the output side

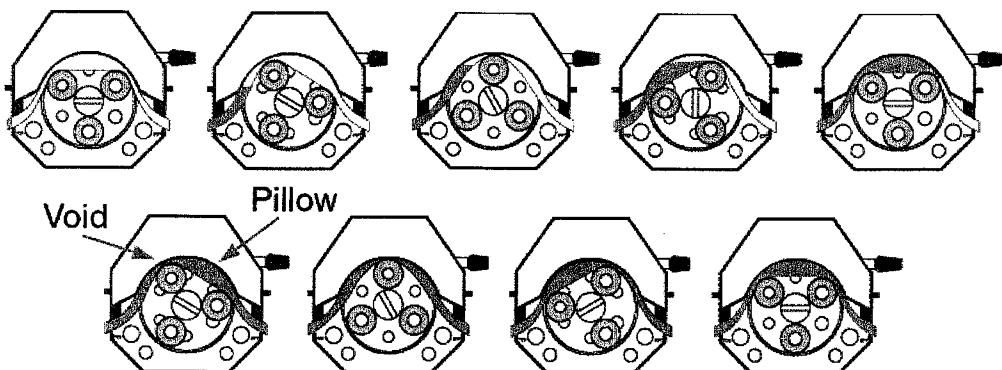

Figure 5-1: Operational sequence of a conventional peristaltic pump.

of the pump. Figure 5-1 shows the operation of a typical laboratory pump [8]. The fluid trapped between two rollers is referred to as the *pillow* and the occluded section of tubing is the *void*. When the void is released, a small amount of fluid can flow back causing pulsation. Ideally, the void should be as small as possible, in the limit having no volume at all. Practically speaking this is unrealistic so pulsation is typically reduced by the design of the rotor/housing structure or the use of multiple pumps heads that are operated out of phase with similar pillow and void sizes so that the net flow is relatively smooth.

While a structure like that of the rotor and housing in the laboratory pump can be made with MEMS [9], the tube would most likely be made separately and installed manually. Such a device could use a microfabricated or conventionally fabricated motor, but in the end, that approach does not lend itself to integration using general MEMS techniques. Rotary and linear translational motion with MEMS actuators can be difficult to achieve with high enough force to squeeze an elastomer tube. However, suppose that the motion was discretized so that a section of tubing was sequentially squeezed by a number of closely spaced actuators as shown in Figure 5-2. In this case, pillows are formed between the first and last actuator in a series of three or more and voids are created by the closing and opening of an actuator. In terms of the output, there will be forward flow based on the volume and speed with which the central sections of the tube are occluded and potentially a reverse flow due to the void caused by the last actuator

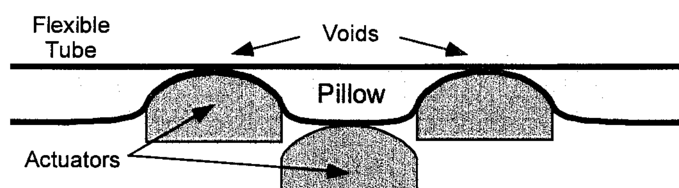

Figure 5-2: Peristaltic operation with discrete linear actuators.

(depending on the operational sequence). Since the fluid is pumped in discrete steps, more stages result in smoother flow with less pulsation due to the void created at the last stage.

At a minimum, a peristaltic pump can be demonstrated with three sequential stages of actuators. Each stage must displace a fixed volume of fluid and prevent flow in either direction (seal) when actuated. A number of patterns can be used to drive such a system, but the most straightforward are the three patterns in Figure 5-3. Like the motion of the rotor, they are symmetric and flow direction is dependent on the order of the phases. Assuming ideal actuators with equal rise and fall times, the intermediate states between phases are shown in gray for Patterns A and B. Pattern C is not especially dependent on actuator performance and the intermediate positions of actuators don't influence the flow to first order. It also more closely approximates the behavior of the rotor based pump as fluid is swept through by the overlap (even) cycles. On the other hand, Patterns A and B are very dependent on actuator performance to the extent that Pattern A will most likely not pump at all. Pattern C contains the phases of Patterns A and B, and can even be thought of as Pattern A with explicit overlap between phases.

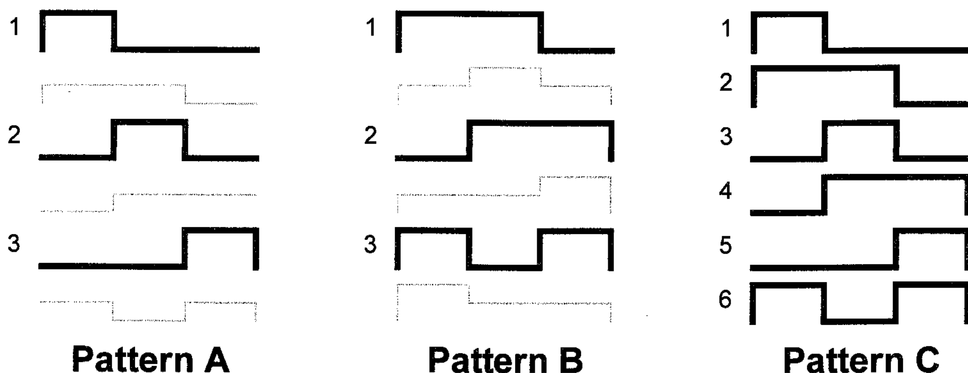

Figure 5-3: Different actuation patterns for a three stage peristaltic pump. Intermediate patterns are shown in gray for A & B and show the transitory behavior assuming that the actuators have equal rise and fall times.

Assuming each of the three stages has equal volume, it is possible to estimate the flow rate for a specific operational pattern. Pattern A is highly dependent on flow restriction inside the pump, the relative pressure across the pump, and the motion of the actuators. It is extremely sensitive to backpressure as there is no sealing from input to output (all actuators open somewhat) in between phases. While in general this is not a useful pattern for a generic pump, a particular design has certain advantages as discussed in Section 5.6.1 For the six phase pattern (Pattern C), one unit volume is pumped per cycle even though two unit volumes are displaced in the middle of the cycle. At the end of the cycle, there is a single unit volume reversion due to the transition to the beginning of the next cycle. This is similar to the operation of the laboratory pump although the void is very small in the lab pump compared to the volume of the pillow. In comparison, the three phase pattern (Pattern B) also pumps one unit volume per cycle assuming that the first actuator is not fully closed (sealed) before the middle actuator is fully off. While both patterns don't generate smooth flow (that is constant rate flow throughout the whole cycle), Pattern B exhibits little or no reversion during the cycle. If both patterns are run at the same phase frequency, Pattern B would have twice the flow rate. However, as will be discussed, the experimental results do not match due to non-ideal actuator characteristics.

5.3 Design and Fabrication

A simple three chamber peristaltic pump structure is shown in Figure 5-4. The core of the design is the chamber and membrane assembly. Since only one side of the tube is compressed by rollers in a generic pump, the same effect can be generated by forming the fluid path between a rigid surface and a flexible membrane. Three sequential flexible membrane actuators along with contoured chambers form a discrete analog of the

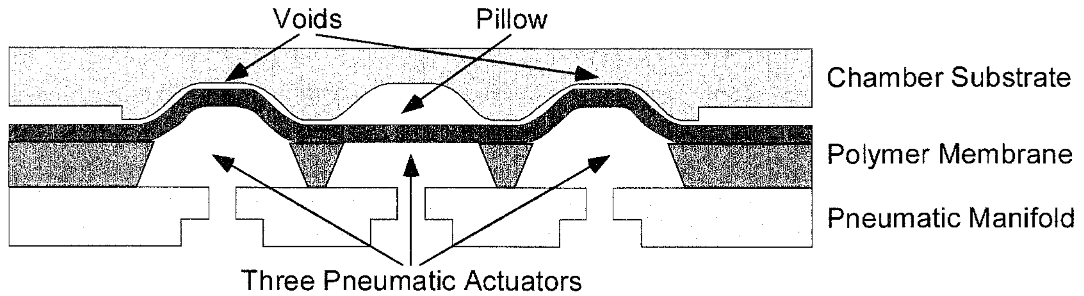

Figure 5-4: A conceptual three chamber peristaltic pump structure.

rotor/tube assembly of a typical laboratory pump. Each chamber is identical in size although that is not necessary for proper operation and it may actually be advantageous for some applications to size the central chamber differently. To pump efficiently, the membrane must perform two functions: sealing and compression.

In the past [10], rigid materials such as silicon and silicon nitride were used to form the membrane. Aside from small deflections due to the large modulus which reduces the swept volume of an actuator, the rigid material does not form a good seal with a corresponding chamber unless they are perfectly matched without any defects that might form a leakage path. Typically some form of bulk isotropic or anisotropic etching is used to form the chamber resulting in large dead volumes and leakage as shown in Figure 5-5.

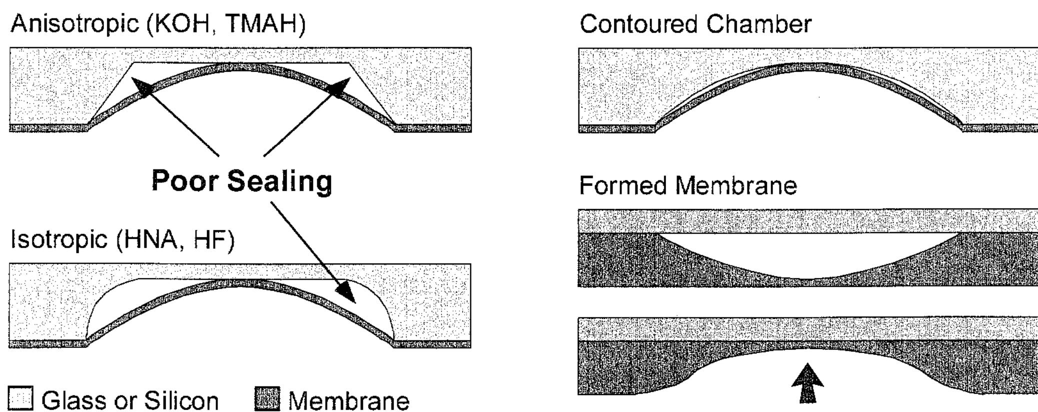

Figure 5-5: Poor matching causing leakage between easily fabricated chamber shapes and deflected membranes along with two possible solutions.

To address this problem, a very flexible polymer membrane is used along with a chamber formed to match the contour of the actuated membrane. This results in good sealing and very little non swept volume in each actuator. Another approach would be the formation of a recess in the membrane by molding such that upon actuation, the membrane deflects and seals against a flat surface. For both approaches, sealing can be accomplished either at the entrance channel, or along the length by forming a tight seal in the center between the membrane and chamber surface.

While a pneumatically driven pump is shown, thermopneumatic actuation can also be used. In addition to the chamber and membrane, a heater is needed to heat the working fluid in a sealed chamber formed by the membrane and heater subassemblies. The theory and operation are discussed in more detail in Sections 3.3 and 5.5.

5.3.1 Membrane

Requirements for the membrane include large elongation, low modulus, high strength, both tear and tensile, chemical resistance to the fluids to be pumped, and compatibility with the processes used to fabricate the underlying structure. In addition, for assembly of the complete pump, the membrane must be bondable in some fashion to the chamber

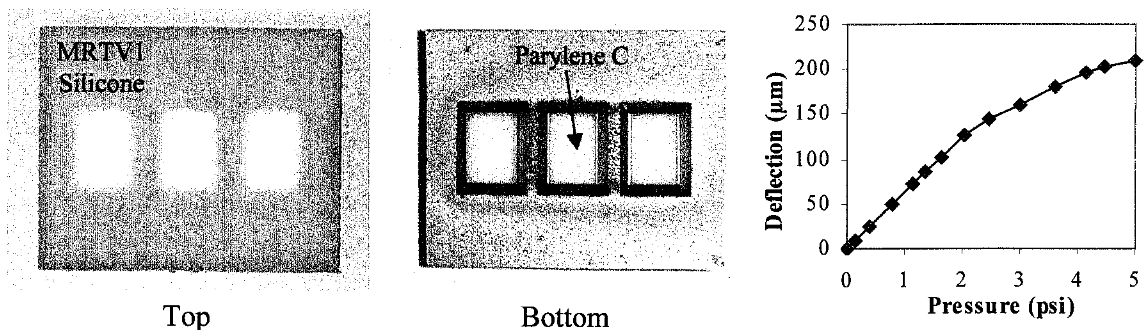

Figure 5-6: Top and bottom views of the composite silicone rubber/Parylene C membrane die. Each membranes measures 2.0 x 2.8 mm. The pressure vs. deflection curve illustrates how flexible the membranes are.

substrate or serve as a compressible gasket for clamping. Silicone rubber fulfills these requirements as outlined in chapter two and is used in macroscopic peristaltic pumps. For thermopneumatic actuation with some working fluids, a vapor barrier is required [11].

Based on lithographic constraints of a 10 mm x 10 mm die size and the need for the perimeter of the silicone layer to serve as a gasket when clamped to the chamber substrate, three 2.0 mm x 2.8 mm membranes were fabricated on a silicon die 10 mm x 8 mm as shown in Figure 5-6. A 2 μm thick layer of Parylene C was used with 200 μm of MRTV1-10RE silicone rubber spin coated over that. The fabrication process is described in Section 2.5.1. No sacrificial layer was used underneath the Parylene to allow independent sizing of the active membrane area and the backside pneumatic cavity so a 2.8 mm membrane pitch was used to allow for material lost due to the 54.7° sidewall formed by anisotropic etching in <100> wafers. Figure 5-6 shows a pressure vs. deflection curve for a composite membrane showing that large deflection can be obtained for relatively low pressures.

5.3.2 Chamber

Previous work [10] has typically used chambers fabricated from glass or silicon substrates using chemical etching. Due to the nature of most anisotropic and isotropic wet etchants, limited geometries can be formed from a single mask. Using grayscale lithography [12], thick photoresist films, and dry etching, fairly complex features can be transferred to silicon, but it is desirable to have a clear substrate and this technique does not work as efficiently on glass. Depending on the desired feature sizes, it is possible to use conventional manufacturing techniques with precision cutting tools.

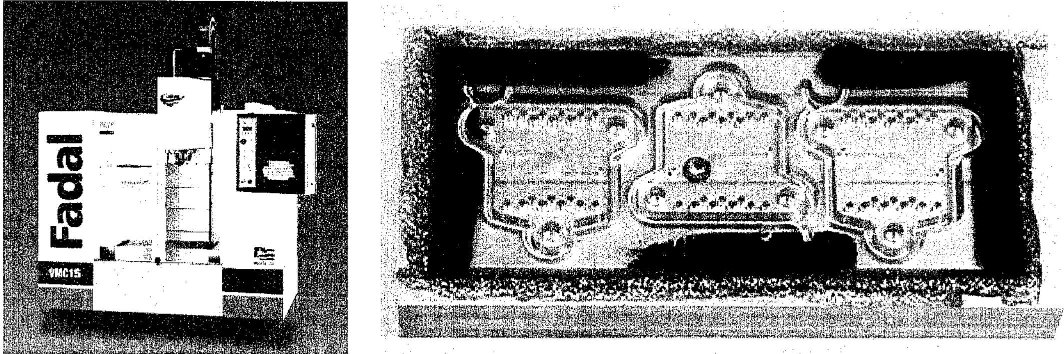

Figure 5-7: The vertical machining center (VMC) used for fabricating chamber prototypes along with the fixture used to hold the acrylic during machining.

Acrylic (PMMA) was chosen as the chamber substrate for its optical clarity, ease of machining, and its common usage along with polystyrene (PS) for injection molded biological and chemical fluidic components. Conventional machining was used for reasons of flexibility and quick turnaround of prototypes. A mass produced part would be made by injection molding or hot embossing from nickel electroforms or silicon and glass masters. A Fadal VMC15 Computer Numeric Control (CNC) milling machine (Figure 5-7) was used to contour cavities and channels, and drill interconnect holes in acrylic substrates. An acrylic blank was held down with adhesive on a fixture block while the top surface was fly cut with a diamond tool bit. This ensured that proceeding machining operations would have a flat reference plane regardless of nonuniformity in the original substrate. Then the inlet and outlet holes were conventionally drilled. A spherical (ball) endmill was used to contour the three cavities after which a smaller square endmill cut the interconnecting channels. Two more setups were used to drill from the inlet and outlet sides of the substrate for external fluidic access. This technique along with the tooling used limits the accuracy of features to roughly 10 μm. Each chamber is designed to approximate the shape of an inflated membrane and measures 140 μm deep

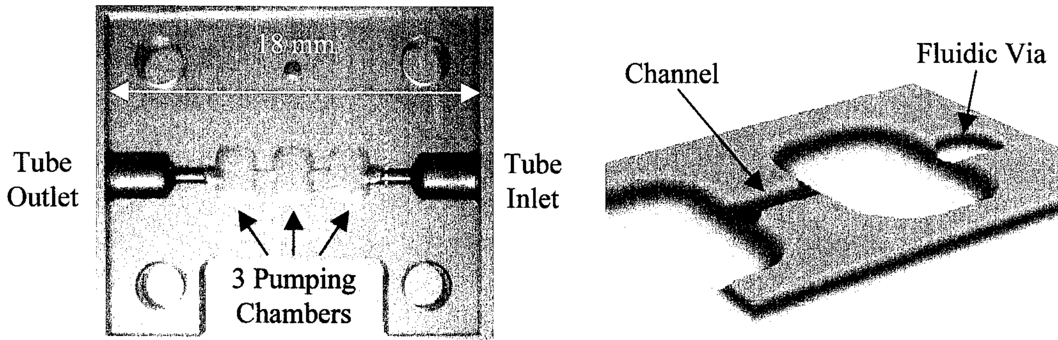

Figure 5-8: Acrylic pump plate with three sequential chambers, connections for tubing on the sides, and four holes for clamping to a base plate. A Wyko scan of an inlet/outlet chamber is on the right with details of the channel and chamber.

in the center. The small channels connecting adjoining chambers are 60 μm deep and 500 μm wide.

Because of the machining method, surfaces are not very smooth with several microns of surface roughness, but the conformability of the silicone rubber layer ensures a good seal nonetheless. External fluidic connections were initially made with 2.4 mm Tygon® tubing, but because of excessive dead volume at the joints, 0.5 mm ID stainless hypodermic tubing along with 0.5 mm ID silicone tubing was substituted. While the overall part (Figure 5-8) is fairly large, most of that area is to allow for clamping to a test fixture and the actual active area of the pump is 10 mm x 3 mm. The Wyko scan in Figure 5-8 shows the measured topography of a chamber along with the inlet hole and interconnecting channel. The calculated volume of a chamber (not including channels) from the Wyko data is 0.4 ul. The curvature of the sidewalls does not quite match the inflated membrane resulting in a small dead volume around the perimeter when the membrane touches the roof of the chamber. However, a good seal is achieved at the chamber/channel interface.

5.3.3 Heater

Previous [13] heater designs have typically been fabricated on glass or silicon substrates and suffer from large heat loss to the surroundings. While it is possible to sandwich a heater in the middle of the chamber so that heat from the top and bottom surfaces is conducted into the working fluid, there is still the issue of heat loss through the substrate laterally and also the tradeoff of power consumption vs. cooling time (for a passively cooled system). Gold on nitride membrane heaters [11] exhibit very good thermal isolation, but suffer from slow cooling and poor heat distribution through the working fluid as the heat is very localized to the resistive heater which also causes problems with early failure at high power due to hot spots.

The goal for the pump heater was a design with uniform heat distribution to the working fluid with large surface area, and a good tradeoff between power consumption and cooling times which is a function of thermal isolation from the surroundings. To this end, it was decided to fabricate a heater with a plate acting as a heat spreader to avoid the highly localized heat distribution of the nitride membrane heater described in [11]. To control heat lost through the substrate, this plate would have to be suspended by small tethers or a thin membrane. The considerations then were the material to be used, specifically the material of the plate and how it would be formed, and how it would be suspended. Silicon was chosen, partly due to availability (silicon wafers being the

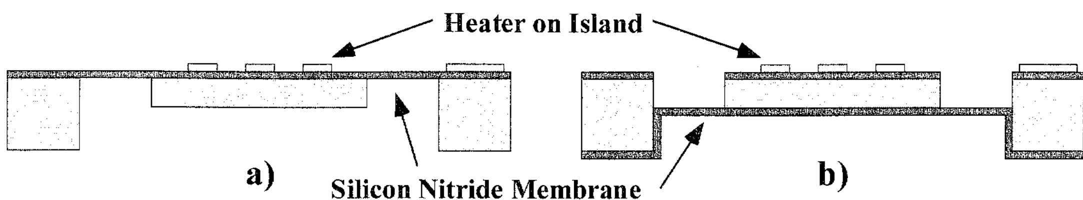

Figure 5-9: Island suspension from the top (a) vs. below (b).

standard substrate for many MEMS processes), and it's relatively high thermal conductivity (1.57 W/cm-°C). The options for suspending the plate are silicon tethers, tethers made of another material, or a thin membrane attached to the top or bottom of the plate. Making silicon tethers of different thickness than the plate itself adds extra complexity and the thermal path though the tethers would have been substantial. Tethers made from silicon nitride or silicon dioxide would be very fragile leaving a silicon nitride membrane as the optimal choice. At the time of this design, Deep Reactive Ion Etching (DRIE) was not available, which limited the methods for defining a silicon island floating on a silicon nitride membrane.

A choice had to be made between suspending the silicon island from the bottom or top as shown in Figure 5-9. With DRIE, either could be easily made although with metallization on the top surface, it is more expedient to suspend the plate from the top so that an additional bridge is not required for electrical interconnect. Once a thin silicon membrane is formed to define the plate material, it is very difficult to perform accurate lithography and patterning inside a small cavity. While a small trench could be pre-etched to define the island and then the membrane formed, the corners would be rapidly destroyed by KOH/TMAH as there would be no mask for corner compensation. However, if the island is defined from the top side, the sizing of the cavity and island are independent as they are formed from separate sides, and an oxide or nitride mask can be used for corner compensation. With this approach, a top layer of nitride has to be used to form a bridge for the resistive heater, while the bottom layer forms the suspension. With a nitride thickness on the order of 1 μm, the thermal conductivity of the membrane is still at least an order of magnitude lower than a small silicon tether.

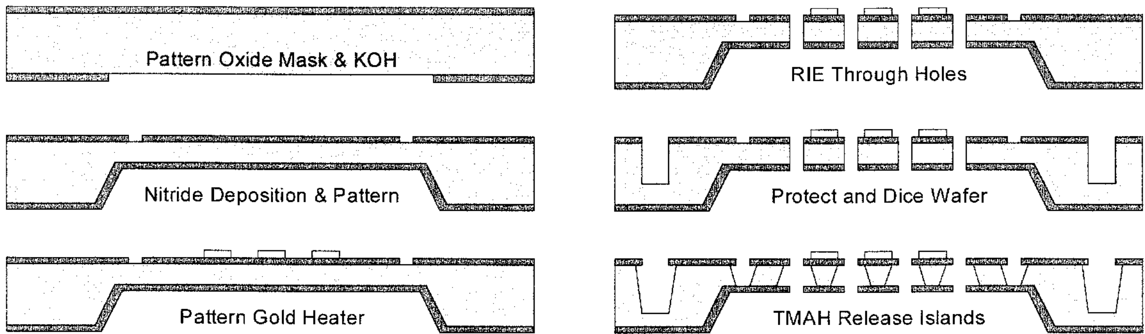

Figure 5-10: Process flow for suspended island heater using TMAH release.

The fabrication process for a single heater (there are three per die) is shown in Figure 5-10. Windows are patterned in 1.8 μm thick silicon dioxide and KOH is used to form 30 μm thick silicon membranes. The oxide is then stripped and 7000 Å of low stress silicon nitride is deposited on both sides forming the supporting membrane on the back and the bridge material (for the resistive heater) on the front. The KOH etching is done at 58°C in 20% KOH which resulted in a slightly rough surface which transferred to the backside silicon nitride. The front side nitride is then patterned to form the bridges and define the mask for freeing the silicon. A 0.7 μm layer of Cr/Au is deposited to form the

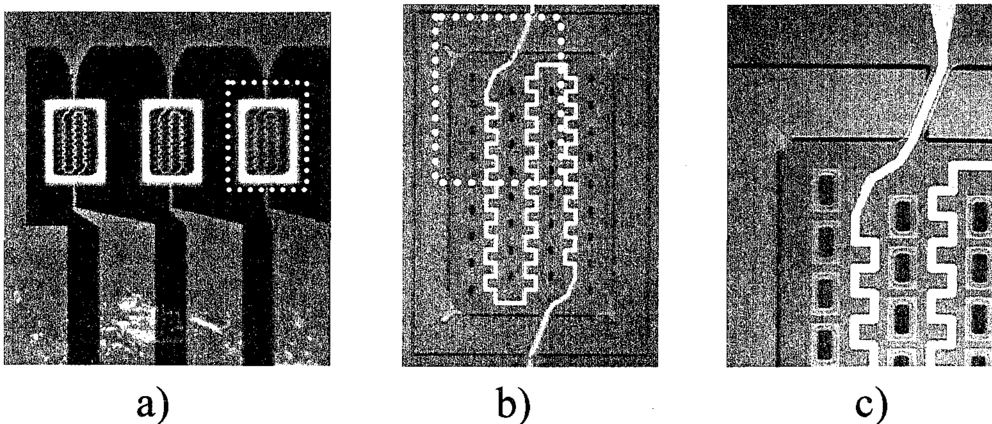

Figure 5-11: (a) A view of the heater die. (b) A single heater showing the meandering gold resistor on a silicon island suspended by a silicon nitride membrane. (c) A closeup of one corner (white dotted outline) with detail of the corner compensation, silicon nitride bridge for the resistor, and through holes.

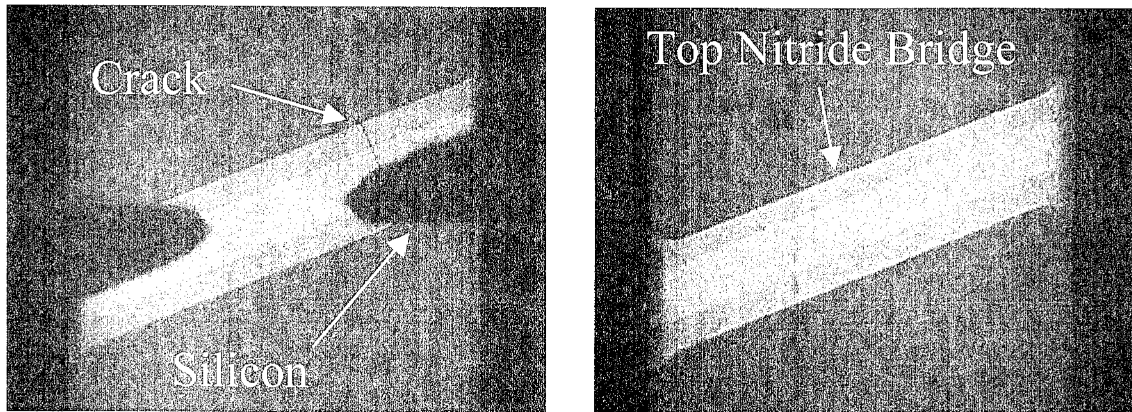

Figure 5-12: A view of the top nitride/gold bridge viewed from the back through the suspension nitride. Note the crack in the beam on the left initiated by the incompletely etched silicon outcropping vs. the good beam on the right.

heater and small holes are etched through the silicon plate to form pressure equalization holes using SF_6/O_2 RIE. The wafer is then diced, leaving approximately 250 μm of silicon so that it can still be handled as a single piece. Finally the islands are released using TMAH to etch the exposed silicon using nitride as a mask. TMAH is used due to its 20:1 selectivity between <111> and <100> planes which results in better undercut of the bridges. Figure 5-11 shows the completed heater and detail of the islands.

To prevent excessive corner rounding of the island, small nitride beams at 45° were used for corner compensation to slow down the attack of the corners formed by two <111> planes. The electrical bridges are angled slightly from square so that planes other than <111> are exposed for faster undercut. However, a significant amount of overetch is still required to fully undercut the bridges. If the silicon is not completely removed back to the transition between the bridge and the substrate, the bridges will crack easily at the sharp interface between nitride and silicon (Figure 5-12). With the silicon completely undercut, the stress risers are removed and the area of maximum stress is the center of the

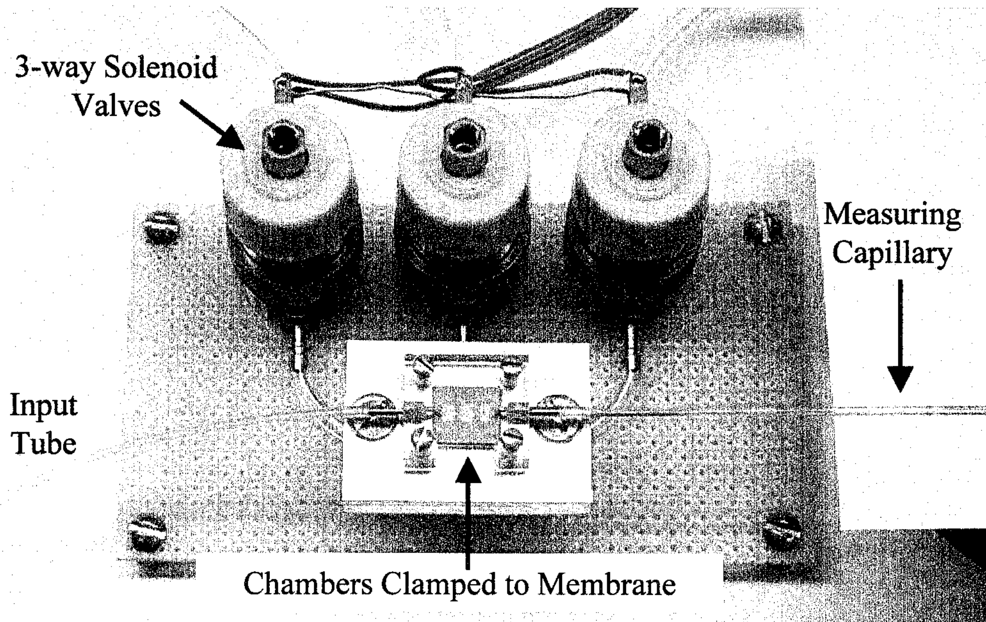

Figure 5-13: Pneumatic testing setup. A silicone membrane die is glued to an aluminum block which serves serves as a manifold for connection to the three solenoid valves. Acrylic pump plates are clamped onto the membrane. A calibrated capillary is attached to the outlet for flow rate measurement.

bridge which makes it more resistant to rough handling. The TMAH also undercuts the small through holes resulting in overhanging nitride ledges top and bottom.

5.4 Pneumatic Operation

Pneumatic testing allows characterization of the membrane and chamber designs without the additional variables introduced by thermopneumatic actuation. It also allows operation at higher frequencies than possible with the thermopneumatic actuators designs presented in this work.

5.4.1 Testing Setup

To verify the design of the peristaltic pump, a membrane die was assembled to a fixture (Figure 5-13) to allow pneumatic operation of the membranes with an external compressed air source and three-way solenoid valves (Clippard ETO-3-6). The use of three-way valves allows each membrane to either be pressurized from an external source

or vented to atmosphere. The response time of the valves is rated at 5 – 10 ms and large diameter tubing (1/8" ID) is used to minimize pressure lag. Using a digital control circuit, the membranes can be driven by arbitrary patterns at various frequencies to explore the behavior of the pump. A chamber substrate is gently clamped on top of the membrane. Along with forming the floor of each chamber, the silicone rubber membrane also serves as a seal or gasket. Excessive clamping force reduces the volume of each chamber and can extrude material into the small channels.

Flow rate is measured by observing the time necessary for fluid movement through a calibrated capillary tube (5 μl) on the output except in the case of backpressure measurements where it is more expedient to measure flow rate on the inlet (for liquid

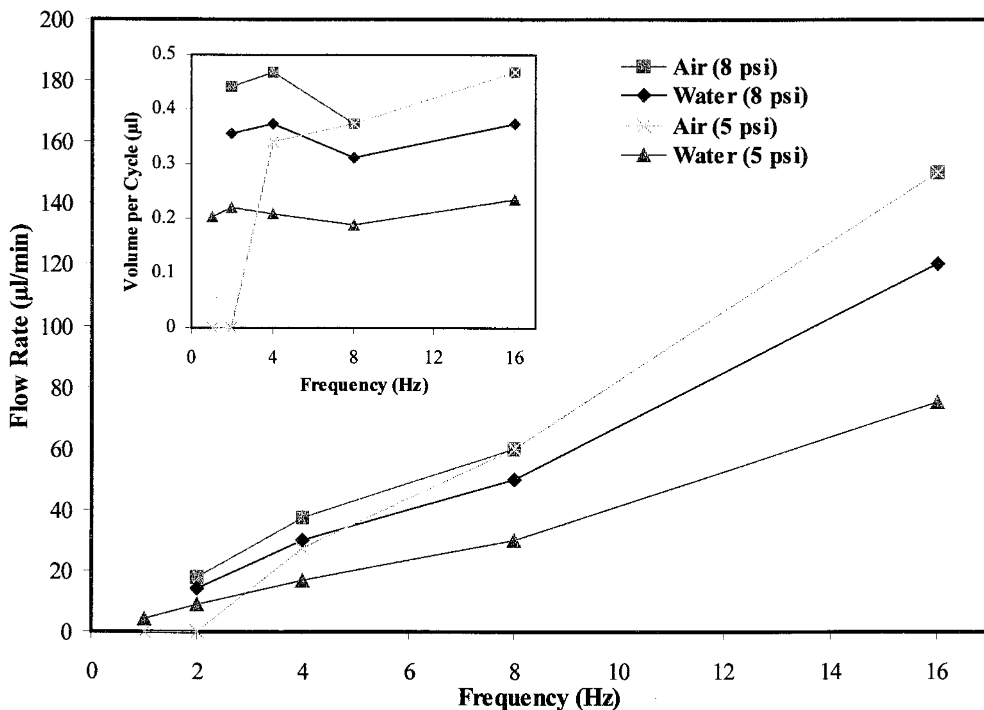

Figure 5-14: Flow vs. frequency for three phase pneumatic operation (Pattern B). Operation is shown for air and water pumping with two membrane actuation pressures. The inset graph shows volume pumped per cycle. Lower actuation pressures result in less membrane deflection which results in less swept volume.

only). To measure the flow rate for pumping air, a small water bubble is introduced in the measuring capillary to serve as a marker.

5.4.2 Testing Results

Initial pneumatic testing was done using Pattern B hereafter referred to as three phase. Membranes were actuated with two different pressures, 5 psi and 8 psi to investigate the effects of sealing and incomplete stroke. The flow rates (for zero backpressure) along with volumes pumped per cycle are shown in Figure 5-14 for air and water at different frequencies. It is interesting to note that the flow rates for air are approximately 25% higher than for water. The ability of the device to pump air demonstrates that it is self priming although at lower frequencies with reduced actuation pressure, it is not due to poor sealing (an inability to generate sufficient vacuum). The flow rate vs. frequency is fairly linear except for the 16 Hz data points which is partly due to the small volume of the measuring capillary and the difficulty of measuring times less than 2 seconds accurately. While a larger capillary could have been used, it would not have presented a consistent outlet condition for all the experiments.

Further testing was done using Pattern C, the six phase cycle. As will be explained in Section 5.5.2, this can be more appropriate for thermopneumatic operation. The centerline of the chamber was placed slightly after the centerline of the corresponding

Figure 5-15: Offset membrane location (to the left) to improve sealing. The blue dye illustrates the resulting dead volume.

membrane, as shown in Figure 5-15. This offset improves the sealing of each chamber, but restricts flow to a single direction and reduces the swept volume. This could be eliminated with improvements to the design of chamber to more closely match the inflated membrane.

Figure 5-16 shows flow rate vs. frequency for six phase operation (liquid flow) along with an overlay of three phase operation for comparison. With six phases, the pump is still self-priming and can easily pump mixed phase fluids. The flow rate is fairly linear with respect to frequency allowing us to calculate a normalized flow rate equivalent to the flow rate at 1 Hz. To measure the effects of backpressure for liquid pumping, a pressure meter was connected to the outlet (either a mechanical gauge or a vertical column of water) and a capillary was attached to the inlet for flow rate measurement. This arrangement allows the continuous measurement of flow rate without interrupting operation. Figure 5-17 shows the backpressure vs. normalized flow rate for two actuation pressures. The normalized flow rate was used as data was taken for different actuation frequencies. To measure the performance of the structure as a vacuum pump, a six phase

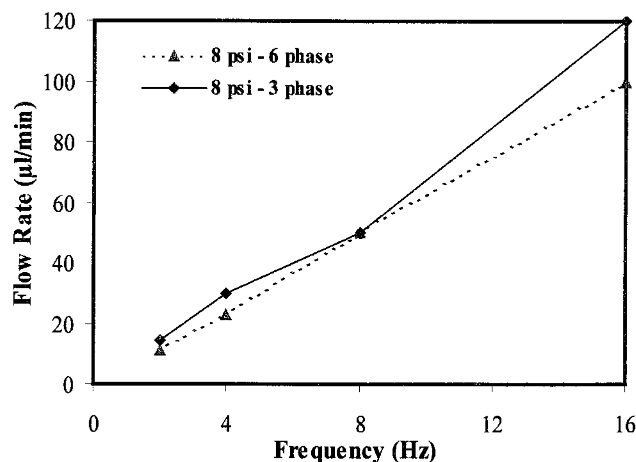

Figure 5-16: Flow rate vs. frequency for 6 phase pneumatic operation as compared to 3 phase for water at an actuation pressure of 8 psi.

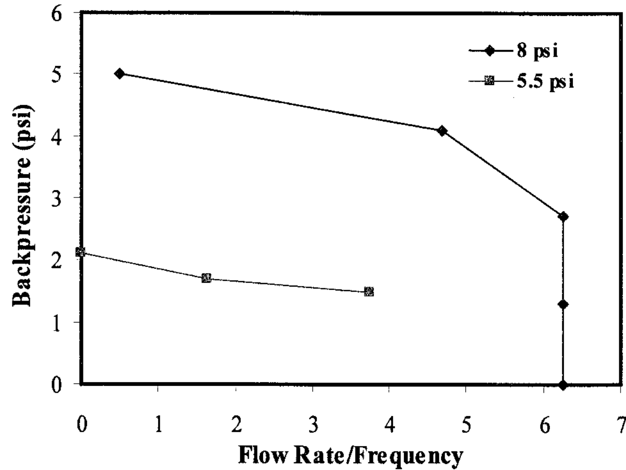

Figure 5-17: Backpressure vs. normalized flow rate (the equivalent flow rate if operated at 1 Hz) for pneumatic operation (six phase) at two pressures.

cycle at 8 Hz was used with an actuation pressure of 8.3 psi with a manometer on the inlet. While continuously pulling a vacuum, a capillary preloaded with a small drop of water was used to determine the flow rate vs. vacuum as shown in Figure 5-18.

5.4.3 Three Phase Analysis

For three phase actuation, the volume of the central chamber determines the flow rate. The first and last chambers simply act as valves and thus could be made different volumes, although this can generate pulsation in the flow if the first and last chambers

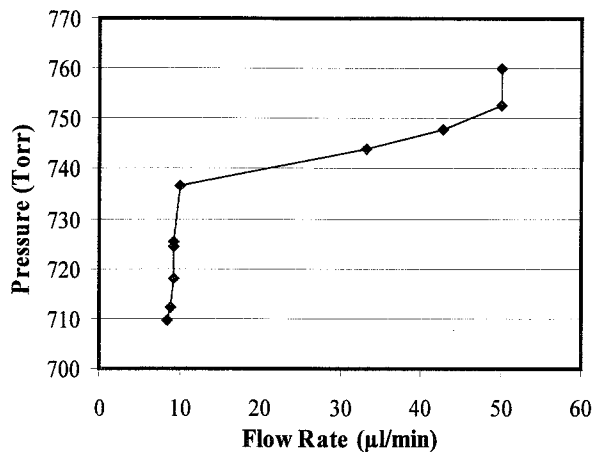

Figure 5-18: Vacuum (measured at the inlet) vs. flow rate using Pattern C at 8 Hz.

have larger volumes than the central one. Consider the transition from the second to third phase of the three phase cycle (Pattern B) in Figure 5-3. Depending on the whether the rise and fall times of the acutators are similar or not, three different situations arise. In the case of pneumatic actuation, inflation is very fast due to the reserve of pressurized gas behind the valve. Deflation tends to take longer as the driving mechanism is simply the restoring force of the stretched membrane. The vacuum created in the central cavity as the second actuator drops from phase two to phase three generates the suction necessary to fill it, but if the first actuator seals too quickly, the central cavity will not be completely filled. Furthermore, since the membranes are very flexible, instead of returning to a perfectly flat rest position it may stay slightly inflated, thus reducing the effective volume of the central chamber.

The average volume pumped per cycle for water is 0.35 μl and 0.44 μl for air. While Wyko data approximates the volume of a chamber as 0.4 μl, measurements made by observing flow in a calibrated capillary while actuating chambers individually show the swept volume of a chamber with no backpressure is almost 0.5 μl when actuated at 8 psi. Clearly then, the three phase cycle is not achieving complete filling of the central chamber. This can be explained by taking into account the slow return to rest time of the membranes vs. inflation and the ease of filling the central chamber for water vs. air. Since the first chamber seals prior to the central membrane fully returning to rest, there is incomplete chamber filling. Furthermore, the higher viscosity of water vs. air and the hydrophobic nature of the silicone membrane and acrylic chamber increase the resistance to filling the central chamber. Since there is no monotonic trend in the volume per cycle vs. operational frequency, it would appear that the time constant of filling for water or air

is significantly less than the phase period which is at a minimum, 62 ms for these experiments. The time constants and overlap of the actuators determine the effective filling rate rather than the operational frequency.

5.4.4 Six Phase Analysis

The six phase pumping results differ from theory by almost a factor of two. In fact, the flow rates are almost identical for the three and six phase patterns when operated at the same frequency. Referring to Figure 5-3, the six phase cycle has pumped two chambers worth of fluid (the central chamber volume), but in the transition from phase six to phase one of the next cycle, there is a flow reversion equal to the volume of the final chamber. If the volume of each chamber is identical (which they are for this device), the net flow per cycle should only be one chamber volume or approximately 0.35 μl (the smaller swept volume is due to the offset chambers to improve sealing as described above). Instead, the average volume per cycle is 0.6 μl for pumping water. Given the incomplete filling of the chambers for three cycle operation, this results in almost a factor of two difference in flow rates.

The most likely possibilities are reversion is less than expected and/or the volume of a chamber has increased. Since the floor of the chambers are flexible, it is very possible to overfill a chamber, but that requires extra pressure to overcome the restoring force of the membrane. The output volume vs. phase was monitored by measuring the movement of the fluid in the capillary. As expected, two unit volumes were observed being pumped out, but at the transition between cycles (from phase six back to phase one), only 30 to 40% of a unit volume was observed going back into the pump. Also, the middle chamber membrane was observed to be slightly bowed down on phase six of the

cycle. This indicates that during the phase five to phase six transition, more than a normal volume is being trapped in the middle chamber. As the first chamber seals in phase six, the fluid in that chamber can either go forward or backwards depending on the relative restrictions. Most likely, most of the fluid would go backwards leaving a normal volume in the central chamber. However, in the six phase cycle, the center of the membrane die is biased slightly behind the center of the chamber substrate to enhance sealing on the input of each chamber. What can then happen is at some point during the actuator stroke, the resistance to flow on the inlet side gets very high and the remaining fluid in the chamber is forced to the next chamber. In this case, the central chamber would end up with more than the 0.3 to 0.4 μl expected, or as measured 0.6 μl on average. For the actual pump to behave exactly like the theoretical model, the swept volume of each chamber would have to be constant (the downward deflection of the silicone membrane past horizontal would have to be restricted physically) and the chambers would have to present low flow resistance until the membrane was fully actuated. Both of these are not satisfied with this design which poses a problem if very precise flow rates are required over a wide range of pressure drops across the pump.

5.5 Thermopneumatic Operation

While pneumatic operation of the peristaltic pump (or a complete system) allows the control of very small volumes which makes it suitable for applications requiring transport and analysis of very small samples, other situations arise where the size of the device or system is important. An alternative self-contained actuation method is then required. As the membrane is flexible, either a source of pressure inside a cavity or some form of attractive force between the membrane and chamber surface is necessary for actuation.

The options include thermal expansion of a fluid or solid [14, 15], vapor pressure changes, or electrostatic attraction [16]. As explained in chapter three, thermal expansion of a fluid seems to be the most suitable method.

5.5.1 Pump Assembly

The thermopneumatic actuator is assembled as follows. A small electrical connector is soldered to the gold pads of the heater die taking care to minimize solder wicking into the bonding area. The dissolution of gold in standard tin/lead solder is very quick [17] so the joint must be formed quickly with a minimum of heat. However, this method is often unsatisfactory and a better technique is outlined in Section 6.4.3. The flux is chemically removed with 1,1,1-trichloroethane and all surfaces to be bonded are cleaned with acetone and isopropanol. The membrane die is coated with a thin layer of epoxy (either NHP 12 minute epoxy or Scotch-Weld™ DP-100) and aligned to the heater die. It is important to get complete adhesive coverage so that the three cavities are well sealed from each other without having excess bleed into the cavity.

After curing, the cavity (actually two separated by the perforated silicon island of the heater) is filled with the working fluid and a glass backplate is attached with the same epoxy. For air filled actuators, this process is very straightforward. However, some assemblies were filled with 3M PF5080 (chosen for its low vapor pressure) and due to the small through holes in the silicon island along with the overhanging nitride, bubbles would form in the holes and a complete fill could not be achieved with gravity alone. To solve this, a membrane and heater assembly was submerged in PF5080 and put in a vacuum chamber. This evacuated the air and resulted in a 100% fill of liquid in the cavities. As epoxy does not readily mix with PF5080, the epoxy was applied after filling

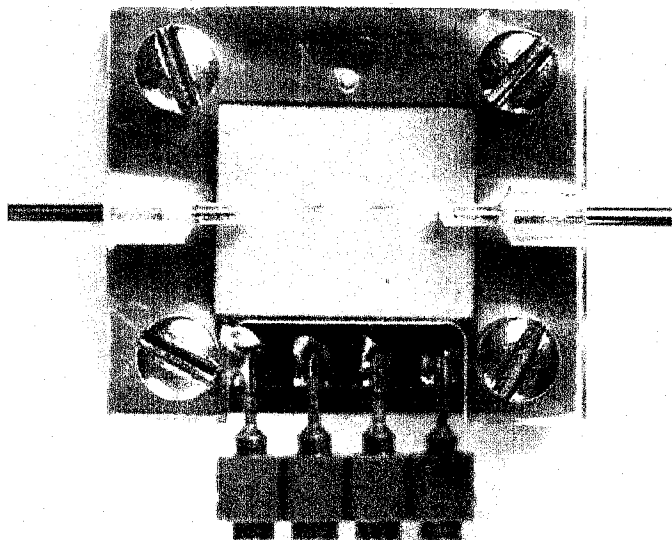

Figure 5-19: Thermopneumatic pump assembly. Heater/membrane package is sandwiched between an aluminum plate and the acrylic chamber plate. The inlet and outlet are stainless steel hypodermic tubing while electrical connections are made to the green 4-pin header on the bottom.

and then the fluid was sealed with the glass backplate by applying pressure until the adhesive sets (typically five minutes). To form the pump assembly, the actuator is placed on an aluminum backplate and the acrylic chamber substrate is clamped on top with four screws as shown in Figure 5-19.

5.5.2 Testing

The heater was designed to provide a large surface area at uniform temperature (the silicon island) while minimizing heat conduction to the substrate. To verify proper operation, the heater was mounted on a hot chuck (to improve signal to noise ratio as compared to ambient) set to 60°C and an infrared microscope (Infrascope™) was used to measure the temperature distribution. With 190 mW of applied power, the island reached 126°C or 66°C above the substrate temperature. As can be seen in Figure 5-20, the heat is

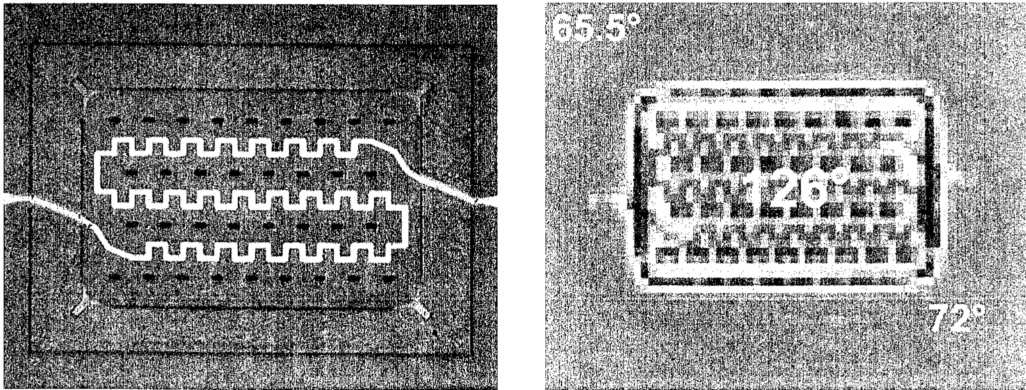

Figure 5-20: Thermal image of a heater showing strong heat localization on the silicon island. Input power is 190 mW and the substrate is on a 60°C hot chuck.

fairly well localized to the suspended silicon island with minimal temperature rise on the surrounding silicon frame.

To determine the proper working fluid, the deflection of a membrane was measured vs. applied power with both air and PF5080 as shown in Figure 5-21. PF5080 achieves less deflection for an equivalent power and the time response is very slow [18]. While Parylene seems to form a fairly effective vapor barrier, there are still problems with leakage of PF5080 during use. Since an air filled actuator achieves about 150 μm of deflection, the chamber substrate was offset slightly to guarantee a good seal at the

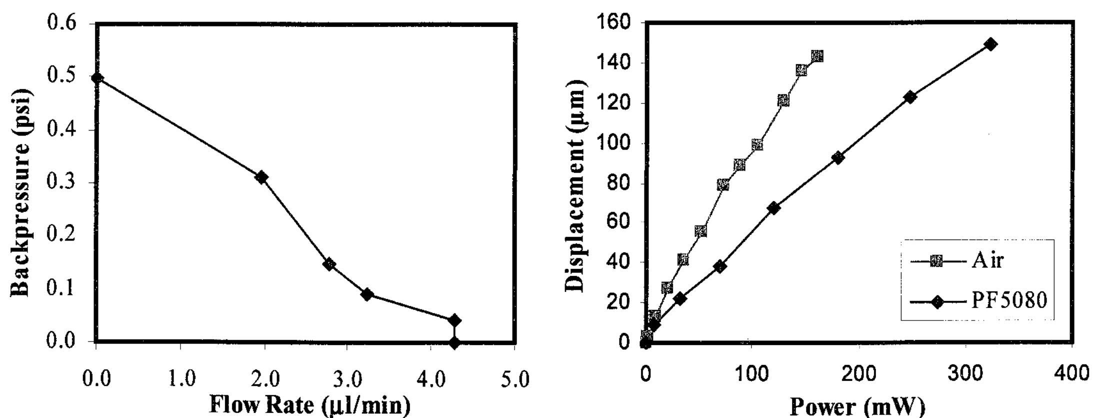

Figure 5-21: Power vs. deflection for air and PF5080 filled actuators and flow rate vs. backpressure for an air filled pump operating at 2 Hz.

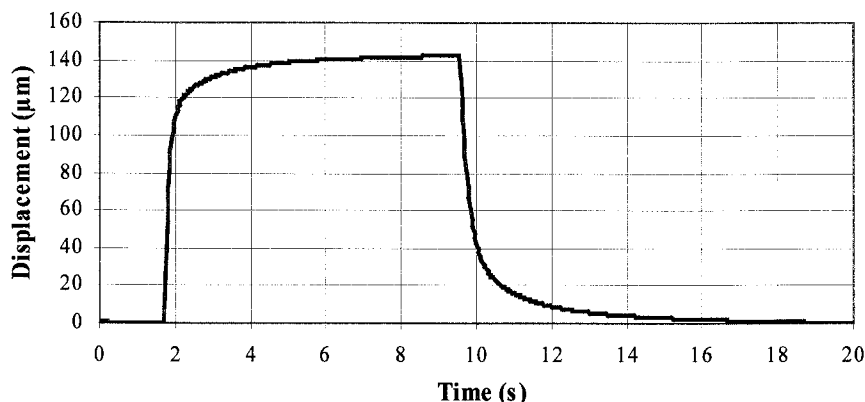

Figure 5-22: Step response of air filled actuator in response to 161 mW input.

entrance of each chamber (with respect to the flow direction). Because of an incomplete stroke, the unit volume per cycle was expected to be less than for pneumatic operation.

With the air filled actuators, flow rate data was taken using a six phase cycle at two and four Hertz. The three phase cycle was not used as the membranes takes longer to return to rest than actuate which would result in very poor filling as discussed in Section 5.4.3. By operating on six phases, the actuators have sufficient time to return to the off state although at 4 Hz operation (which corresponds to 2 Hz for each individual actuator as they are on for two consecutive phases), it is clear that the response time is affecting the operation since the flow rate isn't linear with frequency. For an input power of 291 mW (on average, 1.5 actuators are on per cycle for the six phase pattern) or individual heater power of 194 mW, the flow rate was 4.3 μl/min at 2 Hz and 6.3 μl/min at 4 Hz operation. Flow rate vs. backpressure is shown in Figure 5-21. Figure 5-22 shows the response of an air filled actuator for a 161 mW input step as measured with a (brand name) PD-1000 interferometer. The rise time (10% to 90%) is 0.8 s and the fall time is 1.4 s. Clearly, a 0.5 s period (equivalent to 4 Hz operation) results in incomplete actuator stroke and correspondingly lower volume flow rate.

5.5.3 Operation as a Valve

As mentioned earlier, the basic building block of a peristaltic pump stage is very similar to a valve. To verify this notion, a single pumping chamber was also tested as a normally open valve. A fixed pressure of air was provided at the input using a regulator and the flow rate was measured at the output using an electronic flowmeter (Cole Parmer xxxxx). Flow vs power for two inlet pressures is shown in Figure 5-23. As the pumping structure depends on relative flow restrictions rather than absolute sealing, the structure was not optimized for pure valving applications. For general pumping applications, a symmetric chamber structure is optimal for bidirectional pumping. However, for simple valving, a structure with an inlet bias has better sealing characteristics and the potential for lower dead volume.

5.6 Enhancements

5.6.1 Asymmetric Sealing

If an application only requires fluid flow in one direction, a small optimization can be made to the membrane/chamber design. The shape of the chamber can be adjusted so that

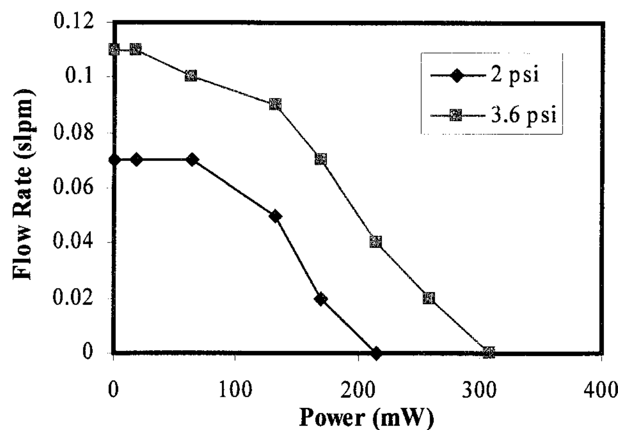

Figure 5-23: Flow rate of air vs power for a single chamber and thermopneumatic actuator used as a valve. Data for two different inlet pressures is shown.

the inflated membrane contacts one side earlier than the other. Then a strong seal is formed prior to complete displacement of the fluid in the chamber. In this case, each chamber acts as the combination of a very small valve and a larger fluid displacing actuator. Two possible scenarios result. Since the silicone membranes can deflect downwards, the first actuator can be inflated while the last actuator is still sealed. Then the volume of fluid that was in the first chamber is displaced into the second chamber deflecting its membrane downwards. In this manner, almost two chambers of fluid are pumped per cycle.

The other possibility does not depend on the flexibility of the membranes and uses Pattern A for actuation. Referring to the sequence of phases in Figure 5-24, consider the transition from phase 3 to phase 1. At the end of phase 3, the pumped volume is equal to two chambers. As the third actuator is turned off and the membrane begins to fall, the first membrane is actuated and seals the inlet. A very small volume is lost accomplishing the seal, but the first chamber is still almost full of liquid. As the first actuator completely deflects and sweeps that volume through, the third actuator has fallen sufficiently that the seal is broken and the liquid in the first chamber is swept into the middle one, while the liquid in the middle fills the last chamber. If the rise and fall times are carefully

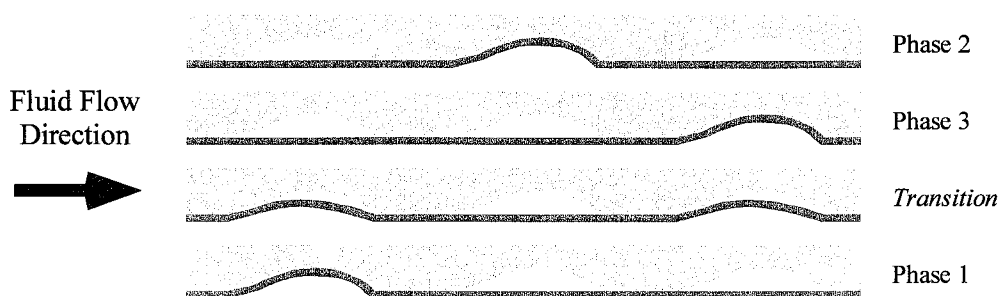

Figure 5-24: Optimization of pumping speed and power by using an asymmetric chamber to seal the inlet side of the chamber before the full stroke is complete.

controlled, there is little to no reversion in the transition except for the volume lost by sealing the inlet. This pattern when used for thermopneumatic operation consumes the least power as only one actuator is on at any time. However, an attempt to fabricate such a chamber using conventional machining was unsuccessful.

5.6.2 Integrated Heater/Membrane

One of the general drawbacks of this design is the alignment and bonding of several dies required to form a complete assembly. The bonding of the heater die to membrane die is especially critical with a fine balance between enough adhesive to ensure a leak free seal and excess extruding into the cavity and affecting the thermal isolation of the heater. The membrane die was made separate because of the difficulty of applying a thick sacrificial layer on the heater die. The removal of silicon from the front side to free the island generated significant topography which along with the through holes made spin coating of photoresist impractical. The ideal heater would be fully planar on one side allowing the application of a sacrificial layer to define a membrane of silicone rubber.

Thermal isolation can also be achieved by using thin beams to support the heater. Using DRIE, beams 100 μm wide and the thickness of the wafer (typically 500 μm) high can be fabricated. Since the DRIE is done from the backside, the front of the wafer is left free for other processes including an integrated membrane. A process is shown in Figure 5-25 for a device with a Parylene C membrane using photoresist sacrificial layers. Thermally grown silicon dioxide is used as a DRIE mask and patterned using BHF. The DRIE process is done in loops where each loop consists of a coating step followed by etching. The silicon etch rate varies from 0.5 to 0.7 μm/loop while oxide etches at roughly 30 Å/loop. Thus, roughly 2 μm of oxide is necessary to etch through the wafer.

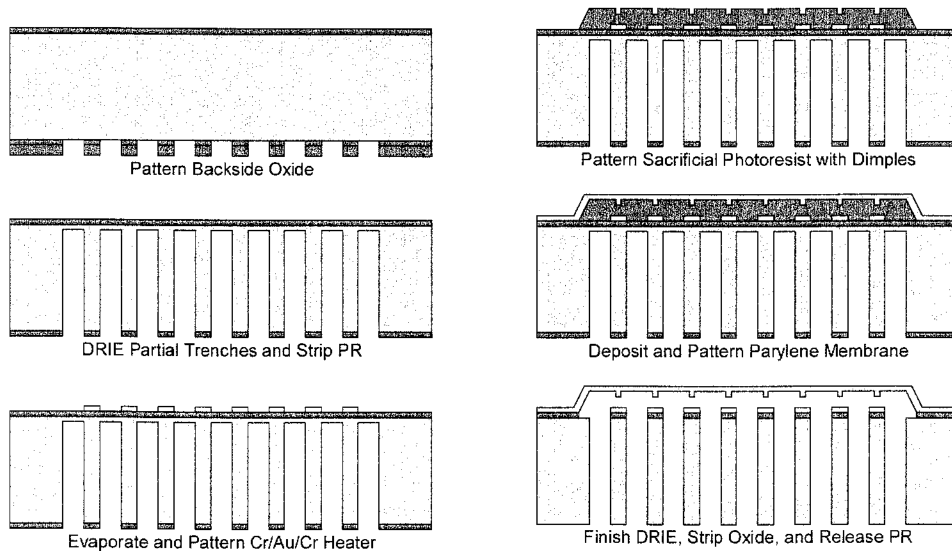

Figure 5-25: Process flow for a DRIE heater with integrated membrane.

The heater and beam pattern is etched through most of the wafer leaving 10 to 20 μm so that further processing can be performed on the front side. Cr/Au/Cr is evaporated and patterned to define the resistive heater. The Cr layer on top of the gold serves to improve adhesion for the Parylene. A photoresist sacrificial layer is defined along with small dimples (by using multiple exposures) after which a 2.0 μm layer of Parylene C is deposited. The dimples in the photoresist define small posts in the Parylene layer which serve to reduce contact area when it touches the substrate. The remaining silicon is removed using DRIE and the oxide mask from the first step with the photoresist and oxide layer serving as an etch stop. The remaining front side oxide is removed with BHF and the photoresist with acetone. After a thorough rinse, the device is ready to be filled and sealed.

Figure 5-26 shows the resulting freed structure along with a cross section showing the highly vertical sidewalls produced by DRIE. Of interest is the discrepancy in beam width as viewed from the bottom vs. the top. The cross section shows that the beam walls

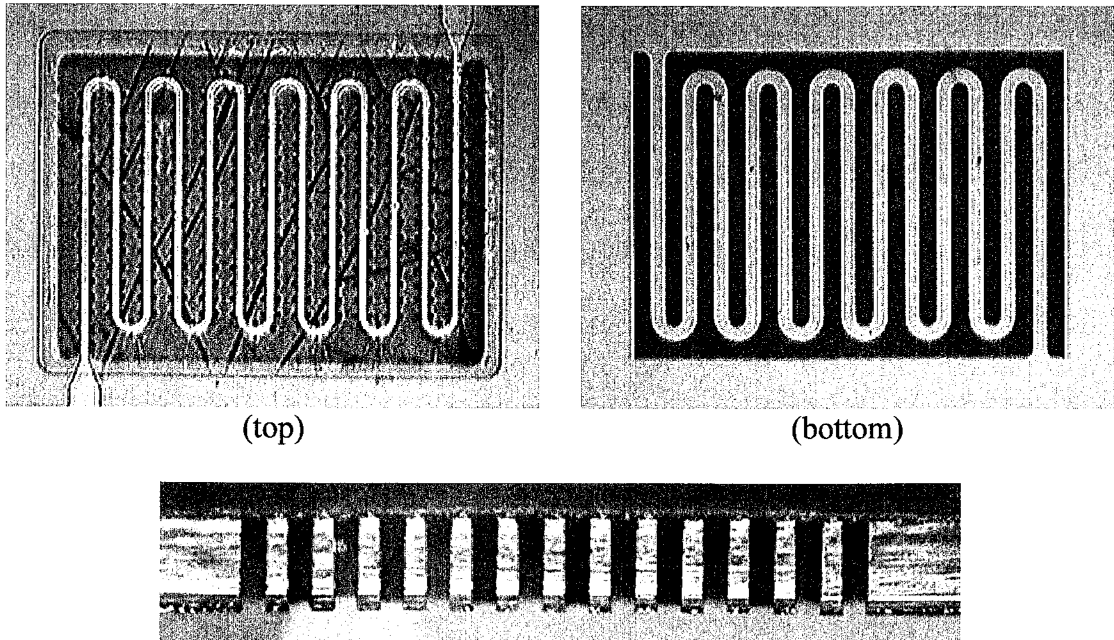

Figure 5-26: Top and bottom views of a meandering silicon beam formed by DRIE. A gold resistor is deposited on the beam to serve as a heater. The cross section below shows the vertical sidewalls and high aspect ratio of the beam.

are parallel and untapered. The narrowness of the beam at the top is due to the oxide stop layer which results in rapid undercoat at the interface. After release, the Parylene membrane would stick to the heater in spite of the dimples. Stiction between the gold and Parylene was very strong making the membranes unusable. At the time, CO_2 critical drying [19] was not available and the device was abandoned. However, portions of the technology will be revisited in Chapter 6.

5.7 Conclusion

A peristaltic micropump structure has been successfully demonstrated using both pneumatic and thermopneumatic actuation. The combination of a highly flexible membrane and a matching chamber that conforms to the shape of the inflated membrane results in good sealing and low unswept volumes. The resulting structure is planar and can be readily integrated with valves and channels to form a fluidic system. A new heater

design using a suspended silicon island has been fabricated and demonstrated to be faster than previous designs while maintaining low power dissipation. Self-priming operation with a maximum flow rate of 6.3 μl/min at 291 mW was achieved using thermopneumatic actuation. With external pneumatic operation, flow rates higher than 100 μl/min are possible due to faster membrane actuation.

References

[1] D. J. Harrison, A. Manz, Z. Fan, H. Ludi, and H. M. Widmer, "Capillary Electrophoresis and Sample Injection Systems Integrated on a Planar Glass Chip," Analytical Chemistry, Vol. 64 (17), pp. 1926-1932, 1992.

[2] C. T. Culbertson, R. S. Ramsey, and J. M. Ramsey, "Electroosmotically Induced Hydraulic Pumping on Microchips: Differential Ion Transport," Analytical Chemistry, Vol. 72 (10), pp. 2285-2291, 2000.

[3] M. Richter, R. Linnemann, and P. Woias, "Robust Design of Gas and Liquid Micropumps," Sensors & Actuators A 68, pp. 480-486, 1998.

[4] K.-P. Kamper. J. Dopper, W. Ehrfeld, amd S. Oberbeck, "A Self-Filling Low-Cost Membrane Micropump," Proceedings of IEEE Workshop on Micro Electro Mechanical Systems (MEMS '98), pp. 432-437, Heidelberg, Germany, January, 1998.

[5] J. Tiren, L. Tenerz, and B. Hok, "A Batch-Fabricated Non-Reverse Valve with Cantilever Beam Manufactured by Micromachining of Silicon," Sensors and Actuators, Vol. 18, pp. 389-396, 1989.

[6] X. Q. Wang and Y. C. Tai,"A Normally Closed In-Channel Micro Check Valve," Proceedings of IEEE International Conference on Micro Electro Mechanical Systems (MEMS '00), pp. 68-73, Miyazaki, Japan, January, 2000.

[7] J. D. Evans and D. Liepmann, "The "Spring Valve" Mechanical Check Valve for In-Plane Fluid Control," Technical Digest, International Conference on Solid-State Sensors and Actuators (Transducers '99), Vol. 2, pp. 1796-1799, Sendai, Japan, June 1999.

[8] Animated GIF from `http://www.coleparmer.com`.

[9] A. S. Dewa, K. Deng, D. C. Ritter, C. Bonham, H. Guckel, and S. Massood-Ansari, "Development of LIGA-Fabricated Self-Pumping, In-Line Gear Pumps," Technical Digest, International Conference on Solid-State Sensors and Actuators (Transducers '97), Vol. 2, pp. 757-760, Chicago, USA, June 1997.

[10] J. A. Folta, N. F. Raley, and E. W. Hee, "Design, Fabrication and Testing of a Miniature Peristaltic Membrane Pump," Technical Digest, IEEE Solid-state Sensor and Actuator Workshop, pp. 186-189, Hilton Head Island, South Carolina, USA, June 1992.

[11] X. Yang, C. Grosjean, and Y. C. Tai, "Design, Fabrication, and Testing of Micromachined Silicone Rubber Membrane Valves," IEEE/ASME Journal of Microelectromechanical Systems, Vol. 8 (4), pp. 393-402, December 1999.

[12] D. Purdy, "Fabrication of Complex Micro-Optic Components Using photo-sculpting Through Halftone Transmission Masks," Applied Optics, Vol. 3, pp. 167-175. 1994.

[13] P. L. Bergstrom, J. Ji, Y.-N. Liu, M. Kaviany, and K. D. Wise, "Thermally Driven Phase-Change Microactuation," Journal of Microelectromechanical Systems, Vol. 4 (1), pp. 10-17, 1995.

[14] M. J. Zdeblick, *A Planar Process for an Electric-to-Fluidic Valve*, Ph.D. Thesis, Stanford University, 1988.

[15] E. T. Carlen and C. H. Mastrangelo, "Paraffin Actuated Surface Micromachined Valves," Proceedings of IEEE Workshop on Micro Electro Mechanical Systems (MEMS '00), pp. 381-385, Miyazaki, Japan, January, 2000.

16] C. Cabuz, E. I. Cabuz, W. R. Herb, T. Rolfer, and D. Zook, "Mesoscopic Sampler Based on 3D Array of Electrostatic Activated Diaphragms," Technical Digest, International Conference on Solid-State Sensors and Actuators (Transducers '99), Vol. 2, pp. 1890-1891, Sendai, Japan, June, 1999.

[17] B. R. Allenby, et al., "An Assessment of the Use of Lead in Electronic Assembly," Surface Mount Council.

[18] X. Yang, *Micromachined Silicone Rubber Membrane Valves for Fluidic Applications*, Ph.D. Thesis, California Institute of Technology, 1998.

[19] G. T. Mulhern, D. S. Soane, and R. T. Howe, "Supercritical Carbon Dioxide Drying of Microstructures," Technical Digest, International Conference on Solid-State Sensors and Actuators (Transducers '93), pp. 296-299, Yokohama, Japan, June 1993.

Chapter 6

Planar Fluidic System

6.1 Introduction

The peristaltic pump described in Chapter 5 is planar and integration with channels is a natural consequence of the fabrication process. Thus, a planar system of pumps, valves, reservoirs, and channels can be made without assembling the components individually. This offers the possibility of batch fabricated, low cost fluidic systems, potentially disposable depending on the technology used for the actuators. However, comparing the volume pumped per cycle to the total volume of the three chambers, the spatial efficiency of the design seems somewhat lacking. For a system with many different liquids to be pumped, this can be a significant penalty, both in area and power consumption. Also, the six phase cycle (Pattern C in Figure 5-3) has significant reversion which can be undesirable. Conceptually, the peristaltic design can be changed into a diaphragm pump with active valves by changing the operational sequence and resizing the chambers. It will be shown that such an architecture has advantages for an integrated system.

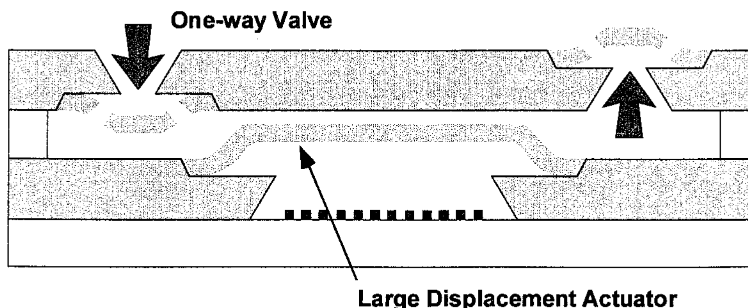

Figure 6-1: Conceptual diaphragm pump with passive check (one-way) valves.

6.2 Diaphragm Pump Operation

Most MEMS mechanical pumps [1] are diaphragm pumps. Conceptually, they are formed with two passive one-way (check) valves and a variable displacement chamber, typically a flexible diaphragm bounding a rigid cavity as shown in Figure 6-1. This design is popular as only a single actuator is required. Since the actuator is often a piezoelectric element attached separately to a pumping structure, this greatly simplifies assembly. Also, the pumping cavity is usually large to maximize flow rate and the compression ratio ε

$$\varepsilon = \frac{\Delta V}{V_0} \tag{6.1}$$

where ΔV is the swept volume and V_0 is volume left that is not displaced both in the chambers and channels, often referred to as the dead volume. Too small of a compression ratio results in an inability to self-prime. Typically, the check valves are integrated into the cavity structure so that manual alignment isn't required. However, fluid flow is out of plane with respect to the substrate although newer planar check valve designs [2] can potentially eliminate this limitation.

While it isn't commonly done, the passive check valves can be replaced with active valves with similar operation. At first, this would seem to be detrimental, in terms of more complex assembly, potentially greater power consumption, and larger area. However, in the context of a system with many inputs and pumps, a very interesting optimization can be performed. Consider a simple system with several reagent reservoirs feeding into a common reaction chamber. Each input reagent requires its own pump. The output check valve prevents other pumps from contaminating each others reservoirs so

active valves are not necessary. If active valves are added to each reservoir, then a single pump can be used assuming that contamination in the inlet channel is not an issue. Consider now the elimination of the input check valve in the pump. Correctly sequenced, the active valves can be used to route the correct liquid or liquids to the pump. Furthermore, if the outlet check valve is replaced with one or more active valves, the inputs can be routed to various outputs. Finally, since the active valves are not directional, any port can serve as an inlet or outlet. In this way, an arbitrary structure can be formed with many small active valves and a single pumping chamber.

In its simplest form, the pump can be realized with two valves and one pumping chamber. Unlike the peristaltic pump, the pumping chamber does not have to form a good seal, all that is necessary is a large swept volume in comparison to the dead volume of the valves and connecting channels. Also, the valve design should be optimized for power consumption and speed since there may be many of them in a system.

6.3 Integrated Heater and Membrane

The peristaltic pump required manual alignment and bonding of the various components that formed the final structure. One of the most troublesome steps was the bonding of the membrane die to the heater die. The opaque silicone membrane prevented visual alignment from the top and the silicon island on the heater obstructed most of the view from the back. Also, the epoxy used for bonding had to be carefully applied to prevent excess from covering the heater and affecting its thermal isolation. Two process changes were investigated to address these issues. First, a clear silicone rubber was used to allow visual alignment through the membrane. Second, a process was designed that integrated the heater and membrane on a single substrate.

6.3.1 Design and Fabrication

Conceptually, to integrate the heater and membrane processes, most of the heater processing must be finished prior to application of silicone rubber to allow maximum process latitude. Furthermore, some sort of sacrificial layer will be necessary to define the membrane. Based on previous experience with the Parylene membrane structure in Section 5.6.2, a similar structure was explored. For a fluidic system, electrical connections to the heaters would preferably be made from the backside to leave the frontside free for channels and other structures. That way, a large actuator die could be bonded to a fluidic plate forming the complete system and allowing each part to be fabricated separately using the optimal materials and processes. A conceptual system is shown in Figure 6-2 with two silicon based actuators and a sensor chip attached to an acrylic (PMMA) fluidic board.

A process flow is shown in Figure 6-3 for the combination membrane/heater

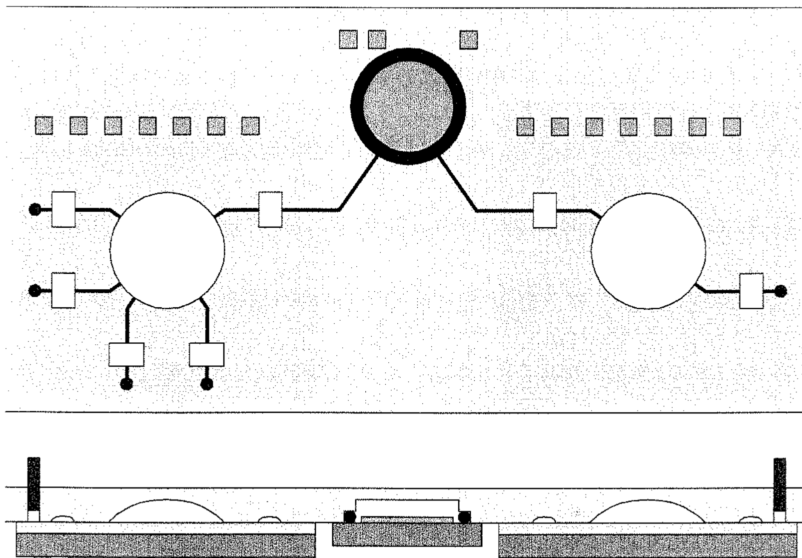

Figure 6-2: A conceptual fluidic system. The rectangles represent active valves with the large circle a pumping chamber. The actuator die on the left has four inputs that can be arbitrarily pumped to the sensor chip in the top center.

structure. First, alignment marks are patterned on both sides of the wafer using a double side alignment jig. Then, a 0.5 μm layer of thermal oxide is grown on a 4" silicon wafer. As DRIE will be used for structural definition, crystalline orientation is unimportant, but <100> is the standard for circuit fabrication and thus the most commonly available. The oxide layer is stripped from the front side with BHF. Next, a layer of Cr/Au is deposited and patterned to form the resistive heater on the backside. This type of metallization is used as it can be soldered if necessary and doesn't oxidize ensuring low contact resistance with mechanical probes. Heavily doped silicon could have been used for the heater, but metallization would still have been required for the external connections. Also, the silicon dioxide layer is used as an etch mask so this process is actually simpler compared to the masking and diffusion or ion implantation step that would have been necessary otherwise. A double spin of AZ4400 photoresist for an 8 μm thick film is patterned to define a meandering silicon beam, the oxide is etched in BHF for 5 minutes, and then the wafer is etched from the backside using DRIE until a thin layer of silicon (nominally 20 - 40 μm) is left after which the remaining photoresist mask is removed with stripper. The etch rate varied from 0.62 – 0.8 μm/loop depending on aspect ratio and how long the machine had been run. A sacrificial photoresist layer is defined on the front side of the wafer using the alignment marks defined at the beginning of the process. Typical front to back alignment accuracy is within 15 μm depending on mask calibration. A thick sacrificial layer is desirable and certainly achievable using multiple spins of AZ4620 or AZ9260 resist. However, the exposure equipment (GCA MANN 4800) is not well suited for thick films due to the 10X reduction optics and so a 9 μm thick layer was used. The surface is cleaned with O_2 plasma followed by a dilute HF dip and then primed

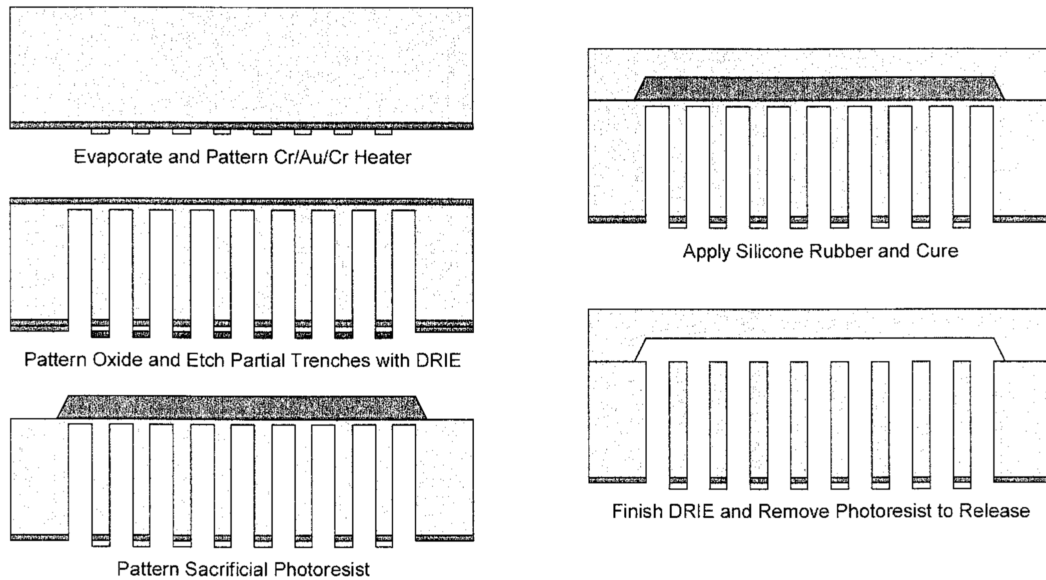

Figure 6-3: Process flow for integrated heater and membrane.

using Dow Corning Sylgard Primecoat by wiping. A layer of X32-1502 silicone rubber is applied by spinning once at 500 rpm to coat, and then at 800 rpm for 40 s to define a nominal 150 μm thick layer. Following cure, the remaining silicon is removed in the DRIE using the photoresist sacrificial layer as an etch stop. The mask for this step is the combination of the Cr/Au resistor and the patterned oxide insulation layer. Then the wafer is diced. Finally, the sacrificial photoresist is removed with acetone freeing the membrane. The front and back of a completed actuator are shown in Figure 6-4. There are six small heaters for valves surrounding a single large heater for the pumping chamber. The two small holes in the upper right and left corners of the dies are through holes for physical alignment with other components.

6.3.2 Discussion

After dicing, it was found that the dicing tape used to secure the wafer to the vacuum chuck had sufficient adhesion to the Cr/Au to peel it off. The adhesive bond had to be attacked with acetone. Normally this is not a problem as metallization on the bottom of

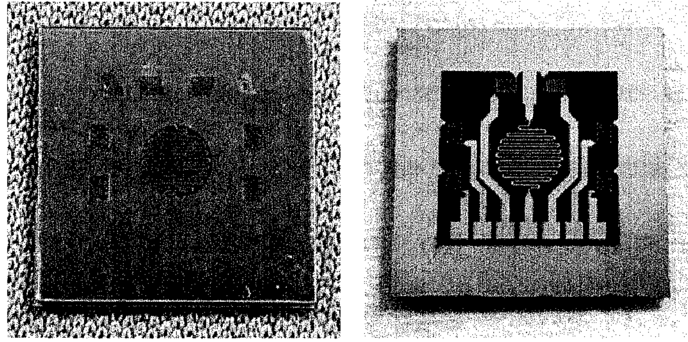

Figure 6-4: Top (left) and bottom (right) view of the integrated heater/membrane. The silicone layer is transparent. Gold is used for the heater metallization.

the wafer is an uncommon practice. After releasing the silicone membranes, it was found that most of them were stuck to the silicon beams. The flexibility of the silicone rubber is so great that a thin sacrificial layer isn't enough to ensure separation during release. Some structures were successfully released by using compressed N_2 to blow the isopropanol used to displace the acetone out from between the beam and membrane. While techniques such as CO_2 critical drying [3] may prevent this behavior, a thicker sacrificial layer is really necessary along with potential surface modification of the silicon beam and/or silicone rubber membrane to reduce contact area so that the restoring force of the membrane is sufficient to prevent stiction. One possibility is the patterning of dimples in the sacrificial layer to form posts in the silicone rubber membrane. However, this requires very thick sacrificial layers to form posts with sufficient aspect ratio. For working with thick resists, a 1X contact or projection aligner with highly collimated UV source is necessary.

To perform testing, electrical contact had to be made to the backside of the die. This could potentially be done with solder bump bonding in a production environment. However, for testing, spring contact probes (Ostby Barton Pylon A-S-C) were used. An

aluminum plate was machined with a row of probes on a 0.05" pitch. The aluminum was anodized to provide electrical insulation. The actuator/membrane assembly was then clamped between a fluidic board machined from acrylic and the aluminum plate as shown in Figure 6-5. Performance of the valves was very poor. In fact, for any reasonable amount of power (< 1 W), there was almost no deflection. This is due to the large amount of heat loss through the silicon tethers. Even though they are only 100 μm wide by 500 μm tall, that is still a very thermally conductive path compared to the 1 μm thick nitride membranes use for earlier heaters. For a 2 mm diameter heater structure, the equivalent cross sectional area of a silicon nitride membrane is roughly 6000 μm^3 vs. 10,000 μm^3 for two silicon tethers. Factor on top of that the 9 times difference in thermal conductivity and the thermal resistance for similar lengths is 14 times higher for the silicon structure! This is further exacerbated by the distributed nature of the resistor on the silicon beam leading to uniform power vs. length. For the nitride membrane heaters, the power is localized to the center.

To make the silicon structure work, the length of the beams must be greatly increased (to increase the thermal resistance), the thickness decreased, or the width decreased. Increasing the length of the beams consumes a large amount of area which is

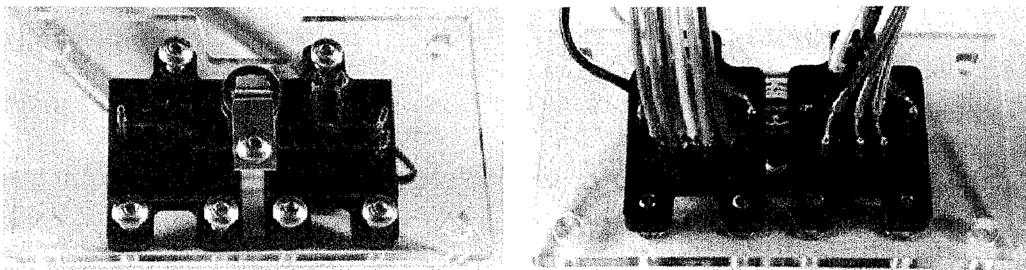

Figure 6-5: Front and back views of actuators assembled to the acrylic fluidic plate along with backside electrical connections.

already at a premium for the valve structures. The thickness of the beams is nominally defined by the wafer thickness and while thinner wafers could be used, fragility during processing would be an issue. It is possible define the thickness of the beams independently of the wafer thickness. However, the metallization could not be applied from the backside. If the metallization is on the front, then other approaches can be used that are superior. Finally, the beam width could be reduced although aspect ratios greater than 10:1 are difficult to achieve when etching through the wafer. In the end, this approach was abandoned although some elements of the process were applied to a later design.

6.4 Improved Nitride Membrane Heater

The major issue for all the pump designs has been the optimal thermal actuator which in large part depends on the heater design. The design outlined in Chapter 5 is fragile and limited to rectangular shapes which limits the membrane geometry to some extent although sacrificial layers can be used to make the two somewhat independent. However, because of the stiction problems encountered, it was desired to make a membrane without a sacrificial layer. Using DRIE, it's possible to make arbitrary geometry membranes; the question then becomes can DRIE be used to make nitride membrane heaters?

6.4.1 Design and Fabrication

The main issue to be solved is the definition of a silicon island on a nitride membrane that is a different thickness than the starting wafer. Once etching begins, the topography is such that photolithography cannot be easily performed. Thus, all lithographic steps must be done prior to the wafer being etched with DRIE. If photoresist and oxide are

used as masking layers, the initial etching can be defined by the photoresist mask and the final pattern can be defined with the oxide. This can be extended to more than two layers by using other mask materials such as metal. Using this technique, the island can be defined initially with the depth etched defining the final thickness of the island, and then a larger area is etched down, stopping at the nitride membrane.

A process is outlined in Figure 6-6 for a nitride membrane heater. Since we wish to stop on the nitride membrane without etching it, an etch stop is required as silicon nitride is etched by SF_6 albeit at a slower rate than silicon. First, a thick layer of thermal oxide is grown on both sides of the wafer. This will be used as the backside DRIE mask. The selectivity between oxide and silicon is roughly 200:1. Thus, to etch 400 μm, 2 μm of oxide is necessary. Then, one side is stripped using buffered HF (BHF) and another thin

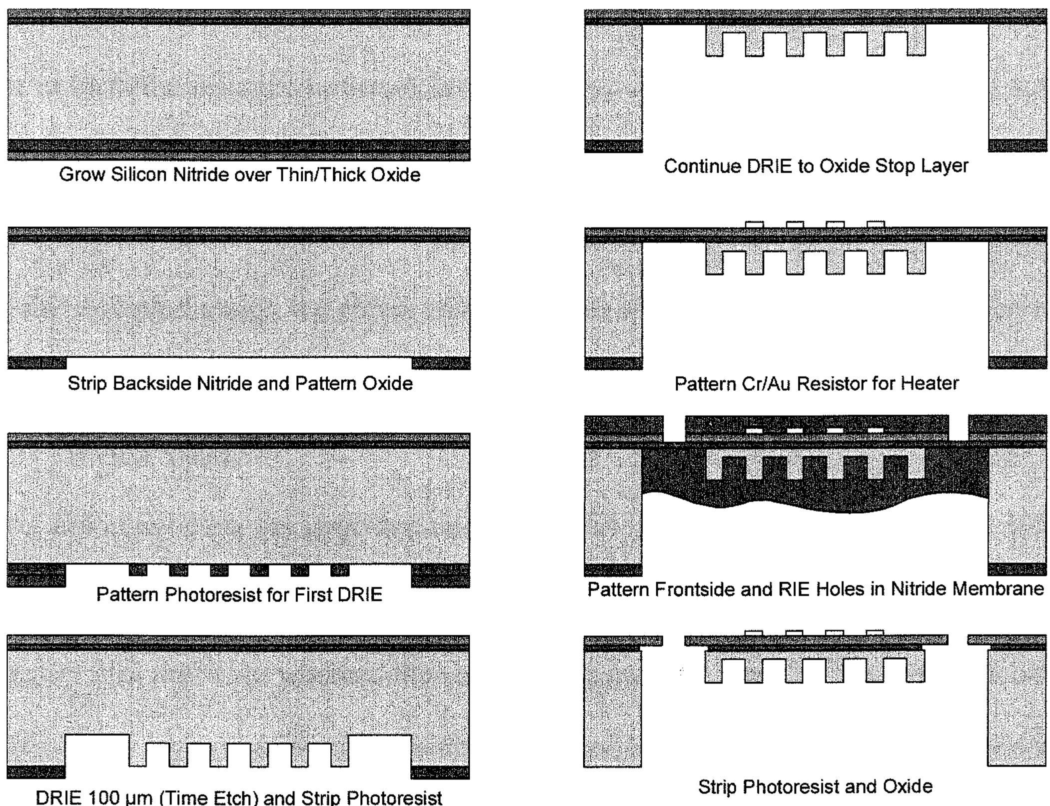

Figure 6-6: Process flow for the nitride membrane heater made with DRIE.

oxide layer is grown. This will form the etch stop and given a nonuniformity on the order of 20 μm across the wafer, should be at least 1000 Å thick. In this case, 2000 Å was grown. A 7000 – 8000 Å layer of low-stress LPCVD silicon nitride is deposited on both sides of the wafer. It is then removed from the backside using SF_6/O_2 plasma to expose the thick oxide which is then patterned to define the second DRIE mask. Then a layer of photoresist is patterned to define the first mask. The selectivity between AZ positive photoresist and silicon is roughly 100:1. However, the first etch is not very deep so 4 μm thick resist is used. This pattern is etched for 140 loops which produced a structure about 100 μm deep depending on aspect ratio. Then the photoresist is stripped and etching continued using the oxide as a mask. Etching continues until the oxide stop layer is reached. Some overetch is necessary as there is approximately 5% nonuniformity across the wafer in the DRIE. Cr/Au is then evaporated and patterned on the front side of the wafer to form the resistive heater. A layer of photoresist is patterned on the front surface to etch pressure equalization holes in the membrane using SF_6/O_2 RIE. Photoresist is also applied to the backside of the wafer to protect the backside of the oxide/nitride membrane from the etching. Finally, the photoresist and oxide stop layers are stripped and the wafer is diced.

6.4.2 Process Specifics

During the initial etch, the large openings for the moat and through holes etched 105 μm while the small openings for the fins only etched 90 μm. The large openings were nominally 200 μm wide whereas the fin defining grooves were 20 μm. After etching to the oxide stop layer, the remaining silicon membrane was 30 to 40 μm thick underneath the fin openings, while the island itself was 80 μm thick (the 20 μm difference is due to

6.4.3 Heater Testing

Since the metallization was on the front side for this generation, contact had to be made to the pads by probes from the top, wire bonding, or soldering. For general electrical and thermal test, a small 0.050" pitch header was soldered to heater dies. As previously mentioned, the tin in conventional solder causes dissolution of the gold pad. This is slightly alleviated by the use of solder with some silver content. However, Indium containing solders provide superior results. Indalloy #2 solder along with Kester #186 flux was used. Because the high thermal conductivity of the silicon substrate made it difficult to get enough heat into the joint with a small soldering iron, the heater die was preheated on a 120°C hot chuck. After removing the flux, the die was then bonded to a glass slide to simulate the backing plate used to seal the working fluid cavity in the thermopneumatic actuators. To provide some indication of the temperature on the surface of the membrane during operation, the TCR was measured using a Delta 2300 convection oven, an Omega HH23 thermocouple, and an HP34401A multimeter. The curves for seven different heaters are shown in Figure 6-7 and the nominal TCR was found to be .0025/°C. These measurements were taken with a uniformly heated die.

The next step was measurement of the spatial temperature distribution on the heater die surface. Theoretically this could be done by fabricating many small resistors on the substrate. Another option is the use of a thermal imager, in this case a Quantum Focus (formerly EDO Barnes) Infrascope™ I. The instrument operates by generating an emissivity map of the surface by measuring the radiance of the sample at two different temperatures. Then, it can calculate the temperature during operation by measuring the radiance. For accurate measurements, it is very important that the emissivity calculation

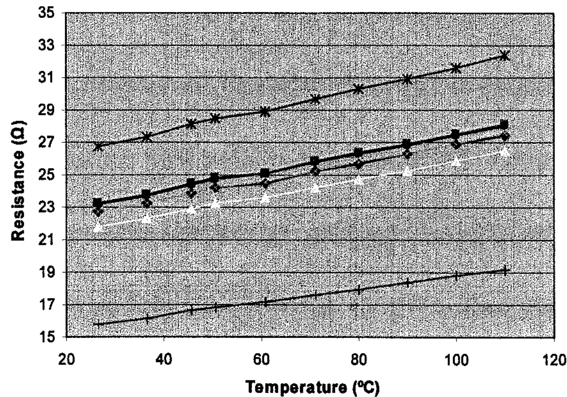

Figure 6-7: Heater TCR measurements

be performed correctly. The sample is heated using a thermoelectric cooler/heater (Peltier junction). Since there are free-standing membranes, it is important to verify that the entire sample reaches a uniform temperature on the hot chuck. This was done by measuring the island temperatures using the calibrated heaters as temperature sensors. Agreement between the set temperature (a closed loop system with a thermocouple attached to a large aluminum heat spreader with the Peltier junction) and the membrane temperatures was within 0.8% over a range of temperature from 40°C to 80°C, while the emissivity was calculated using radiance values at 60 and 80°C. Once the emissivity was calculated, the stage was turned off and allowed to return to room temperature. It is important to note that the set temperature was not simply adjusted to room temperature. In this case, it would still be in closed loop operation trying to maintain room temperature on the surface, leading to it possibly cooling the chuck to compensate for the heating of the device under test. These measurements simulate the packaged heater on a very large heat sink in ambient conditions.

One of the valve heaters and the central pumping chamber heater were measured. Figure 6-8 shows the results for both. Clearly, the heat is localized to the center of the membrane. For the small heater, 110 mW generates an 83°C increase in temperature on the membrane. Given a gap between heater and substrate of 400 μm, the approximate amount of heat lost to conduction through air to the substrate is 8 mW. Conduction through the nitride membrane accounts for approximately 32 mW. Thus, roughly 70 mW is lost elsewhere. These values are similar to those obtained for a nitride membrane hotplate [4]. Since the nitride and silicon membranes are not completely opaque, the emissivity map includes some details from the backside of the die including the silver epoxy used to bond the die to the glass backplate. Thus, the only reliable temperatures are from the gold surfaces and bulk silicon substrate. However, that is enough to safely conclude that the substrate stays close to room temperature while the islands reach elevated temperatures. Another experiment was done with a die which had not been completely etched, that is the membrane holding the heaters consists of a silicon nitride

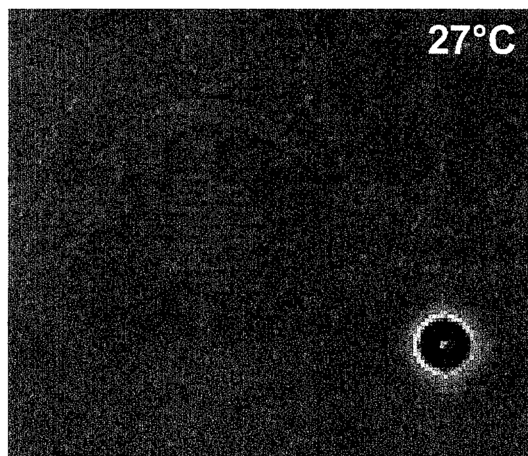

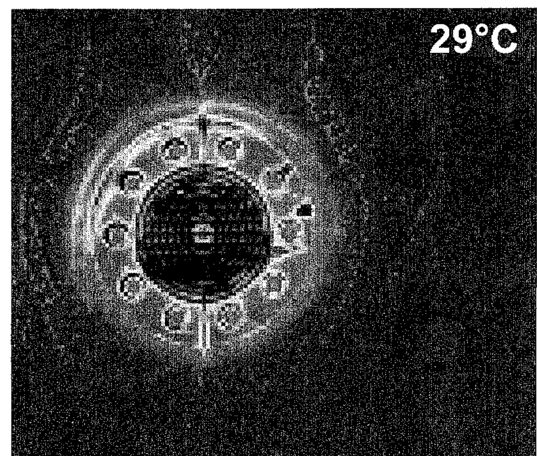

Figure 6-8: Thermal image of small heater on the left and large heater on the right. The gray regions are areas where no data was acquired due to the low emissivity of gold.

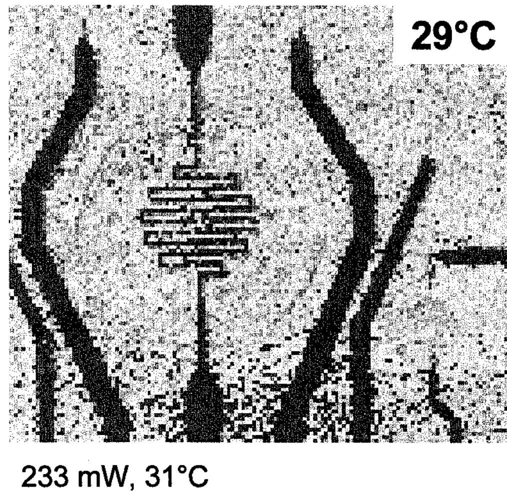

Figure 6-9: Thermal image of a small heater with 233 mW applied power. The membrane suspending the heater is composed of silicon nitride and silicon resulting in very high thermal conduction to the substrate.

membrane, the oxide stop layer, and approximately 5 μm of silicon. The results are shown in Figure 6-9. Clearly, the addition of what seems like a small amount of silicon greatly detracts from the thermal isolation of the heater. With a 5 times increase in cross section, and a thermal conductivity 8 times higher than silicon nitride, there is roughly 40 times increase in conductivity. It is interesting to note that the resistances measured for the heaters while testing do not correlate to measured temperature. The small heater went from 23 Ω to 41 Ω. This would correspond to a temperature increase of more than 300°C. A more likely explanation is the nonuniform heating of the membrane and differing coefficients of thermal expansion for the various materials leading to strain in the gold.

6.5 Diaphragm Pump

To complete the pump, two other components are necessary. A membrane to form the flexible wall of the sealed working fluid filled cavity, and a fluidic substrate with matching features to form the valves and pumping chamber. These are then assembled into a complete pump.

6.5.1 Membrane

Circular membranes are formed using a simpler version of the process in Section 6.3.1. Openings are defined in an oxide mask and cavities are partially etched in a silicon wafer leaving a small amount of silicon. A photoresist sacrificial layer is defined on the front side followed by spin coating and curing of silicone rubber. The silicone rubber is added late in the process so that it doesn't interfere with cooling in the DRIE which uses helium on the backside to cool the substrate during etching. Finally, the etching is continued from the backside until the photoresist stop layer is reached. Then, the photoresist is removed using acetone releasing the membrane. For the valves, 1.4 mm diameter membranes 150 μm thick were formed with Shin Etsu X32-1502. The pumping chamber membrane was 4.0 mm in diameter. Theoretical calculations for the valve membranes are found in Chapter 3.

6.5.2 Fluidic Substrate

Acrylic was used for the fluidic substrate. It is commonly used for microfluidic components and typically fabricated using hot embossing or compression molding for prototyping and injection molding for mass production. The use of acrylic for compact discs (CDs) and polycarbonate for digital versatile discs (DVDs) has provided the technology for high throughput manufacture of very precise low cost substrates. However, the costs to manufacture an appropriate mold are very high. Theoretically, a silicon master can be made using a variety of fabrication techniques, transferred to a nickel electroform, and then used to mold parts. However, for making prototypes, conventional milling as in Section 5.7 was used instead. Starting with a 0.125" piece of cast acrylic sheet, the surface was surfaced with a diamond flycutter. Then, a 3 mm

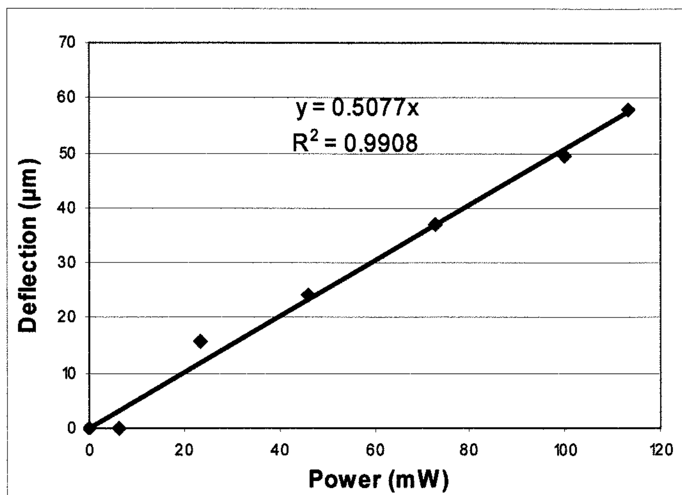

Figure 6-10: Power vs. deflection for valve actuator.

spherical endmill was used to machine the cavities for the valves and pumping chamber. The pumping chamber was made hemispherical while the valve cavities closely match the sinusoidal profile of the inflated membrane. Channels were milled using 0.005" or 0.010" endmills. Finally, 0.020" holes were drilled to make external connections to tubing. Two different channel configurations were fabricated, one 125 μm wide and 40 μm deep, the other 250 μm wide and 100 μm deep except near the valves where it was 25 μm deep. Surface roughness of the flycut surface was on the order of 1 μm p-p. This did not form a good seal against the silicone rubber so the acrylic parts were lapped on 5 μm silicon carbide lapping paper and then polished with 1.0 μm sapphire paste. This resulted in a loss of 2 – 3 μm of acrylic.

6.5.3 Thermopneumatic Actuator

A membrane die was bonded to a heater die and glass backplate to investigate the static and transient characteristics of the actuator. As before, a microscope stage was used to focus on the center of the membrane and chart deflection vs. applied power. The resulting curve is shown in Figure 6-10. The deflection is linear with power which is expected

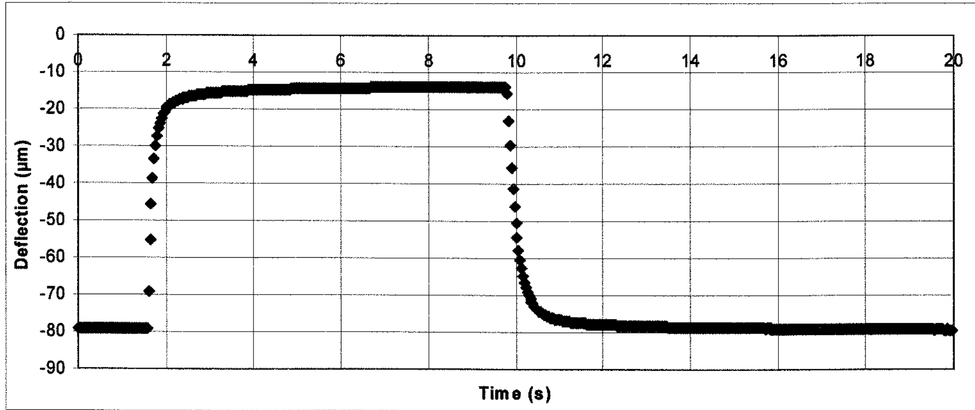

Figure 6-11: Transient response of small valve actuator in response to 2.0V input

from the simulation of deflection vs. temperature in Section 3.3.3. However, the deflection is much less than expected given the temperature on the heater membrane at 110 mW power input. Simulation shows that a 10°C increase in temperature of all the air in the cavity should result in a 50 µm deflection. In this case, that deflection is being achieved with close to a 125°C increase in temperature (assuming a linear relationship between input power and surface temperature). This indicates that the temperature falls off much more rapidly inside the sealed cavity than would be explained by a simple conduction model.

Transient performance was also evaluated using a laser interferometer. Previously, the smallest time constant achieved for a nitride membrane based actuator [5] was 1.2 s. A deflection vs. time curve for the valve actuator is shown in Figure 6-11 and the results for both the small valve and large pumping actuators are summarized in Table 6-1. 2.0 V was applied to both devices for actuation.

Actuator	Power	Deflection	τ Heating	τ Cooling
1.4 mm valve	100 mW	65 µm	0.12 s	0.24 s
4.0 mm pump	210 mW	298 µm	0.37 s	0.74 s

Table 6-1: Time constants for thermopneumatic actuators.

Performance is significantly better than the previous design. There is also a second time constant on the order of seconds that is not listed which is due to the package whereas this shorter time constant is associated with the heater structure and working fluid and dominates the performance.To determine if the time constant was dominated by the working fluid (air) or the structure, the time constant of the heater resistance was measured. Of interest was the effect of air. As the results in Table 6-2 show, the time constant is dominated by the structure as the time constant in vacuum is very similar to that of the package structure. This would not necessarily be the case for a working fluid such as water. Considering only conduction, and using conservation of energy, we can write

$$I^2 R - \frac{Ak\Delta T}{L} = \rho V C_v \frac{dT}{dt} \tag{6.2}$$

and then define thermal resistance and capacitance as follows

$$R_{th} = \frac{L}{kA} \qquad C_{th} = \rho V C_v \tag{6.3}$$

where L is the length, A the cross sectional area, V the volume, C_V the specific heat, k the thermal conductivity, and ρ the density. A simple calculation of the time constant for cooling considering only air is 19 ms which is clearly too fast. Considering the mass of the silicon island and the nitride membrane, the time constant is 0.25 s which compares very well to the measured value of 0.24 s.

Device	**τ Heating**
Heater & Backplate	98 ms
Heater, Backplate & Membrane	98 ms
Heater & Backplate in Vacuum	96 ms

Table 6-2: Measurements to determine effects of air on time constants

6.5.4 Thermopneumatic Pumping

With passive check valves, only the pumping actuator needs to be controlled. The valves operate automatically based on the relative pressure difference between the pumping chamber and the inlet/outlet. With active valves, the opening and closing must be correctly sequenced with the motion of the pumping actuator. Also, the central pumping actuator is not designed to form a tight seal between inlet and outlet so a valve must always be closed. A basic sequence with 6 phases is shown in Figure 6-12. First the inlet is sealed, the fluid in the chamber is displaced, the outlet is sealed, the chamber is refilled, and then the inlet sealed again prior to opening the outlet before the cycle repeats.

Both the large and small actuators were actuated with 2.0 V for power dissipations of roughly 100 and 200 mW respectively. All testing was done with water at room temperature unless otherwise noted. The depth of the small chambers ranged from 40 to 45 μm with the large chambers ranging from 140 to 160 μm. Based on the interferometer measurements, the valves should have been completely sealed and the pumping membrane should have touched the roof of the chamber. The first pump tested had 125 μm wide, 40 μm deep channels. Considering a slight compression of the silicone rubber layer due to clamping and the actual channel height was probably closer to 35 μm. It was

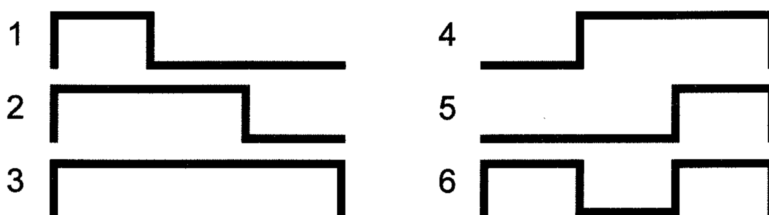

Figure 6-12: Basic 6 phase sequence for diaphragm pump. Note that a valve is always closed to prevent free flow through the structure.

observed that it took roughly 5 – 6 s to fill the pumping chamber. However, operation of the valves was quite fast, more or less as expected from the time constant measurements. The flow rate was 0.5 μl/cycle and reversion was very small as expected due to the large swept volume of the pump chamber vs. the small valve chambers. However, given the 5 – 6 s necessary to fill the pump chamber plus additional time for valving and it is clear that the overall flow rate is very low, 2 – 3 μl/min. To allow for sequenced rather than manual operation, a slightly modified 6 phase pattern was used as shown in Figure 6-13. Because the fill phase is so slow, the output valve can seal quickly enough to omit a separate sealing phase between phases 2 and 3. That is to say, the output valve is sealed before the inlet and pumping membranes have gone to their rest positions. Phases 4 and 5 allow additional time for filling. The acrylic chamber chip was changed to the one with dual-level channels, mostly 100 μm deep with a small section 25 μm deep next to the valves. It was noted that the fill time was reduced to 3 s so that the 5 phase sequence could be safely operated at 0.5 Hz. Flow rate was 1.7 μl/min. It was noted that the volume per cycle was 0.33 μl/cycle. This may have been due to misalignment of the membrane and chamber.

Given that the actuators are fairly fast, the slow fill times limit the performance of the pump. By assuming the filling occurs uniformly, the flow rate is roughly 0.1 μl/s for both types of channels. Since the same actuator was used for both pumps, the relative pressure drop from inlet to outlet is also similar. Inflation requires roughly 2000 Pa. Assuming then that the pressure drop from inlet to outlet is also 2000 Pa as the membrane deflates, the following equation [6] can be used to estimate pressure drop. This assumes

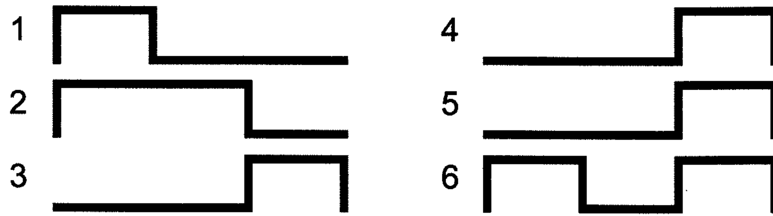

Figure 6-13: Modified sequence used for thermopneumatic operation. The slow filling of the pump chamber and fast rise vs. fall times of the valves allows the transition from phase 2 to phase 3.

that the flow is incompressible, the channel height is much smaller than the width and length, and the flow velocity is zero except along the length of the channel. Then

$$\Delta P = \frac{12 Q_v \mu L}{h^3 w} \tag{6.4}$$

where L is the length of the channel, h is the height, w is the width, μ is the viscosity, Q_v is the volumetric flow rate, and ΔP is the pressure drop. The essential channel parameters along with the calculated pressure drop are shown in Table x. While the channel dimensions don't strictly satisfy the assumptions with respect to h << w, this provides a useful approximation to determine the cause of the slow filling. For both channels, a flow rate of 0.1 μl/s was assumed. In design 2, the pressure drop for the deep (100 μm) channels is neglected as it is very small compared to the shallow sections.

Design	Height	Width	Length	ΔP
1	35 μm	125 μm	4 mm	896 Pa
2	20 μm	250 μm	1.3 mm	780 Pa

Table 6-3: Channel dimensions for two different acrylic fluidic substrates and the corresponding pressure drops assuming a flow rate of 0.1 μl/s.

This compares well with the approximate pressure difference available for filling from the restoring force of the membrane. The pressure drop is actually a function of membrane deflection so the average from full inflation (2000 Pa) to rest (0 Pa) is 1000 Pa with a similar change in flow rate.

To determine if surface forces were also cause for the slow filling, two experiments were performed. First, acrylic and silicone surfaces are hydrophobic. Silicone can be temporarily rendered hydrophilic by plasma treatment, but the effect is not permanent. Acrylic can be made hydrophilic using potassium hydroxide. One of the acrylic substrates was soaked for 10 minutes in concentrated potassium hydroxide until the channel surface was mildly hydrophilic. No significant difference was noted in fill time. However, this is not fully conclusive as the membrane surface was still strongly hydrophobic. Also, 3M PF-5080 (a perfluorocarbon fluid) with a viscosity of 1.4 cp (close to the viscosity of water, 1.0 cp at 25°C) was tried. PF-5080 wets acrylic and silicone very well. However, fill times were found to be similar indicating that surface effects weren't on the same order as pressure drop in the channels.

The pump with both channel designs was found to be unable to pump air. This is simply due to poor sealing. Most likely the major leakage path is the valve itself which is masked when pumping water due to its much higher viscosity and the hydrophobicity of the surface. However, there was also a leakage path between the acrylic and the silicone rubber. X32-1502 is harder than the MRTV1-10RE used previously and does not form as good a seal under mild compression. Increasing the clamping force results in extrusion of the silicone into the channels greatly reducing their height and increasing the flow resistance significantly. The leakage in the valve is due to misalignment and mismatch between the actuated membrane shape and the corresponding chamber. Misalignment is simply due to the manual nature of assembly and could be greatly improved with interlocking components or an apparatus similar to a wafer bonder or contact aligner. The process could also be modified to provide some degree of self-alignment as will be

discussed. At this feature size, the limitations of conventional machining are apparent. Aside from the limitations of positioning accuracy, the tooling itself starts to become an issue. A 0.001" error in the diameter of a spherical endmill causes significant change in the final shape of a machined cavity.

6.6 Conclusion

A diaphragm pump using active valves has been successfully demonstrated. This design lends itself to integrated fluidic systems. However, the softness of the pumping membrane leads to slow filling when coupled with the large pressure drop across inlet channels. This can be addressed by stiffening the pumping membrane and/or distributing the pumping actuator over many small actuators. With either approach, the compression ratio should be maximized to reduce reverse pulsation in the flow.

References

[1] See Chapter 1 for an extensive list of references.

[2] X. Q. Wang and Y. C. Tai,"A Normally Closed In-Channel Micro Check Valve," Proceedings of IEEE International Conference on Micro Electro Mechanical Systems (MEMS '00), pp. 68-73, Miyazaki, Japan, January, 2000.

[3] G. T. Mulhern, D. S. Soane, and R. T. Howe, "Supercritical Carbon Dioxide Drying of Microstructures," Technical Digest, International Conference on Solid-State Sensors and Actuators (Transducers '93), pp. 296-299, Yokohama, Japan, June 1993.

[4] R. P. Mamginell, D. A. Rosato, D. A. Benson, G. C. Frye-Mason, "Finite Element Modeling of a Microhotplate for Microfluidic Applications, MSM '99, San Juan Puerto Rico, 1999.

[5] X. Yang, *Micromachined Silicone Rubber Membrane Valves for Fluidic Applications*, Ph.D. Thesis, California Institute of Technology, 1998.

[6] S. Wu, *Integrated Polysilicon Thermistors for Microfluidic Sensing*, Ph.D. Thesis, California Institute of Technology, 2000.

Chapter 7

Conclusion

7.1 Summary of Research

The suitability of silicone rubber as a material for microfabrication, specifically for integration with conventional silicon processing, was investigated. An addition cure material was tested and found to have a very low Young's modulus, 5 orders of magnitude smaller than single crystal silicon or silicon nitride, both commonly used as membrane materials. In addition, the low durometer of the material lends itself to sealing, especially for fluidic applications. A variety of RTV addition cure formulations were investigated for mechanical and chemical properties conducive to MEMS with one standing out as especially suited for large deflection actuators, Shin Etsu X32-1502. Several processes were developed to integrate silicone rubber with conventional MEMS processes such as bulk and surface micromachining of silicon.

Using silicone rubber membranes, two types of micro balloon actuators for aerodynamic control were investigated. The first was made on a silicon substrate using a Parylene release layer. This provided a high yield dry-release mechanism with independent sizing of the membrane vs. the pneumatic access hole. The second was made on metal substrates, both brass and copper, to form a flexible actuator skin for distributed use on a leading edge. Both actuators were successfully used to control a delta wing taking advantage of small perturbations in the boundary layer near separation inducing large changes in the vortices developed by the delta wing. At high angles of attack where

the vortex development is most pronounced, aerodynamic moments on the same order as conventional flaps were achieved. This indicates that these actuators can be used for flight control in applications requiring high maneuverability and low observability such as unmanned aerial vehicles (UAVs) for surveillance.

A peristaltic pump structure was fabricated using the combination of a large deflection silicone rubber membrane and a plastic chamber structure with cavities closely matching the shape of the inflated membrane. Unlike previous work, sealing with this design was fairly good and the dead volume was low which allowed self-priming operation and the ability to pump vacuum on the inlet. These features had only been demonstrated with diaphragm pumps using passive check valves previously. In addition, the design was inherently planar and the pumping structures could also be used as a valve. As such, all the components for a microfluidic system were embodied in the implementation of the pump, that is channels, valves, and pumps. For self-contained operation, a thermopneumatic actuator was developed using a novel floating silicon island heater to improve thermal transfer to the working fluid, reduce heat lost to the substrate and thus power consumption, and improve operating frequency. Previous work used silicon islands suspended by silicon beams with resultant high power consumption, nitride membranes with no heat spreader, or glass substrates with poor thermal isolation. The use of a silicon nitride membrane to suspend the silicon island reduced power consumption while ensuring fast heat transfer to the working fluid. Using this thermopneumatic actuator, a self-contained, self-priming, peristaltic pump was demonstrated with a flow rate of 6.3 μl/min operating at 291 mW. Previous peristaltic

pumps have not been self-priming and their designs do not lend themselves to integrated systems.

With the availability of DRIE, the heater structure was improved in terms of robustness, density, and speed. Using a multilevel etching process, the heater island can be optimized for the size of the fluidic cavity and very large surface area structures can be made. By using the proper sacrificial layer materials, it is possible to integrate the membrane and heater into one device to simplify assembly. Along with the new heater, a generic pumping structure was devised employing multiple active valves and a single pumping actuator. This structure allows arbitrary pumping from an input port or ports to any output. A plurality of pumps and valves can be replaced by a single structure and the planar nature of the design lends itself towards easy integration. The heaters required for the various valves and pumps are made on a silicon substrate. The matching channels and chambers are fabricated on a polymer card. The assembly then consists of channels, reservoirs, pumps, and valves which can be used for a variety of fluidic systems. A simple system consisting of two valves and one pumping structure was successfully demonstrated as a bi-directional pump.

7.2 Directions for Future Work

The largest hurdle to using this technology to make integrated fluidic systems is assembly. Clearly, a method other than manual alignment and clamping is needed for commercial quality systems. Some suggestions for improvement follow.

Integration of the membrane and heater structure is possible and some initial experiments were done. With the appropriate exposure tools and process chemistry, thick photoresist can be used as a sacrificial layer and incorporated into the suspended island

DRIE heater process. In this case, the pressure relief holes would be etched prior to freeing the nitride membrane. Anti-stiction measures can also be taken, such as roughening the surface, forming posts in the membrane or surface to reduce contact area, and possibly CO_2 critical drying. While there will be a decrease in actuator volume (due to the loss of the silicon membrane substrate) with a resulting increase in the flexibility (expressed as λ in Chapter 3), this becomes less important as the size of the pumps and valves are scaled down. It can also be compensated for by stiffening the membranes. In Chapter 6, it was seen that membrane stiffness is important in defining sufficient restoring force to maintain the desired flow rate. While it is simplest to make all the membranes the same thickness, different thickness sacrificial layers can allow independent definition of membrane thickness. Also, composite membranes can be used in some areas to increase the stiffness of larger structures.

The polymer fluidic cards are best fabricated by some form of molding, compression, injection, or hot embossing. These require a mold insert, typically made of nickel in production. Prototype molds can be made from silicon or glass. To achieve the contoured shapes necessary for the valve and pump chambers, grayscale lithography in concert with dry etching pattern transfer is the most expedient method of making such structures with submicron accuracy. Rather than clamping the fluidic cards to the actuator substrates, they can actually be bonded. One approach is lamination to the silicone membrane prior to curing the silicone rubber, thus using it as an adhesive layer and a mechanical layer. This can be achieved with suitable surface treatment on both surfaces and a specialized formulation of silicone rubber. Another approach is bonding the polymer card directly to the cured elastomer layer using suitable pretreatment

(plasma) and a silane coupling agent. This alignment step is best performed optically using techniques similar to those used in wafer bonding. With such measures, flow systems with minimum dimensions on the order of 10 μm can be made using today's technology.